I. STUDIES OF COLLISION BROADENING OF ION CYCLOTRON RESONANCE LINESHAPES

II. STUDIES OF THE GAS PHASE ION CHEMISTRY OF FLUOROETHANES

Thesis by

Douglas P. Ridge

In Partial Fulfillment of the Requirements

For the Degree of

Doctor of Philosophy

California Institute of Technology

Pasadena, California

1973

(Submitted September 18, 1972)

ACKNOWLEDGMENTS

The author gratefully acknowledges the assistance, advice, direction and discussion of Professor J. L. Beauchamp. He also acknowledges the contributions of his fellow students in hours of discussion and scientific debate. He acknowledges the efforts of Mrs. Joyce Lundstedt, who typed the manuscript. Finally he acknowledges his mother and father, and his wife and daughter. Without their help and encouragement this work could not have been completed.

ABSTRACT

In Section I theoretical calculations of gas phase ion mobilities are reviewed. The results of measurements of ion cyclotron resonance linewidths of ions in methane and ions in hydrogen are presented. The relationship between ion mobilities, collision frequencies and ion cyclotron resonance linewidths is reviewed. The results of the linewidth measurements are compared with DC mobility measurements and theoretical calculations of the mobility. The results of previous ion cyclotron resonance linewidth measurements are in serious disagreement with DC mobility measurements. The results of the present study, however, agree well with recent mobility measurements. Except for H^+ and H_3^+ in hydrogen the results of the linewidth measurements are consistent with the theory of Mason and Schamp which is based on a three term 12-6-4 ion molecule interaction potential. It is concluded that weak chemical bonding occurs between hydrocarbon ions and methane and that the anisotropy of the H_2 molecule plays a significant role in determining the cyclotron resonance linewidths of ions in hydrogen. The parameters which determine the 12-6-4 potentials which best characterize the interaction between the ion-neutral pairs studied are estimated. It is concluded that the interaction of H^+ and H_3^+ with H_2 are too energetic to be adequately represented by a 12-6-4 potential. Measurements of the linewidths of Na^+ ions in the C_3H_6O isomers are found to increase linearly with dipole moment in quantitative agreement with a simple model. The implications of this result are discussed.

In Section II a series of fluoride transfer reactions between fluoroalkyl cations and fluoroalkanes in the gas phase are described. In one case ($CH_3CHF^+ + CH_3CF_3 \rightarrow CH_3CF_2^+ + CH_3CHF_2$) equilibrium is observed so that a free energy change can be assigned from the final ratio of the ionic products. From this result and from observations of competitive fluoride transfer reactions in mixtures of fluoroalkanes a sequence of fluoride affinities of fluoroalkyl cations is deduced (the fluoride affinity of R^+ is $-\Delta H$ for the reaction $R^+ + F^- \rightarrow RF$). Including the results of previous studies the sequence in order of decreasing fluoride affinities is $C_2F_5^+ > CF_3^+ > CH_3^+ > CH_2F^+ > CHF_2^+ > CHF_2CHF^+ > CH_2FCHF^+ > CH_3CF_2^+ > CH_3CHF^+ > C_2H_5^+$. The effects of fluorine substituents on ethyl cation stability are discussed. A simple electrostatic model is proposed to account for the destabilization of fluoroethyl cations by β fluorine substituents.

The base induced elimination of HX from alkyl halides (RX) in the gas phase is proposed and its observation reported. The reaction $CH_3O^- + C_2H_5F \rightarrow CH_3OHF^- + C_2H_4$ is shown by isotopic labelling and kinetic studies to be a based induced 1,2 elimination. Analogous reactions are observed between CH_3O^- and CH_3CHF_2, CH_3CF_3, CH_2FCHF_2, and CHF_2CHF_2. It also appears that F^- reacts with fluoroethanes in an analogous way. Other substrates from which bases appear to eliminate HX are β-chloroethanol, ethylene bromohydrin and CH_3CCl_3. Proton transfer between fluoroethanes and CH_3O^- is also observed. The fluoroethyl anions formed transfer F^- to the parent fluoroethanes. The thermochemical consequences of the observed reactions with regard to the binding in species of the type XHY^- and with regard to the electron affinities of the fluoroethyl anions are discussed.

TABLE OF CONTENTS

SECTION I

Studies of Collision Broadening of Ion Cyclotron Resonance Lineshapes

CHAPTER 1

Review of Calculations of Ion Mobilities

Classical Calculations

In December of 1895 Roentgen astounded the scientific world with his announcement of the discovery of X-rays. One of the intriguing properties of this new kind of radiation was its capacity to render normally insulating gases conducting. Experiments by Ernest Rutherford and J. S. Townsend and others established that the charge carriers moved through the gases at velocities proportional to the applied field. These early experiments also suggested that the charge on these particles was the same as that on univalent ions in solution.[1] Soon after these results were obtained Paul Langevin applied Boltzman's kinetic theory to the motion of charged species in a gas under the influence of an applied field where v_d and E are the drift velocity of the ion and the electric field strength respectively.[2] The mobility, K, of an ion is defined by Eq. (1). Applying the methods of Boltzman, Langevin obtained Eq. (2).

$$v_d = KE \tag{1}$$

$$K = \frac{3e}{n_0\, 32[2\pi M_r\, kT]^{\frac{1}{2}} \int_0^{\infty} q(v_0)\exp(-z^2)\, z^5\, dz} \tag{2}$$

where

e = electronic charge

n_0 = neutral number density

M_r = reduced mass of ion neutral pair

kT = product of Boltzman's constant and absolute temperature

$z = (M_r\, v_0^2/2\, kT)^{\frac{1}{2}}$

v_0 = relative velocity of ion neutral pair

$q(v_0)$ = a collision cross section for ion-neutral pair, proportional to diffusion cross section .

The collision cross section $q(v_0)$ is defined by

$$q(v_0) = \int_0^\infty \cos^2\Phi \; b \; db \tag{3}$$

where b is the impact parameter and Φ is related to Θ, the scattering angle in the center of mass system by $2\Phi = \pi - \Theta$. The diffusion cross section, $q_d(v_0)$ is defined by

$$q_d(v_0) = 2\pi \int_0^\infty (1 - \cos\Theta) b \; db \tag{4}$$

so that

$$q_d(v_0) = 4\pi \, q(v_0) \quad . \tag{4a}$$

Physically, the diffusion cross section is a measure of the average momentum in the incident direction lost by an ion on collision with a neutral.

Integration of the Legrangian equations of motion for Φ gives Eq. (5)

$$\Phi = \int_0^{\rho^*} \frac{d\rho}{\sqrt{1 - \rho^2 + \dfrac{2V(r)}{M_r \, v_0^2}}} \tag{5}$$

where $\rho = b/r$ and b and r are the impact parameter and the ion-neutral distance, respectively. The upper integration limit in Eq. (5), ρ^*, is equal to ρ^0, the smallest positive root of the quantity under the radical sign. Langevin chose the potential defined in Eq. (6) where α is the

angle averaged polarizability of the neutral and D_{12} is the sum of the radii

$$V(r) = \frac{\alpha e^2}{2r^4} \qquad r > D_{12}$$
$$V(r) = \infty \qquad r < D_{12} \tag{6}$$

of the ion and the neutral. For this potential ρ^* is equal to ρ^0 unless $\rho^0 > b/D_{12}$ in which case ρ^* is equal to b/D_{12}.

Physically this is a mathematical description of a model in which the ions and molecules are hard impenetrable spheres of combined radius ν_{12} that attract each other with an ion-induced dipole force proportional to r^{-5}.

The angle Φ in Eq. (5) can be evaluated in terms of elliptic integrals. Langevin uses the expressions obtained in evaluating Φ to calculate collision trajectories in a number of typical cases. Figures 1, 2, and 3 show trajectories calculated for various values of the reduced parameters μ/z and β defined by Eqs. (7) and (8).

$$\frac{\mu}{z} = \left(\frac{\alpha e^2}{2\, D_{12}^4}\right)^{\frac{1}{2}} \left(\frac{1}{\frac{1}{2} M_r v_0^2}\right)^{\frac{1}{2}} \tag{7}$$

$$\beta^2 = \left(\frac{M_r v_0^2}{4\alpha e^2}\right)^{\frac{1}{2}} b^2 = \frac{b^2}{b_0^2} \tag{8}$$

Here b_0 is the critical impact parameter or the impact parameter for which the orbiting discussed below occurs so that β is a reduced impact parameter. μ/z is just the radio of the potential energy due to

the polarization interaction at a distance D_{12} to the relative kinetic energy of the interacting pair. Thus μ/z is the reciprocal of a reduced relative velocity. In the figures two other parameters, ψ and ϵ, are used. These are related to μ/z and β^2 by Eqs. (9) and (10).

$$\frac{\mu}{z} = \sin \epsilon \qquad \text{(used only if } \frac{\mu}{z} \leqslant 1\text{)} \tag{9}$$

$$2\beta^2 = \sin \psi + \frac{1}{\sin \psi} \qquad \text{(used only if } \beta \geqslant 1\text{)} \tag{10}$$

In Fig. 1, $\mu/z = 4$. For this small value of the reduced relative velocity attractions play an important role. The reduced trajectories in the figures give the motion of a molecule reduced to point size relative to a stationary ion of radius D_{12}. For $\beta > 1$, no hard sphere collisions occur. The trajectory is simply curved inward and consists of two symmetrical portions separated by the point of nearest approach. For $\beta = 1$ orbiting occurs, and the molecule moves around the ion in a circle of radius $r_0 = b_0/\sqrt{2}$. For $\beta < 1$ the trajectories spiral inwards and a hard sphere collision occurs. The trajectory is symmetric about the point of contact.

As the reduced velocity increases and μ/z decreases the trajectories are less curved and hard sphere collisions become more important. Figure 2 corresponds to $\mu/z = 0.9$. In this case some trajectories lead to hard sphere collisions that would not result in inward spiralling. Finally where the velocity is very large, as in Fig. 3, in which $\mu/z = 0.01$, hard sphere collisions play the essential role and curvature of the trajectories is no longer important.

Figure 1

Collision trajectories calculated by Langevin for $\mu/z = 4$. When $\beta = 1$ (i.e., when $b = b_0$) the trajectory closes on itself and orbiting occurs at a radius r_0. The distance of closest approach of the trajectory that passes through A is r_1. The point of closest approach is A. The angle bisected by AD is equal to 2Φ for this trajectory and is therefore the supplement of the scattering angle Θ ($\Theta = \pi - 2\Phi$). Figure from Reference 2.

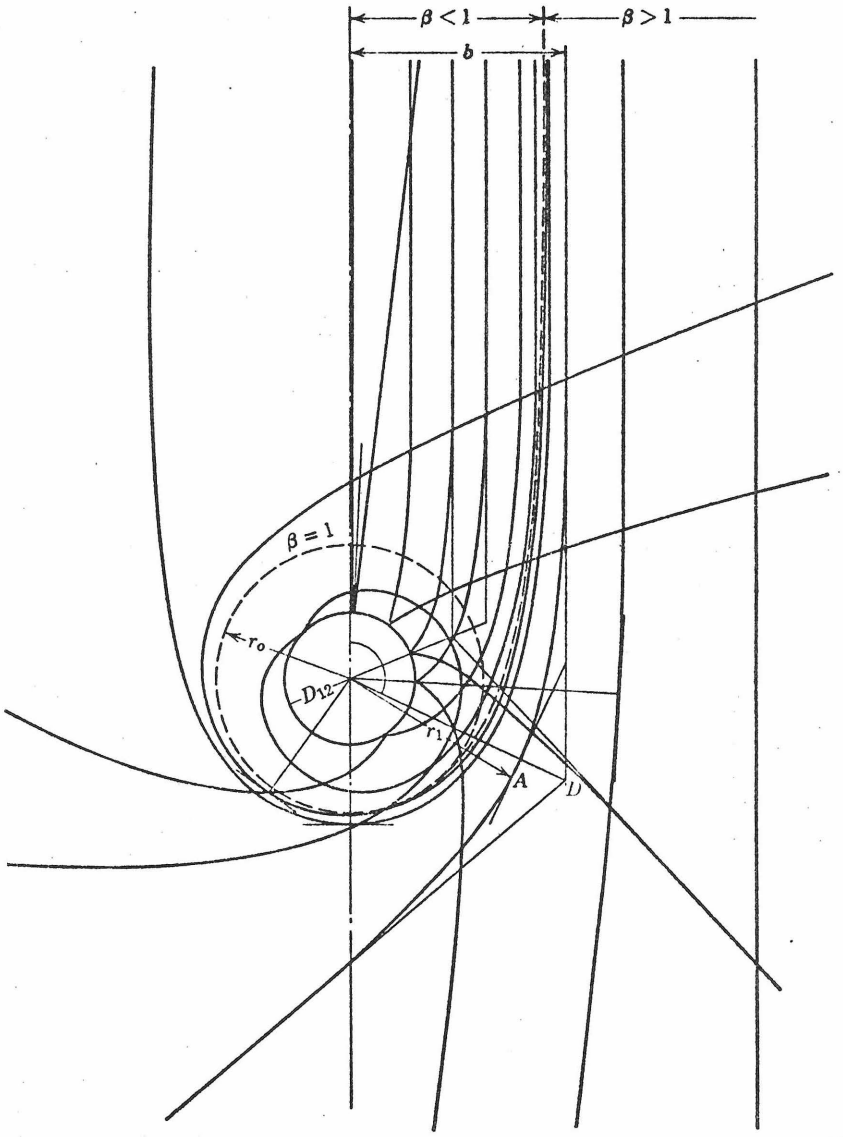
β < 1
β > 1
b
β = 1
r0
D12
r1
A
D

Figure 2

Collision trajectories calculated by Langevin for $\mu/z = 0.9$.
Figure from Reference 2.

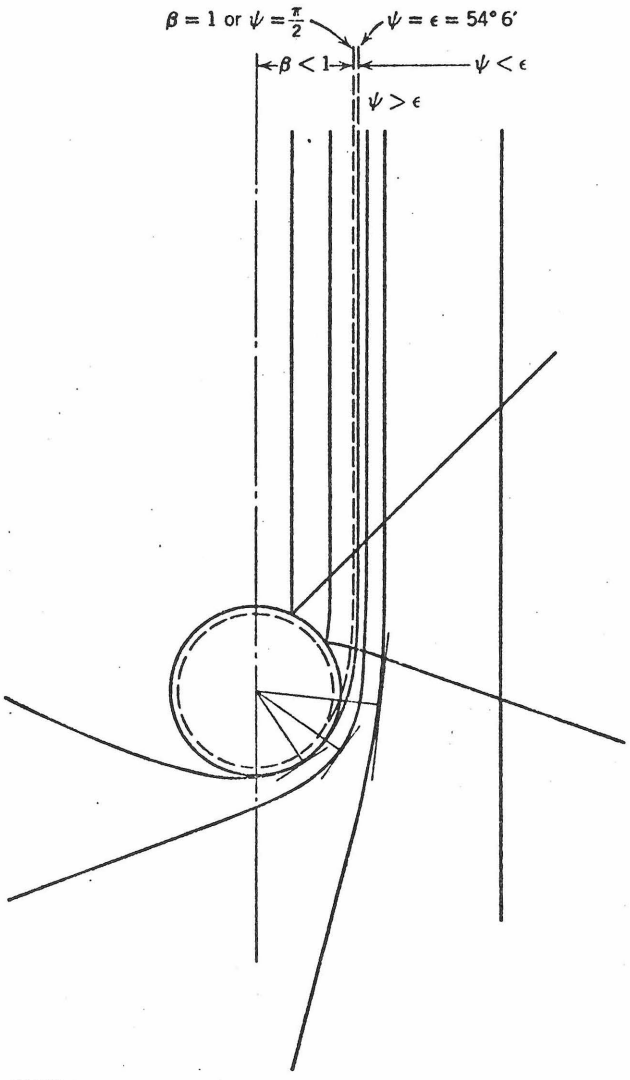
$\beta = 1$ or $\psi = \frac{\pi}{2}$
$\psi = \epsilon = 54° 6'$
$\beta < 1$
$\psi < \epsilon$
$\psi > \epsilon$

Figure 3

Collision trajectories calculated by Langevin for $\mu/z = 0.01$.
Figure from Reference 2.

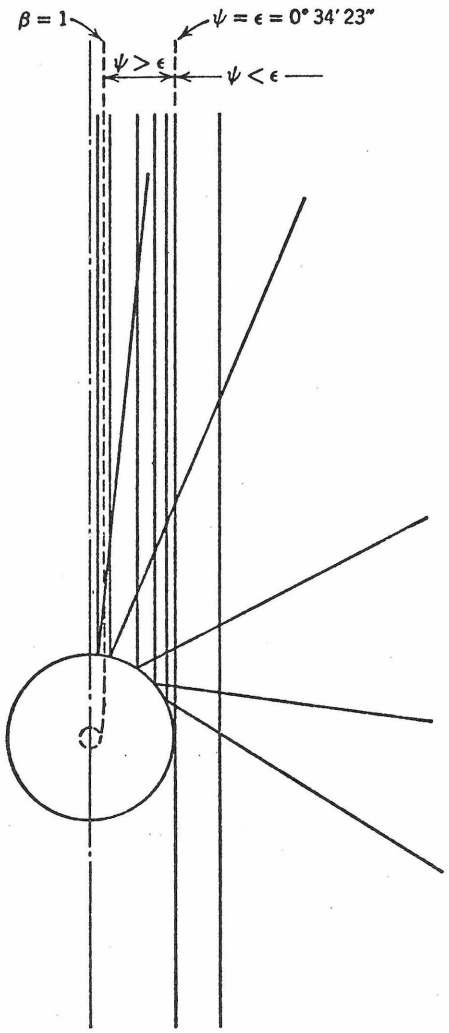
β = 1
ψ = ϵ = 0° 34′ 23″
ψ > ϵ
ψ < ϵ

Langevin evaluates the integral in Eq. (3) by graphical methods. He does it for a number of different values of μ/z and then evaluates the integral in Eq. (2) also by graphical methods. The results of the calculations are illustrated in Fig. 4. The ordinate and the abscissa are given in terms of Y and $1/\mu$, which are defined in Eqs. (11) and (12)

$$Y = \left(\frac{2\,kT}{\alpha\, e^2}\right)^{\frac{1}{2}} \int_0^{\infty} q(v_0)\exp(-z^2)\, z^5\, dz \tag{11}$$

$$\frac{1}{\mu} = \left(\frac{2\,kT}{\alpha\, e^2}\right)^{\frac{1}{2}} D_{12}^2 \tag{12}$$

Substituting from Eqs. (11) and (12) into Eq. (2) gives Eq. (13)

$$k = \frac{1}{n}\ \frac{3}{16Y[4\pi\alpha M_r]^{\frac{1}{2}}} \tag{13}$$

The mobility is thus proportional to 3/16Y. Since $1/\mu$ depends on the ionic radius and the temperature, Fig. 4 shows how the mobility varies with increasing ion size at fixed temperature or with temperature at fixed ion size.

The two limiting cases of this model are of interest. In the case of a large ion where collision trajectories are little effected by the attractive potential, we may obtain $q(v_0)$ from Eqs. (4) and (5) by setting V(r) equal to zero for r greater than D_{12} and infinity for r less than D_{12}. The result is given in Eq. (14). The mobility for this limiting case can now be determined by substituting Eq. (14) into Eqs. (11) and (13). The results of these substitutions are given in Eqs. (15), (16) and (17).

Figure 4

The variation of ion mobility with ion size and temperature. The quantity on the ordinate is proportional to the mobility and the quantity on the abscissa increases with temperature and ion size. Figure from Reference 2.

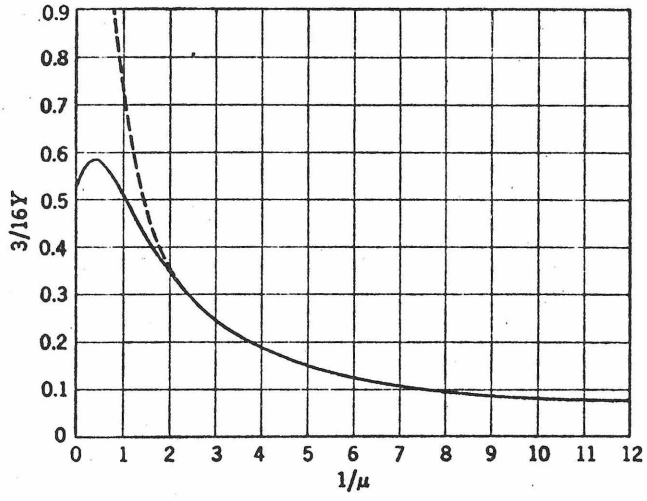
0.9
0.8
0.7
0.6
0.5
0.4
0.3
0.2
0.1
0
3/16Y
0 1 2 3 4 5 6 7 8 9 10 11 12
1/μ

$$q(v_0) = \int_0^\infty \cos^2 \Phi \, b \, db = \frac{D_{12}^2}{4} \tag{14}$$

$$Y = \left(\frac{2kT}{\alpha e^2}\right)^{\frac{1}{2}} \frac{D_{12}^2}{4} \tag{15}$$

$$\frac{3}{16Y} = \frac{3}{4}\left(\frac{\alpha e^2}{2kT}\right)^{\frac{1}{2}} \frac{1}{D_{12}^2} \tag{16}$$

$$K = \frac{1}{n} \frac{3e}{8(\pi kT M_r)^{\frac{1}{2}} D_{12}^2} \tag{17}$$

The broken line in Fig. 4 illustrates the variation of the expression for 3/16Y in Eq. (16) as a function of $1/\mu$. From the definitions given above for z and μ/z it is evident that $1/\mu$ is given by Eq. (18). The broken line thus indicates what the variation of the mobility with

$$\frac{1}{\mu} = \left(\frac{2kT}{\alpha e^2}\right)^{\frac{1}{2}} D_{12}^2 \tag{18}$$

temperature and ion size would be if there were no attractive potential.

The value of K in the limit of very small ions or in the polarization limit is given by taking the value of 3/16Y, at $1/\mu = 0$ from Fig. 4. Hasse[3] repeated Langevin's calculations in 1926, and we use his more accurate value for the intercept. Hasse finds that $3/16Y_p = 0.5105$, and Eq. (13) becomes

$$K = \frac{1}{n} \frac{0.5105}{[4\pi\alpha M_r]^{\frac{1}{2}}} \tag{19}$$

Also available from Langevin's calculations are values of the diffusion cross section defined by Eq. (4) for the two limiting cases. For the high temperature-large ion case we obtain Eq. (20) from Eqs. (14), (3) and (4a)

$$q_d(v_0) = \pi D_{12}^2 \tag{20}$$

In the polarization limit (small D_{12}, low temperatures) Langevin shows that $q(v_0)v$ is a constant independent of v_0. This allows us to rewrite Eq. (11) in the form of Eq. (21). Rearranging Eq. (21), evaluating the integral and making use of the definition of b_0 implied

$$Y_p = \left(\frac{M_r}{\alpha e^2}\right)^{\frac{1}{2}} q(v_0) v_0 \int_0^\infty \exp(-z^2)\, z^4\, dz \tag{21}$$

$$q(v_0) = \left(\frac{4\alpha e^2}{M_r v^2}\right)^{\frac{1}{2}} \frac{4}{3} Y_p = b_0^2 \frac{4}{3\sqrt{\pi}} Y_p \tag{22}$$

by Eq. (8) gives Eq. (22). Substituting the value of Y_p into Eq. (22) and making use of the relationship between $q(v_0)$ and $q_d(v_0)$ given in Eq. (4a) gives Eq. (23).

$$q_d(v_0) = 1.105\, \pi\, b_0^2 \tag{23}$$

It is instructive to consider this cross section as divided into two parts on the basis of whether the impact parameter is greater or less than b_0. The expression for the diffusion cross section given in Eq. (4) then becomes Eq. (24). The scattering angle, Θ, is zero for forward scattering and increases as the change in the direction of the relative

velocity increases. For backward scattering Θ is $\pm \pi$. An examination of Fig. 1 suggests that Θ changes rapidly with impact parameter, b, for b less than b_0, the impact parameter at which orbiting occurs.

$$q_d(v_0) = 2\pi \int_0^{b_0} (1 - \cos \Theta) b \, db + 2\pi \int_{b_0}^{\infty} (1 - \cos \Theta) b \, db \qquad (24)$$

In fact Θ oscillates sufficiently rapidly between π and $-\pi$ for vanishingly small D_{12} (or very low temperatures) that $\cos\Theta$ may be set at its average value, zero, in the first integral in Eq. (24). This gives Eq. (25).

$$q_d(v_0) = \pi b_0^2 + 2\pi \int_{b_0}^{\infty} (1 - \cos\Theta) b \, db \qquad (25)$$

A comparison of Eqs. (25) and (23) indicates that collisions at impact parameters greater than b_0 contribute about 10% of the cross section for momentum transfer. The most important momentum transfer process is the inward spiralling collision. The success of the polarization limit of the Langevin model in predicting experimental mobilities thus depends to a large extent on whether such collisions occur in real physical systems.

The most comprehensive classical calculations done since Langevin's were done by Mason and Schamp[4] in 1958. They did classical calculations based on the potential defined in Eq. (26).

$$\varphi(r) = \frac{\epsilon}{2} \left[(1+\gamma) \left(\frac{r_m}{r}\right)^{12} - 4\gamma \left(\frac{r_m}{r}\right)^{6} - 3(1-\gamma) \left(\frac{r_m}{r}\right)^{4} \right] \qquad (26)$$

The r^{-4} term is the same ion induced dipole potential which appeared in the calculations of Langevin. The r^{-6} term arises from ion-induced quadrupole forces and London dispersion forces. The r^{-12} term represents a close range repulsion. There are three disposable parameters in the potential; ϵ, the well depth; r_m, the position of the potential minimum; and γ, the relative size of the r^{-6} term. The experimentally determined mobility and its temperature dependence provide effectively two conditions leaving one parameter to be determined. This third parameter is fixed by the condition given in Eq. (27).

$$\frac{3}{2}\epsilon(1-\gamma)\left(\frac{r_m}{r}\right)^4 = \frac{\alpha e^2}{2r^4} \tag{27}$$

The coefficient of the r^{-6} term can be estimated quantum mechanically for some systems.[4] This provides an auxiliary weak condition to be used if the fit of the temperature data is not totally unambiguous.

The details of the calculation are complex and not very instructive physically, but the main features of the results are interesting. The effect of the short range repulsive term is illustrated in Fig. 5. The quantity on the ordinate is proportional to the mobility. The parameter T^* is a reduced temperature given by $T^* = kT/\epsilon$. The temperature dependence is shown for three different potentials where n is the exponent of the repulsive term and the only attractive term is the r^{-4} term (i.e., $\gamma = 0$ in Eq. (26)). The results for $n = \infty$ are taken from Hasse[3]; the results for n = 8 from Hasse and Cook[6]; and the results for n = 12 from Mason and Schamp's calculations. The same qualitative

behavior is observed in each case, with the maximum increase of the mobility over the polarization limit strongly dependent on the steepness of the repulsive barrier.

The effect of the r^{-6} term is illustrated in Fig. 6. Here a quantity proportional to the mobility is plotted against T^* for n = 12 and various values of γ. As is evident from Eq. (26), increasing γ increases the relative importance of the r^{-6} term in the model potential. A value of $\gamma = 0$ implies a 12-4 potential with no r^{-6} contribution. A value of $\gamma = 1$ implies a 12-6 potential with no r^{-4} contribution. Addition of the dispersion and charge-induced quadrupole attraction has an effect similar to increasing the steepness of the repulsive wall. The height of the maximum above the polarization limit decreases with increasing γ. High values of γ introduce a minimum in K at low temperatures and thus have the rather surprising effect of permitting the mobility to fall below the low temperature polarization limit. All the curves approach the same high temperature mobility.

Quantum Mechanical Calculations

Quantum calculations of ionic mobilities have been done by Dalgarno, McDowell and Williams.[7] They begin with the quantum mechanical definition of the diffusion cross section,

$$q_d(v_o) = \frac{4\pi}{k^2} \sum_{\ell=0}^{\infty} (\ell+1) \sin^2(\eta_\ell - \eta_{\ell+1}) \quad . \tag{28}$$

Figure 5

Dependence of mobility on T^* for various values of the exponent of the repulsive term in a potential of the form $Ar^{-n} - \alpha e^2/2r^4$. T^* is kT/ϵ where ϵ is the well depth. The quantity on the ordinate is proportional to the mobility. Figure from Reference 4.

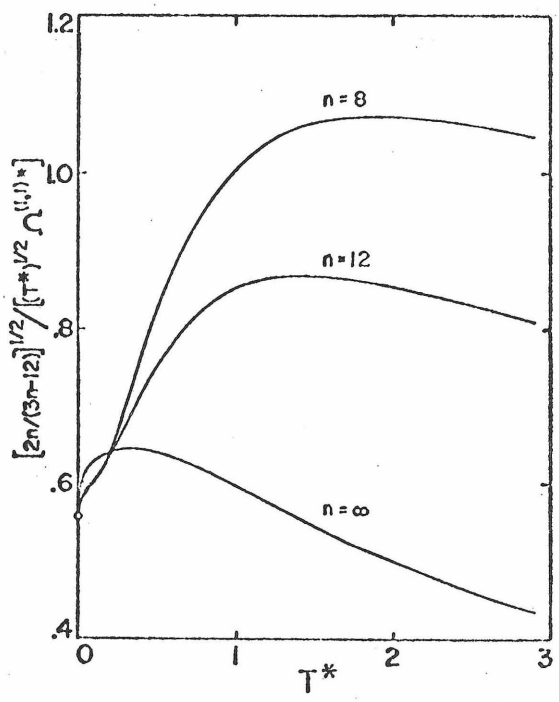
1.2
1.0
.8
.6
.4
0
1
2
3
T*
n = 8
n = 12
n = ∞
[2n/(3n-12)]^1/2/[T*^1/2 Ω^(1,1)*]

Figure 6

Dependence of mobility on γ, the coefficient of the r^{-6} term in 12-6-4 potential. The quantity on the ordinate is proportional to the mobility. Figure from Reference 4.

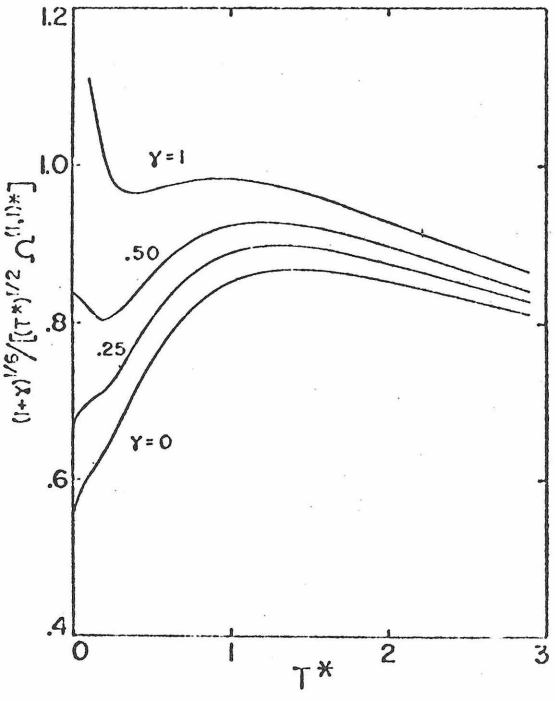
1.2
1.0
.8
.6
.4
0
1
2
3
T*
γ = 1
.50
.25
γ = 0
$(1+\gamma)^{1/6}/[(T^*)^{1/2}\,\Omega^{(1,1)*}]$

Where $k = M_r v_0/\hbar$ is the wave number of the relative motion. The ℓth order phase shift, η_ℓ, is defined by the condition that the regular solution of the radial equation

$$g_\ell''(r) + k^2 \left(\frac{2M_r V(r)}{\hbar^2} - \frac{\ell(\ell+1)}{r^2} \right) g_\ell(r) = 0 \tag{29}$$

behaves asymptotically as

$$g_\ell(r) \sim \frac{1}{k} \sin(kr - \tfrac{1}{2}\ell\pi + \eta_\ell) \tag{30}$$

Three approximate methods are used to calculate the phase shifts: Jeffrey's (WKBJ) approximation; the Massey-Mohr approximation; and the Born approximation.[8] The Jeffrey's approximation assumed that V(r) is a slowly varying function of r. The Massey-Mohr approximation is a modification of Jeffrey's approximation good for large ℓ. The Born approximation assumes that the scattering distorts the incoming only a small amount, i.e., the phase shifts are small. Expressions for η_ℓ in the three approximations are given in Eqs. (31) to (33).

Jeffrey's

$$\eta_\ell = \int_{r_0}^{\infty} \left\{ k^2 - \frac{2\mu V}{\hbar^2} - \frac{(\ell+\frac{1}{2})^2}{r^2} \right\}^{\frac{1}{2}} dr - \int_{r_0^1}^{\infty} \left\{ k^2 \frac{(\ell+\frac{1}{2})^2}{r^2} \right\}^{\frac{1}{2}} dr \tag{31}$$

Lower limits are outermost zeroes of the integrands.

Massey-Mohr

$$\eta_\ell = \int_{r_0^1}^{\infty} \frac{V(r)}{\left\{ k^2 - \frac{(\ell+\frac{1}{2})^2}{r^2} \right\}^{\frac{1}{2}}} dr \tag{32}$$

Born $$\eta_\ell = -\frac{\pi k^2}{M_r v_0^2} \int_0^\infty r\, V(r) \left[J_{\ell+\frac{1}{2}}(kr)\right]^2 dr \qquad (33)$$

$J_{\ell+\frac{1}{2}}$ is the $(\ell+\frac{1}{2})$th or Bessel function of the first kind.

Dalgarno et al. show that for large ℓ for a potential of the form Cr^{-n} the three approximations approach the same value. Table I shows some calculated phase shifts for the r^{-4} polarization potential between Li^+ and He and between Li^+ and Xe. The value of k has been chosen such that $ka_0 = 1$ where a_0 is the Bohr radius.

In the case of the Jeffrey approximation when ℓ is large η_ℓ can be considered a continuous function of ℓ, and the difference in phase shifts can be written

$$\beta(\ell) = \eta(\ell+1) = -\partial\eta/\partial\ell \qquad (34)$$

or, setting $p = (\ell + \frac{1}{2})/k$

$$\beta(p) = 1/k\ \partial\eta/\partial p \ . \qquad (35)$$

It can be shown by substituting Eq. (31) into Eq. (35) that $\beta = \Phi - \frac{1}{2}\pi$, so that if the summation in Eq. (28) is replaced by an integration over p it becomes identical to the classical formula

$$q_d(v_0) = 4\pi \int_0^\infty \cos^2\Phi\ b\ db \qquad (36)$$

where Φ is defined by Eq. (5).

Table I. Phase Shifts for Thermal Energy Ion-Neutral Scattering Calculated Using Three Different Approximate Techniques[a]

	Li^+ in He				Li^+ in Xe		
ℓ	Jeffreys	Massey-Mohr	Born	ℓ	Jeffreys	Massey-Mohr	Born
13	1.335	1.026	1.032	43	1.708	1.549	1.605
16	0.617	0.562	0.564	48	1.187	1.118	1.153
19	0.355	0.341	0.342	53	0.867	0.833	0.858
22	0.226	0.222	0.222	58	0.655	0.637	0.654
25	0.154	0.152	0.152	63	0.508	0.498	0.510
28	0.109	0.109	0.109	68	0.403	0.397	0.405

[a]Taken from Reference 7.

Since the r^{-4} polarization potential is long range at thermal energies, it is large values of ℓ that contribute to the cross section. Thus the physical significance of the results of Dalgarno et al., is that quantum effects are not important in determining ionic mobilities when elastic collisions are the principle mechanism of momentum transfer. They calculate a value of the diffusion cross section for the pure r^{-4} potential using the Massey Mohr approximation. They point out that because of the equivalence of Jeffrey's approximation and the classical description for large ℓ, their result, $1.06\,\pi b_0^2$, is less accurate than the classical result, $1.105\,\pi b_0^2$. They conclude that only in a very favorable case such as the case of protons in helium below 20 °K would quantum effects be observable.

Dalgarno, McDowell and Williams[7] compare experimental results with the classical polarization limit for a number of systems. The reduced mobility is given by

$$K_0 = K \frac{P}{760} \frac{273}{T} \tag{37}$$

where P and T are the pressure in torr and the temperature at which K is measured. K_0 is the density dependent mobility reduced to its value at a density of 2.69×10^{19} molecules cm^{-3}, the density of an ideal gas at 273 °K and 760 torr. Since classical theory predicts that the mobility is inversely proportional to the square root of the reduced mass, Dalgarno et al., report a quantity

$$K' = K_0 \sqrt{M_r} \tag{38}$$

where M_r is in atomic mass units. The polarization limit for K′ (from Eqs. (19), (37) and (38)) is

$$K = \frac{5.31}{\sqrt{\alpha}} \tag{39}$$

where α is in A^3. Table II reports the experimental results and presents $5.31/\sqrt{\alpha}$ for comparison. The fact that the results for A, Kr and Xe are mass independent but different from the polarization limit, leads Dalgarno et al. to postulate a systematic error in the experimental results. They report a value of $5.68/\sqrt{\alpha}$ to show how such a systematic error would effect the results.

Mason and Schamp show that the discrepancy between the polarization limit and the observed mobilities can be more reliably accounted for by including the shorter range r^{-6} and r^{-12} terms in the interaction potential. Table III presents their results for the systems for which temperature dependence data are available. The agreement is indeed impressive.

Thus we see that gas phase ionic mobilities of alkali metal ions in rare gases are quite adequately explained for low field where elastic collisions are the principle method of momentum transfer by a classical treatment based on a three term ion-neutral interaction potential.

The theoretical studies reviewed indicate that the mobilities of gaseous ions are primarily determined by the long range attractive forces between the ions and the neutral molecules of the gas. The shorter range attractive and repulsive forces play a discernible but less

Table II. Comparison of Experimental Mobilities with Mobilities Calculated from the Langevin Model[a]

ion \ gas	He	Ne	A	Kr	Xc[c]
Li	38.6	30.4	11.4	9.4	7.3
	- -	25.2	- -	- -	- -
Na	41.9	26.8	11.5	9.3	7.5
K	41.0	27.4	11.7	9.6	7.4
Rb	39.3	27.2	11.7	9.5	7.4
Cs	36.3	25.5	11.5	9.5	7.4
A	39.9	- -	- -	- -	7.7
In	40.5	27.5	10.9	- -	- -
Tl	37.6	26.7	11.1	- -	- -
Hg	26.5	- -	- -	- -	- -
	37.0	- -	- -	- -	- -
$5.31/\sqrt{\alpha}$ [b]	30.5	21.9	10.8	8.9	6.9
$5.68/\sqrt{\alpha}$ [b]	32.8	23.5	11.6	9.6	7.4

[a]The number reported is K′ which is related to K_0, the mobility at 2.69×10^{19} molecule cm^{-3}, by Eq. (38). Where two values are listed they are results of two different measurements by different workers. Data from Reference 7.

[b]Theoretical values calculated from Eq. (39). The Langevin model predicts that all the K′ values in a given column will be equal to the value of $5.31/\sqrt{\alpha}$ given at the bottom of the column.

[c]See text for explanation of the last row of numbers.

Table III. Comparison of Experimental Mobilities with Mobilities Calculated from the 12-6-4 Potential of Mason and Schamp[a]

T°K	Li^+ - He		Na^+ - He		Cs^+ - He	
	Obs	Calc	Obs	Calc	Obs	Calc
0		20.0		17.2		16.2
20.5	20.0	20.6				
78	21.8	21.8				
79					17.5	17.6
90	22.2	22.0				
92			18.5	18.8	18.0	17.9
195	23.9	24.2	20.9	21.0	19.2	19.2
290			22.8	22.7	18.9	18.9
291	25.8	26.2				
380	27.8	27.7				
392					18.1	18.1
405			24.0	23.0		
477			24.6	24.3		
483	29.2	28.7				
492					17.4	17.4

(Continued)

Table III (Continued)

T°K	K^+ - Ar		Rb^+ - Kr		Cs^+ - Xe	
	Obs	Calc	Obs	Calc	Obs	Calc
0		2.60		1.45		0.91
78	1.30					
90	1.52		1.15	1.51		
195	2.34	2.77	1.57	1.55	1.02	0.98
273			1.575	1.569	1.005	0.994
291	2.81	2.82	1.58	1.58	1.01	1.00
370			1.59	1.62	1.01	1.03
400	3.08	2.92				
450					1.03	1.06
455			1.64	1.66		
460	2.95	2.98				

[a]The number reported is the mobility measured reduced to its value at a standard density. The mobility is in cm^2 $volts^{-1}$. Data from Reference 4.

conspicuous role. Because of the long range nature of the forces, quantum effects are probably not important for the cases examined. The theoretical calculations done so far are only applicable in a strict sense when the ions and neutral molecules have spherical symmetry, but the detailed study of Mason and Schamp in particular seems to provide a very accurate description of these systems. Attempts to apply such a description to the mobilities of polyatomic, non-spherical ions in gases consisting of polyatomic, non-spherical molecules could prove interesting and instructive. The result of such an attempt could be information about how structure effects ion-neutral collision dynamics and perhaps even information about the structure of gaseous ions. If sufficient data are obtained, better descriptions of ion-molecule collision processes may suggest themselves. Such descriptions would be very useful in understanding the kinetics of ion molecule reactions. In addition, the data itself would be useful in helping to develop the growing technology of the manipulation of gas phase ions.

The study described in the following chapter is designed to provide accurate mobilities of polyatomic ions in polyatomic gases to serve as the basis for a discussion of collision processes in such systems. The study is also designed to develop a relatively new technique for measuring mobilities at low pressures.

References

1. For discussion of early work see L. B. Loeb, "Basic Processes of Gaseous Electronics," University of California Press, 1961.
2. P. Langevin, Annales de chimie et de physique, Series 8, 5, 245 (1905). See translation in E. W. McDaniel, "Collision Phenomena in Ionized Gases," John Wiley and Sons, New York, 1964.
3. H. R. Hasse, Phil. Mag. Ser. 7, 1, 139 (1926).
4. E. A. Mason and H. W. Schamp, Jr., Ann. Phys., 4, 233 (1958).
5. H. Margenau, Philosophy of Science, 8, 603 (1941).
6. H. R. Hasse and W. R. Cook, Phil. Mag., Ser. 7, 12, 554 (1931).
7. A. Dalgarno, M. R. C. McDowell, and A. Williams, Phil. Trans. Roy. Soc., A-250, 411 (1958).
8. E. H. S. Burhop, "Quantum Theory of Collisions," in Quantum Theory I, D. R. Bates, ed., Academic Press, 1961.
9. J. L. Beauchamp, J. Chem. Phys., 46, 1231 (1967).
10. J. O. Hirschfelder, C. F. Curtiss, and R. B. Bird, Molecular Theory of Gases and Liquids, John Wiley and Sons, (1951).
11. D. L. Albritton, T. M. Miller, D. W. Martin, and E. W. McDaniel, Phys. Rev., 171, 94 (1968).
12. T. Terao and P. A. Back, J. Phys. Chem., 73, 3884 (1969).

CHAPTER 2

The Interactions of Ions with Nonpolar Neutrals: The Collision Broadening of Cyclotron Resonance Lines of Ions in Hydrogen and Methane

Introduction

Ion cyclotron resonance studies of ion-molecule reactions are normally accomplished in the pressure range between 10^{-7} and 10^{-5} torr.[1-3] In the usual experimental arrangement, the ions generated by electron impact are drifted through the cell by the action of crossed electric and magnetic fields (Fig. 1), with the drift velocity being given by

$$v_d = \frac{cE}{H} \quad . \tag{1}$$

With the typical values E = 0.5 V/cm and H = 7.5 kG, the drift velocity is 6.7×10^3 cm/sec, corresponding to an ion transit time through the resonance region of $\tau = 10^{-3}$ sec. In an ion-molecule reaction, considerable conversion of reactant to product occurs when the quantity $nk\tau$ approaches unity, where n is the number density of the neutral species and k represents the bimolecular reaction rate constant.[4] Ion molecule reaction rate constants are typically 10^{-9} cm^3 molecule^{-1} sec^{-1}.[4] Consequently $nk\tau$ approaches unity at a particle density of $\sim 10^{12}$ molecules cm^{-3}, corresponding to a pressure of $\sim 3 \times 10^{-5}$ torr. Below this pressure, ion cyclotron resonance lineshapes are not significantly collision broadened, since the ion suffers at most one collision as it passes through the cell. At higher pressures, appreciable collision broadening of the absorption peak occurs with a concomitant

Figure 1

Cutaway view of cyclotron resonance cell. The magnetic field is collinear with the electron beam.

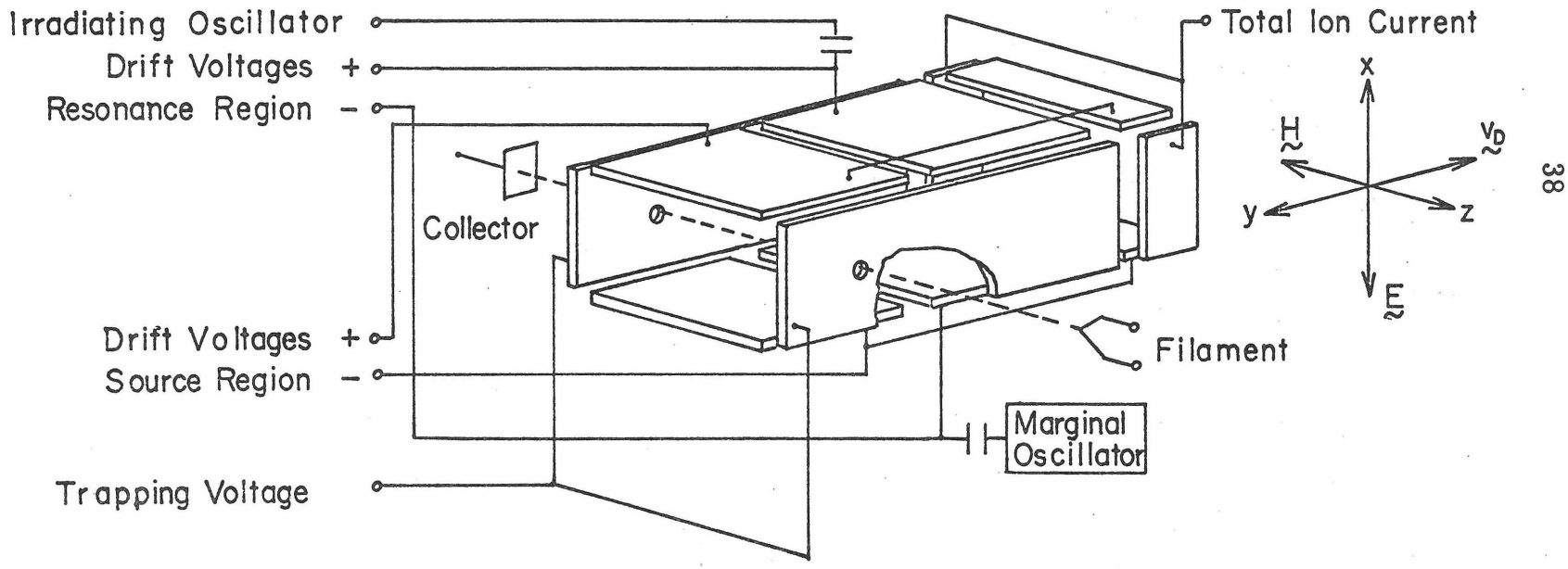
Irradiating Oscillator
Drift Voltages +
Resonance Region −
Collector
Drift Voltages +
Source Region −
Trapping Voltage
Total Ion Current
Filament
Marginal Oscillator
x
H
v_D
y
z
E

FIG. 1.

decrease in resolution. In the case of methane, these various factors are illustrated in Fig. 2. CH_5^+, evident at m/e 17 in Fig. 2, is produced in the well-known reaction

$$CH_4^+ + CH_4 \rightarrow CH_5^+ + CH_3 \qquad (2)$$

which proceeds with a biomolecular rate constant $k = 1.1 \pm 0.1 \times 10^{-9}$ cm^3 $molecule^{-1}$ sec^{-1} at thermal ion energies.[1,4] The reactant has totally disappeared and the product ion peak is significantly broadened at 5.32×10^{-4} torr. At 1.80×10^{-3} torr, the line broadening has increased to the extent that resolution of adjacent mass peaks would be impeded.

While the loss of resolution limits the usefulness of ion cyclotron resonance spectroscopy for the study of ion-molecule reactions, an analysis of the collisional broadening phenomenon can provide important information about non-reactive collision processes. This is in general supported by the experimental results of Wobschall and co-workers.[5] The present study is an examination of the collision broadening of the cyclotron resonance absorptions of ions in methane and hydrogen.

Both methane and hydrogen are extensively utilized as chemical ionization reagents in high pressure mass spectrometric studies. Minor constituents present in methane and hydrogen are ionized by reaction with CH_5^+ and $C_2H_5^+$ in methane and H_3^+ in hydrogen. Using chemical ionization reactions it is possible to generate a wide variety of ionic species in methane and hydrogen for the study of collisional broadening processes. Such studies yield collision frequencies for

Figure 2

Methane spectrum at 14 eV and various pressures. The resonances at 3200 and 3400 gauss correspond to CH_4^+ and CH_5^+, respectively. The points marked on the spectra indicate a fitted Lorentzian line.

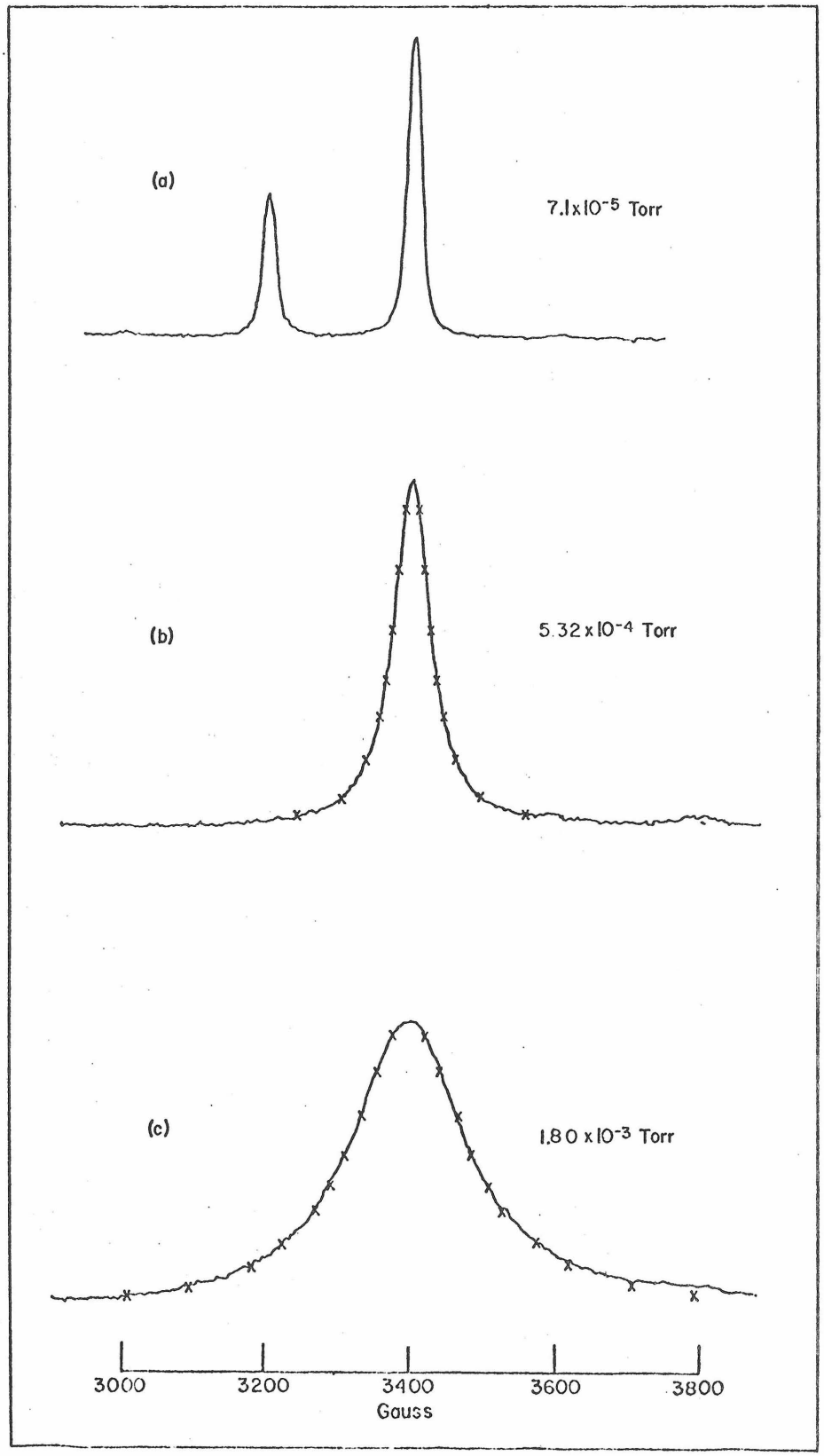
(a)
7.1x10⁻⁵ Torr
(b)
5.32x10⁻⁴ Torr
(c)
1.80x10⁻³ Torr
3000
3200
3400
3600
3800
Gauss

momentum transfer, diffusion cross sections and ion mobilities. These data can then be used to test simple models for the calculation of the corresponding quantities. The information obtained is useful in providing a more complete description of ion motion in chemical ionization experiments, particularly in regard to the important questions of ion source residence times, collision frequencies, and the establishment of thermal equilibrium.

Hydrogen has been widely utilized as a collision gas for ion mobility studies. Using drift tube techniques in conjunction with mass spectrometric analysis, McDaniel[6] and co-workers have recently reported the mobility of H_3^+ in hydrogen. They obtain a value of 11.1 ± 0.6 $cm^2V^{-1}sec^{-1}$ in the limit of low E/P (ratio of electric field strength to pressure). Wobschall[5] subjected the hydrogen system to scrutiny with cyclotron resonance techniques, reporting a value of 7.0 $cm^2V^{-1}sec^{-1}$ for the mobility of H_3^+ in hydrogen, considerably below the value obtained in drift tube measurements. To provide confidence in cyclotron resonance techniques for ion mobility measurements, it is essential that this discrepancy be resolved, particularly since both studies have provided for positive mass identification of the species under investigation.

Patterson has measured the mobility of SF_5^- and SF_6^- in methane[7] at low E/P. The only other study of the mobilities of ions in methane which provided for mass identification of the charge carriers is that of Meisels and co-workers.[8] The apparatus used in this study was designed for chemical ionization studies and only relative drift velocities could be determined with any accuracy.

Experimental

Ion cyclotron resonance spectra were recorded in the absorption mode by modulating the electron energy[9] and feeding the output of the marginal oscillator into a Princeton Applied Research Model HR-8 phase sensitive detector referenced to the modulation frequency (32 cps). Typical spectra are shown in Fig. 2. Linewidths measured from absorption spectra were compared with linewidths from derivative spectra obtained by field modulation. As required for a Lorentzian lineshape the spacing of the maximum and minimum of the derivative spectrum is given by $2\xi/\sqrt{3}$. This yielded collision frequencies identical to those measured from absorption linewidths. Electron energy modulation proved to be more sensitive in the present application because of the limited amplitude of field modulation which could be generated for detecting wide lines. All spectra were recorded by sweeping the magnetic field strength at constant observing frequency.

An MKS Instruments model 90H1E capacitance manometer was employed to determine pressure. The capacitance manometer was calibrated against a Bendix GM-100A McLeod gauge. Both gauges were connected to a test vacuum manifold. Helium gas was used to minimize mercury pumping error.[10] The gas was admitted to the system and the pressure read on both gauges. A portion of the system was sealed off and the remainder evacuated. The gas in the sealed off portion was then expanded into the entire manifold and the resulting pressure again read on both gauges. This procedure was repeated until

the pressure could no longer be read on the McLeod gauge. In Fig. 3 the capacitance manometer readings are plotted against the McLeod gauge readings. The capacitance manometer was operated at 65°C to minimize zero drift so it was necessary to correct the lower pressure readings for thermal transpiration.[10] The capacitance manometer is observed to be linear throughout the range of the calibration. The factory calibration agreed with the McLeod gauge calibration to within less than 1%. Immediately following the calibration the capacitance manometer was removed from the test stand and connected to the ion cyclotron resonance spectrometer and the collision frequency of CH_5^+ in CH_4 measured as described in the Results below. At the time of the calibration the thermal transpiration correction was checked. The gauge was allowed to cool to room temperature and equilibrate overnight. The next day the CH_5^+ collision frequency was measured again. The ratio of the two measured collision frequencies was 1.066 in good agreement with the theoretical thermal transpiration correction, (338/297) = 1.068.[11] The value obtained for the CH_5^+ collision frequency was used as a pressure standard for subsequent collision frequency measurements. At the time of the measurement of other collision frequencies, the CH_5^+ collision frequency was also measured. The measured collision frequency was then multiplied by the ratio of the CH_5^+ collision frequency measured at the time of the calibration to the CH_5^+ collision frequency measured at the time of the subsequent experiment. This was found to produce consistent results when collision frequency measurements were repeated. The measured CH_5^+ collision

Figure 3

Comparison of capacitance manometer readings with the McLeod gauge readings of helium pressure.

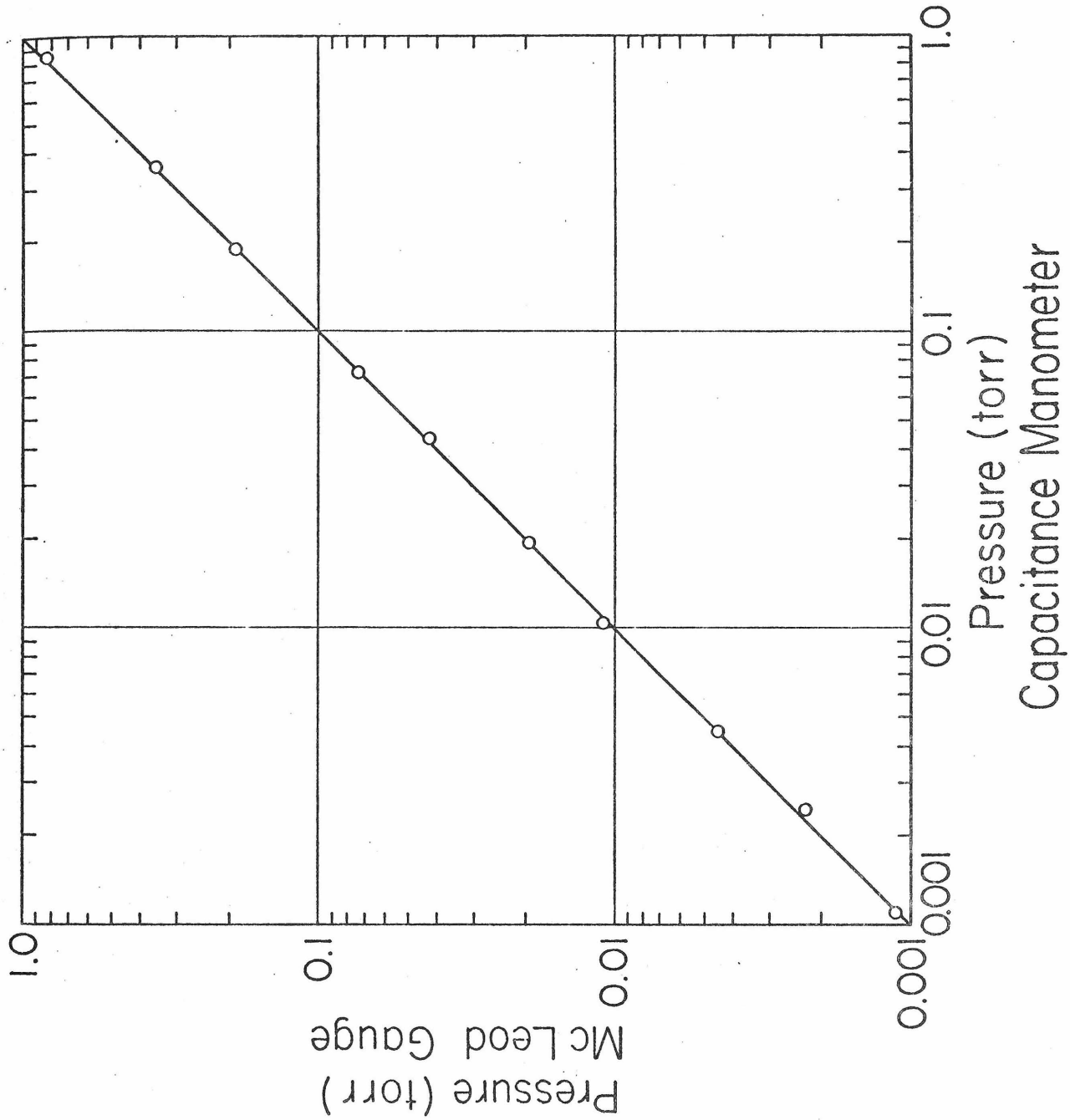
Pressure (torr)
Mc Leod Gauge
1.0
0.1
0.01
0.001
Pressure (torr)
Capacitance Manometer
1.0
0.1
0.01
0.001

frequency in general differed with the standard value by less than 5%. The change in the gauge calibration seemed to depend on whether the controller had been turned off for a period of time or disconnected for use on another experiment.

The spectra from which linewidths were measured were obtained in the following way. The high vacuum pump was valved off from the rest vacuum system and the leak valve was opened and gas admitted. The leak valve was closed and the spectrum taken. After the spectrum was taken, the valve between the pump and the system was opened and the system evacuated. The output of the capacitance manometer was monitored on a recorder during the entire procedure. The measured initial rise in pressure when the gas was admitted was compared with the fall in pressure when the gas was pumped away. The agreement was generally very good. There was no evidence of impurities appearing as a result of pyrolysis of hydrogen, methane or additive gases on the filament. The time that the system was closed off was kept at 3 to 5 minutes to avoid complications from any such pyrolitic processes. Outgassing of the system on this time scale was well below 10^{-6} torr.

Na^+ ions were produced by heating a mineral containing the alkali metal. The mineral was prepared following the description of Blewett and Jones[12] and melted in a platinum crucible. A piece of 5 mil platinum filament was dipped into the melt so that a bead formed on the filament. The filament was mounted on the cell so that the bead went through a hole in the trapping plate in the source region of the cell (Fig. 1). The bead was

just inside the cell wall. The bead was heated by passing a current through the wire. Ions left the surface of the bead and passed through the cell in the same way that ions formed by electron impact would. A current of 1.0 amp or less through the platinum filament was normally sufficient to produce a current at the ion collector of 10^{-11} to 10^{-10} amps. The ion current was modulated by applying a 30 cps square wave to the trapping plate adjacent to the bead ion source. The cyclotron resonance of the ions was thus observed in the absorption mode (rather than the derivative mode). In general more than one kind of ion was observed to be emitted from the sources used. An attempt was made to produce a lithium ion source by melting a mixture of Li_2O, Al_2O_3, and SiO_2 as described above. Some lithium ions were observed, but the major peak was sodium. Potassium ions also appeared. The sodium and potassium were probably present as impurities in the Li_2O used and were preferentially emitted because of their lower ionization potentials. Running the source at high emission current (1 μamp) for several hours in an evacuated glass test chamber increased the relative importance of lithium ion emission and decreased the total emission current at a given filament current. The operating temperatures of the filaments were determined to be on the order of 1000 °K with an optical pyrometer.

The experiments involving the use of the Na^+ source were performed on an ion cyclotron resonance spectrometer constructed as part of the present studies. The major components were identical in design with the commercial spectrometer built by Varian. The trapping and drift voltages were supplied by emitter follower amplifiers.

A schematic of these control circuits is given in Fig. 4. The cell was provided by Varian. The marginal oscillator was constructed by the technical staff of the California Institute of Technology chemistry department using a Varian design. The vacuum system was constructed from commercial components by the technical staff also. The vacuum system is mounted on a cart so that the experiment can be rolled in and out of the magnet gap. The magnet used was a Magnion 12 inch nmr magnet with a hall probe field control and cylindrical pole caps. A PAR Model 122 Lock-in Amplifier was used to detect the signal.

All gases employed were obtained from Matheson and had a stated purity of greater than 99%. Gas mixtures were prepared manometrically, with freeze pump thaw cycles used to degas additives to methane and hydrogen prior to mixing. Single resonance spectra indicated gases used were of stated purity.

Figure 4

Emitter follower circuit used to provide voltages to cell plates. This circuit is repeated three times to provide positive voltage for trapping plates and drift plates. It is repeated three times with modifications to provide negative voltages for drift plates and trapping voltages. The modifications are replacing the NPN transistor (40327) with a PNP transistor (2N4036) and applying -15 V rather than +15 V to the common of the transistor. Switches are provided to reverse the leads to positive and negative drift plates (reversing the direction of the drift fields) and for selecting positive or negative trapping voltages. A switch is provided so that one of the trapping plates can be connected to a square wave modulation signal from the phase sensitive detector.

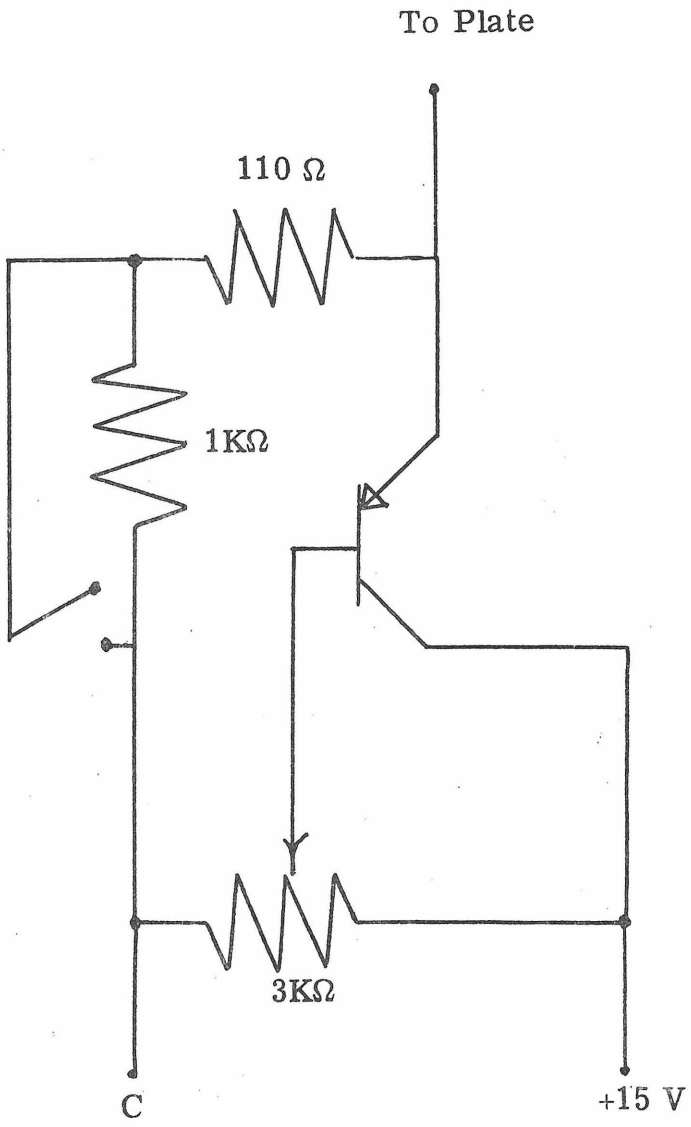

Switch open: 0-10 V

Switch closed: 0-1 V

Analysis of Spectra

The effect of elastic collisions on ion motion can be described as indicated in Eq. (3), by adding to the Lorentz force a term which represents the damping of the ion velocity.[13]

$$\frac{d\underline{v}}{dt} = \frac{e\,\underline{E}(t)}{m} + \frac{e\underline{v}x\underline{H}}{mc} - \xi\underline{v} \tag{3}$$

In Eq. (3) v is the ion velocity, e is the charge on the ion, E(t) is the electric field, m is the mass of ion, H is the magnetic field, and c is the speed of light in a vacuum. If the ion experiences only elastic collisions with the neutral species, the collision frequency for momentum transfer, ξ, is given by[13]

$$\xi = \langle \sigma_d(v_0) v_0 \rangle \; nM/(m+M) \tag{4}$$

where n and M are the number density and mass of the neutral, and $\sigma_d(v_0)$ and v_0 are the diffusion cross section and relative velocity of the ion-neutral pair. The brackets indicate an average over the distribution of relative velocities.

With the observing radio-frequency electric field expressed by

$$\underline{E}(t) = E_1 \sin \omega t \quad , \tag{5}$$

the power absorption calculated from the solution of Eq. (3) has the Lorentzian form

$$A(\omega_c) = \frac{I(0)\tau e^2 E_1^2}{4m} \frac{\xi}{(\omega - \omega_c)^2 + \xi^2} \qquad (6)$$

where $\omega_c = cH/mc$ is the cyclotron frequency of the ion, I(0) is the rate of ion formation at the electron beam and τ is the time the ion spends in the resonance region of the cyclotron resonance cell. The half width at half height for the power absorption expression (6) is equal to ξ. The reduced collision frequency for momentum transfer, ξ/n, can thus be obtained directly from the slope of the variation of linewidth with pressure. Other detailed treatments of power absorption in cyclotron resonance experiments have attempted to include the effect of reactive collisions and the finite lifetime of the ions in the apparatus.[14] Such factors are important when examining reactive ions or working in the low pressure region ($10^{-5} - 10^{-4}$ torr). We have for this reason purposefully selected ionic species for study which are nonreactive toward methane and hydrogen.

The solution of Eq. (3) involves the assumption that the collision frequency ξ is effectively independent of the velocity, v, over the range of velocities sampled as the ion absorbs power from the observing field. An equation of motion for the energy of the average ion, subject to the same limitations of Eq. (3), can be developed and solved with suitable approximations to give (at resonance)[13]

$$E_{ion} = 3/2\ kT + \frac{e^2 E_1^2 (m + M)}{8\xi^2 m^2} \qquad (7)$$

where T is the temperature of the neutral species. Since ξ increases with the neutral number density [Eq. (4)], Eq. (7) indicates that the excess kinetic energy of the ion resulting from its interaction with the observing field is proportional to E_1/P, the ratio of the amplitude of the observing field to the pressure of the neutral. The analysis leading to Eq. (6) can thus be assumed to be valid over the range of E_1/P for which the ratio of linewidth to pressure is found to be independent of E_1/P.

The ratio of field strength to pressure is a parameter frequently used to characterize the results of D.C. drift tube mobility measurements. As pointed out in Appendix I of this chapter, the ion cyclotron resonance experiment can be considered a D.C. mobility experiment in a rotating frame with a D.C. field equal to $E_1/2$. For this reason, the values of E_1/P reported below should be divided by two before comparisons are made with drift tube mobility results.

The pressure range over which experimental data can be meaningfully obtained and analyzed with Eq. (6) is limited at higher pressures by the transverse diffusion of ions which occurs as a peculiar and previously unrecognized feature of the cell geometry illustrated in Fig. 1. In addition to the observing radio frequency electric field, ions in the cell are acted upon by a constant electric field in the -x direction (Fig. 1) which gives rise to the drift motion described by Eq. (1). Equation (1) is obtained from a solution of Eq. (3) for the motion in absence of collisions ($\xi = 0$). It is necessary to consider what effect collisions might have on the drift motion. Since the equation of motion

which includes the effect of collisions [Eq. (3)] is linear in both ion velocity and electric field, it can be solved separately for the drift and radio frequency electric fields and the resulting solutions superimposed to give a complete description of the motion. The time averaged solution to the equation involving the drift field yields[15]

$$\langle v_x \rangle = - \frac{\xi e E}{m(\omega_c^2 + \xi^2)} \tag{8}$$

$$\langle v_y \rangle = - \frac{\omega_c e E}{m(\omega_c^2 + \xi^2)} \tag{9}$$

In the limit of no collisions $\langle v_x \rangle$ is zero and $\langle v_y \rangle$ yields the drift velocity expressed by Eq. (1). Collisions thus give rise to a drift velocity transverse to the usual direction of ion motion through the cell. From simple geometric considerations this motion can result in the collision of ions with the drift electrodes before the ions leave the resonance region. This condition develops when the ratio $\langle v_x \rangle / \langle v_y \rangle$ is greater than half the cell height divided by the distance from the electron beam to the end of the resonance region. This occurs in our apparatus when the ratio $\langle v_x \rangle / \langle v_y \rangle$ is greater than 0.0714. In order to avoid the complicating effects of this ion loss mechanism we have confined the measurements discussed in the following section to pressures such that

$$\langle v_x \rangle / \langle v_y \rangle = \xi / \omega_c < 0.0714. \tag{10}$$

Results

Ions in Methane

As illustrated in Fig. 2, the observed lineshapes of the cyclotron resonance power absorption of CH_5^+ ions in methane fit the Lorentzian description well. The variation with pressure of the linewidth of CH_5^+ in methane is illustrated in Fig. 5. The linewidth is expressed both as the full width at half height in gauss and as the half width at half height, ξ, in sec^{-1}. The reduced collision frequency for CH_5^+ in methane, obtained from a least squares analysis of the data above 5×10^{-4} torr in Fig. 5, is $\xi/n = 9.06 \pm 0.06 \times 10^{-10}$ cm^3 $molecule^{-1}$ sec^{-1} (table I). Below 5×10^{-4} torr the linewidth approaches a low pressure limit. The limit observed is 20 ± 1 gauss. The observed low pressure linewidths are the result of the finite residence time of the ion in the cell and the effect of the trapping field on the ion motion. The departure of an ion from the cell has the effect of a collision in which the ion loses all of its momentum. Thus a calculation of power absorption in the absence of collisions indicates that the linewidth depends on τ, the ion residence time.[14a] As discussed elsewhere[16] the trapping field gives rise to a shift in the resonance frequency. The shift is the same for all ions in the cell only if the spacing between the trapping electrodes is equal to the spacing between the drift electrodes. In the cell employed in our experiments the spacing between the drift electrodes is one-half that of the trapping electrodes. This results in a shift in resonance frequency dependent on the position of the ion in the trapping well, which causes a slight broadening of the absorption line.

Figure 5

Variation of CH_5^+ linewidth in gauss (full width at half height) with pressure. The half width at half height in sec^{-1} (ξ) and the number of collisions suffered by the ion as it passes through the cell [$\xi\tau(m+M)/m$] are also indicated.

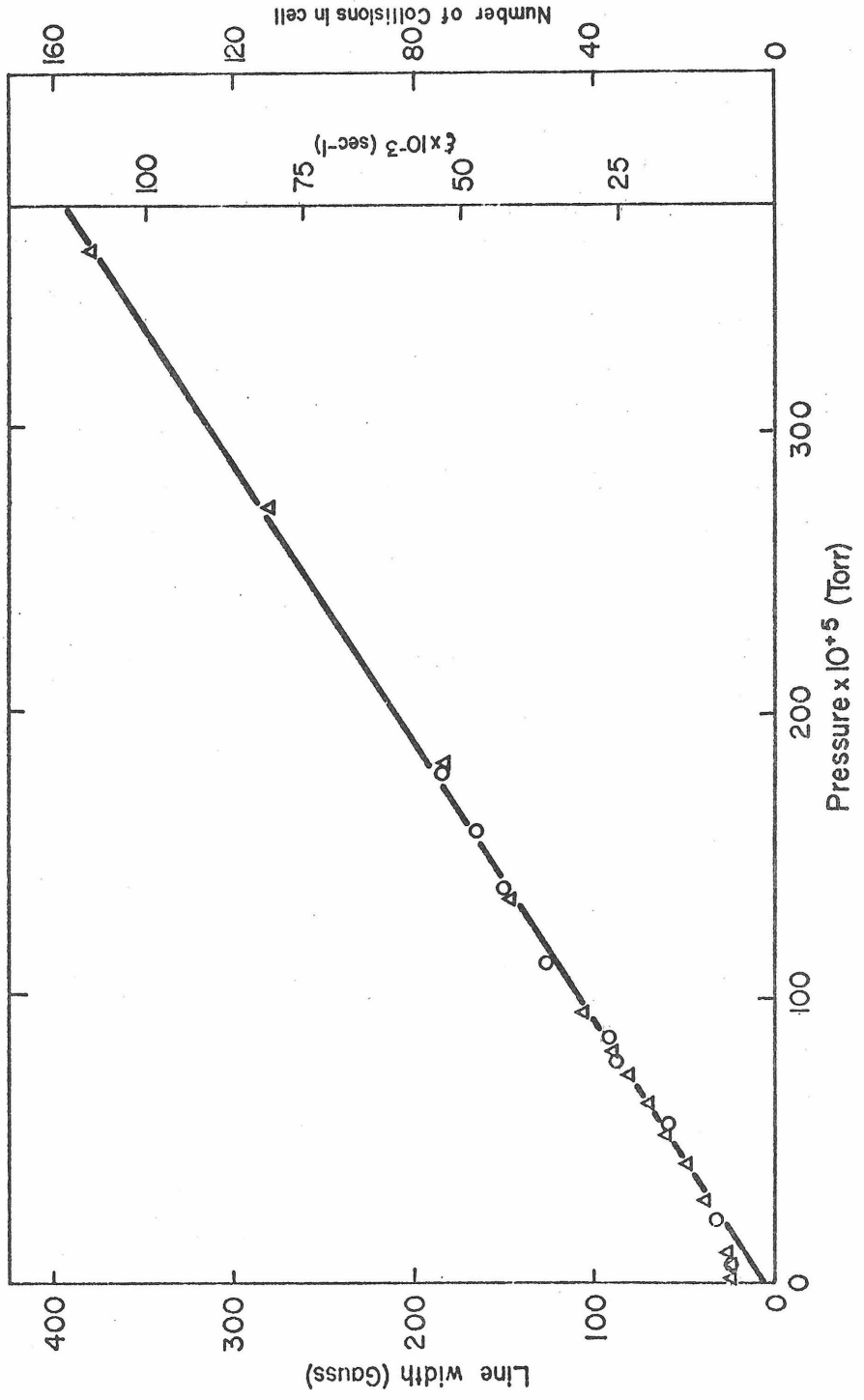
Line width (Gauss)
400
300
200
100
0
0
100
200
300
Pressure x 10^-5 (Torr)
ζ x 10^-3 (sec^-1)
100
75
50
25
Number of Collisions in cell
160
120
80
40
0

Table I. Results of Collision Frequency Determinations

Neutral	Ion	$K_0(cm^2V^{-1}sec^{-1})^b$		$\xi/n \times 10^{10}(cm^3mole^{-1}sec^{-1})^a$		$\sigma_d(Å^2)^c$	
		Measured	Calculated	Measured	Calculated	Measured	Calculated
CH_4	CH_5^+	2.32 ± 0.02	2.99	9.06 ± 0.06	7.04	214.5 ± 1.5	167
	$C_2H_5^+$	2.28 ± 0.06	2.67	5.39 ± 0.12	4.62	194.0 ± 4.0	167
	$C_3H_7^+$	1.99 ± 0.03	2.51	4.18 ± 0.05	3.31	210.0 ± 3.0	167
	$C_4H_9^+$	1.98 ± 0.07	2.43	3.17 ± 0.09	2.59	204.0 ± 6.0	167
	Na^+	3.11 ± 0.06	2.80	5.01 ± 0.09	5.57	150.0 ± 3.0	167
H_2	H^+	16.2 ± 0.6	18.95	21.9 ± 0.9	18.78	107.3 ± 4.2	91.9
	H_3^+	11.03 ± 0.14	14.19	10.78 ± 0.11	8.37	118.3 ± 1.3	91.9
	CH_5^+	11.34 ± 0.04	11.61	1.852 ± 0.006	1.81	94.0 ± 0.3	91.9
	H_3O^+	11.06 ± 0.19	11.54	1.703 ± 0.028	1.63	95.9 ± 1.5	91.9
	N_2H+	11.07 ± 0.10	11.35	1.115 ± 0.009	1.09	94.2 ± 0.9	91.9
	$C_2H_5^+$	11.68 ± 0.21	11.35	1.056 ± 0.017	1.09	89.3 ± 1.4	91.9
	$C_3H_7^+$	11.17 ± 0.07	11.23	0.744 ± 0.004	0.75	92.4 ± 0.5	91.9
	Na^+	11.77 ± 0.18	11.46	1.325 ± 0.020	1.361	89.5 ± 1.4	91.9

Table I (Cont'd)

[a]Determined from ion cyclotron resonance linewidth measurements. The error estimates represent standard deviations determined from a least squares analysis of linewidth versus pressure data.

[b]The mobility at 273 °K and 760 torr calculated from the measured collision frequencies as indicated in the text.

[c]The diffusion cross section at 300 °K calculated from the measured collision frequencies, Eq. (4) and assuming $1/2\ M_r v_0^2 \approx 3/2\ kT$.

The data in Fig. 4 are recorded at a constant observing oscillator level of 0.0365 V cm^{-1}. This corresponds to a variation of the ratio of electric field strength to pressure from 65 to 11 volts cm^{-1} $torr^{-1}$ over the corresponding pressure range from 5.62×10^{-4} to 3.44×10^{-3} torr. Any dependence of ξ/n on E_1/P would cause curvature which is not observed in the data shown in Fig. 4. The linewidth is thus relatively independent of E_1/P over this range. Utilizing Eq. (7), a value of E_1/P of 65 Volts cm^{-1} $torr^{-1}$ corresponds to an estimated ion energy of 0.067 eV in excess of 3/2 kT (= 0.039 eV at 300°K).

$C_2H_5^+$, a second abundant species in methane if produced by the reaction

$$CH_3^+ + CH_4 \rightarrow C_2H_5^+ + H_2 \quad . \tag{11}$$

Like CH_5^+, $C_2H_5^+$ is stable against further reaction with methane. The experimental value of ξ/n, obtained from the slope of a plot analogous to Fig. 5, is 5.39 ± 0.12 10^{-10} cm^3 $molecule^{-1}$ sec^{-1} (table I).

Propyl and butyl cations were generated by the chemical ionization reactions[17]

$$\left.\begin{matrix} CH_5^+ \\ C_2H_5^+ \end{matrix}\right\} + C_3H_8 \rightarrow C_3H_7^+ + \begin{cases} CH_4 + H_2 \\ C_2H_6 \end{cases} \tag{12}$$

$$\left.\begin{matrix} CH_5^+ \\ C_2H_5^+ \end{matrix}\right\} + (CH_3)_3CH \rightarrow C_4H_9^+ + \begin{cases} CH_4 + H_2 \\ C_2H_6 \end{cases} \tag{13}$$

in methane containing 3% propane and isobutane, respectively. The variation with pressure of the single resonance intensities of the main ionic species in the methane-propane mixture is illustrated in Fig. 6. Above 5×10^{-4} torr the decrease in CH_5^+ and $C_2H_5^+$ intensities with a simultaneous increase in $C_3H_7^+$ intensity indicates the occurrence of reactions (12). The chemistry of the methane-isobutane mixture is similar to that of the methane-propane mixture with $C_4H_9^+$ the predominant species at high pressure. The structure of the propyl and butyl cations generated in reactions (12) and (13) are somewhat uncertain. In the case of propane, for instance, the species produced are probably a mixture of 2-propyl and 1-propyl cations. On subsequent collisions with propane, the 1-propyl cations are probably converted to 2-propyl cations. In the present studies, linewidths were recorded over the pressure region from 10^{-4} to 3×10^{-3} torr and most likely samples collision frequencies for several carbonium ion structures. The possibility exists that the collision frequencies may depend on ion structure, as discussed below.

The experimental values of ξ/n for $C_3H_7^+$ and $C_4H_9^+$ are $4.18 \pm 0.05 \times 10^{-10}$ and $3.17 \pm 0.09 \times 10^{-10}$ cm^3 $molecule^{-1}$ sec^{-1}, respectively. No variation of ξ/n with E_1/P was observed for either ion. The measured values of ξ/n were corrected for the presence of the additive gases. The collision frequencies of $C_3H_7^+$ and $C_4H_9^+$ with C_3H_8 and C_4H_{10} were assumed to be equal to the polarization limit discussed below. These estimates of the collision frequences and the known partial pressures

Figure 6

The variation of relative ion abundances of ions in methane containing about 3% propane. The quantity (I_i/m_i) is the ratio of the single resonance intensity of an ion to its mass and is proportional to the relative abundance of the ion (Reference 1).

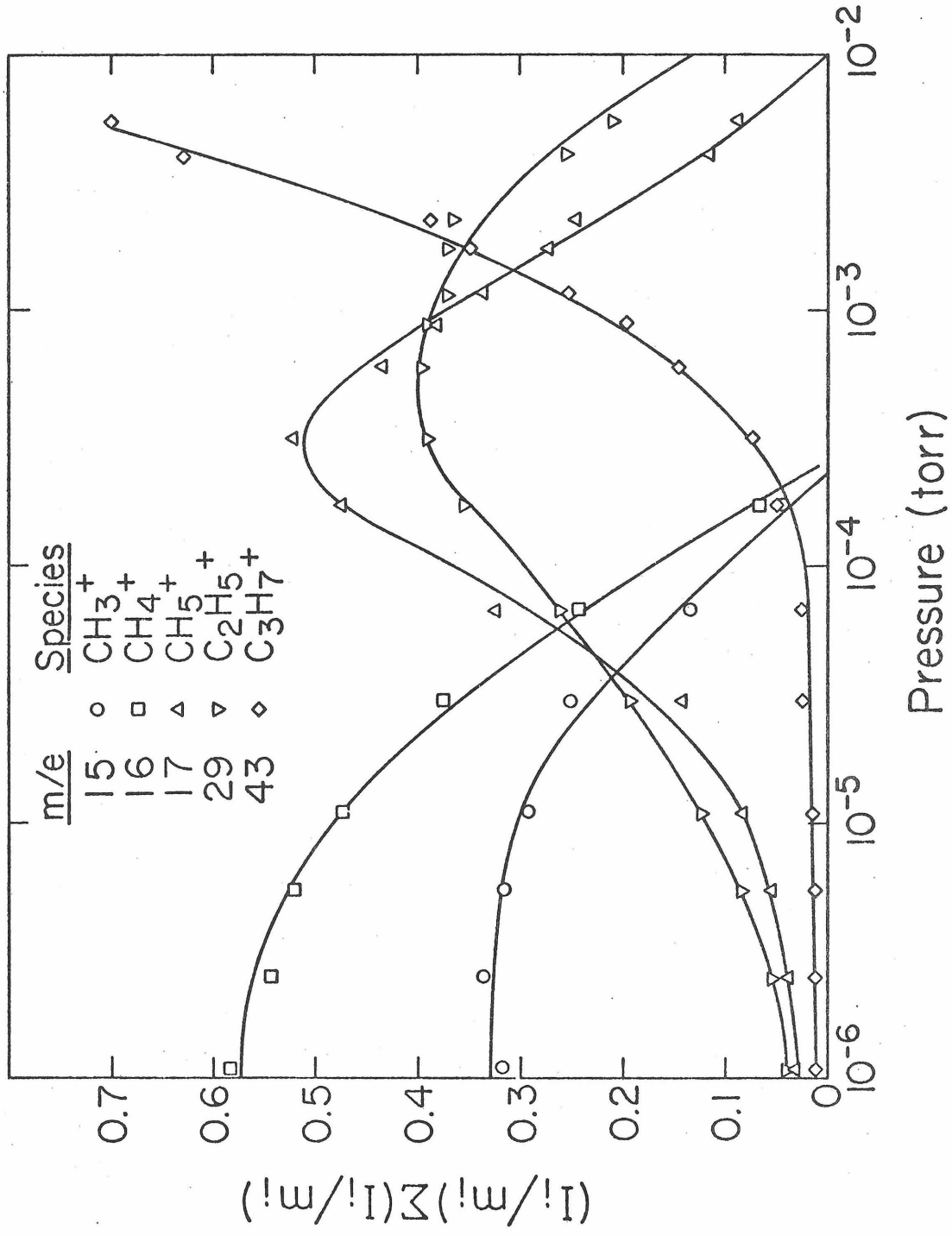
(Ii/mi)Σ(Ii/mi)
0.7
0.6
0.5
0.4
0.3
0.2
0.1
0
10-6
10-5
10-4
10-3
10-2
Pressure (torr)
m/e
15
16
17
29
43
Species
CH3+
CH4+
CH5+
C2H5+
C3H7+

of the additives were used to estimate the contributions of the additive gases to the linewidths. The corrections were found to be very small (0.1 or 0.2%) for the partial pressures used (additives made up approximately 3% of the total pressure).

The Na^+ collision frequency was also observed to be independent of E_1/P, and the value of ξ/n obtained was $5.01 \pm 0.09 \times 10^{-10}$ cm^3 $molecule^{-1}$ sec^{-1}.

Ions in Hydrogen

The ions H^+ and H_3^+ can be directly studied in hydrogen, the latter species being generated in the well-known ion-molecule reaction

$$H_2^+ + H_2 \rightarrow H_3^+ + H \qquad (14)$$

Other ionic species studied in hydrogen include CH_5^+, H_3O^+, N_2H^+, $C_2H_5^+$ and $C_3H_7^+$, generated in the chemical ionization reactions (15)-(19).

$$H_3^+ + CH_4 \rightarrow CH_5^+ + H_2 \qquad (15)$$

$$H_3^+ + H_2O \rightarrow H_3O^+ + H_2 \qquad (16)$$

$$H_3^+ + N_2 \rightarrow N_2H^+ + H_2 \qquad (17)$$

$$H_3^+ + C_2H_6 \rightarrow C_2H_5^+ + 2H_2 \qquad (18)$$

$$H_3^+ + C_3H_8 \rightarrow C_3H_7^+ + 2H_2 \qquad (19)$$

Reactant gases were introduced as in the case of methane except that lower additive concentrations were employed, typically 0.5%. These lower concentrations were necessitated by the fact that because of its low mass, H_2 is very inefficient in comparison to the additives in

momentum relaxation processes. Corrections were estimated as in the case of methane and were found to be small (1 or 2%). In each case the linewidth was found to increase linearly with pressure and to be independent of E_1/P below 50 V cm^{-1} $torr^{-1}$. The resulting values of ξ/n are summarized in Table I. The somewhat large standard deviation of H^+ is dictated by its low abundance in the mass spectrum of hydrogen.

Discussion

Comparison with Mobility Measurements

The mobility of an ion in a gas is the proportionality constant relating the applied field, E, to the observed drift velocity, u, of the ion in the gas (Eq. 20). The mobility is thus a transport property of the ion and the gas. The mobility is related to the collision frequency for momentum transfer, ξ, by Eq. (21).[5a] A derivation of Eq. (21) that relies on the fact that an ion cyclotron resonance experiment can be considered a DC mobility experiment in a rotating frame is given in Appendix I. Substituting from Eq. (4) into Eq. (20) gives Eq. (22) relating the mobility to the neutral number density and the diffusion cross section. Since the mobility is dependent on the neutral number density, the number usually reported is K_0 which is related to K by Eq. (23) where P and T are the pressure and temperature at which K is measured.

$$u = KE \tag{20}$$

$$K = \frac{q}{m\xi} \tag{21}$$

$$K = \frac{q}{n\, M_r \langle \sigma_d(v_0) v_0 \rangle} \tag{22}$$

$$K_0 = K \frac{P}{760} \frac{273}{T} \tag{23}$$

The values of K_0 given in Table I were calculated from the values of

ξ/n in Table I using the relationships given in Eqs. (21) and (23).

Mobilities for several of the systems listed in Table I have been measured by other methods. Comparison of the results of these measurements with the present measurements is given in Table II. Each of the methods used to obtain the tabulated results made provision for mass identification of the charge carrying species.

The agreement between the present ion cyclotron resonance linewidth measurements and the drift tube measurements of McDaniels and co-workers[6] is very good. This agreement indicates that ion cyclotron resonance linewidths are an accurate measure of ion neutral collision frequencies. The disparity between the present results and the early ion cyclotron resonance results of Wobschall and co-workers[5] must be the result of experimental problems with the technique in its early stages of development. The problems restricting the accuracy of Wobschall's measurements may have been the lack of techniques to measure pressures less than a micron very accurately and the difficulty of characterizing the ion motion in the early solenoidal ion cyclotron resonance apparatus. The availability of the capacitance manometer for low pressure measurement, and the development of the cell design illustrated in Fig. 1 have largely alleviated these problems.

The apparatus used by Meisels and co-workers[8] was designed for chemical ionization studies and is not well suited for the measurement of accurate mobilities. The sources of error are systematic however and relative measurements of mobilities of various ions in the same or similar gases should be quite reliable. The agreement between

Table II. Comparison of Mobility Measurements

Neutral	Ion	K_0 (cm^2 $Volt^{-1}$ sec^{-1})[a]			
		This Work	Reference (6)	Reference (8)[b]	Reference (5)
H_2	H^+	16.2 ± 0.6	15.7 ± 0.6		
H_2	H_3^+	11.03 ± 0.14	11.1 ± 0.5	6.2 ± 0.2	7.0
H_2	Na^+	11.77 ± 0.18	12.2 ± 0.6		
CH_4	CH_5^+	2.32 ± 0.02		1.75 ± 0.03	
CH_4	$C_2H_5^+$	2.28 ± 0.02		1.74 ± 0.07	

[a]The mobility at 273 °K and 760 torr.

[b]See text for discussion of accuracy of these measurements.

the present measurements and Meisels measurements can thus be considered satisfactory.

Two different workers have measured the drift velocities of ions formed in discharges in methane.[18] The ions were not identified. The range of E/P values over which the measurements were made is 50 to 200 Volts cm^{-1} $torr^{-1}$. The mobility K_o of the charge carriers was observed to be approximately 2.5 Volts cm^{-2} sec in both cases. This agrees reasonably well with the mobilities of CH_5^+ and $C_2H_5^+$ in Table I.

Comparison with Theory

The polarization limit of the Langevin theory discussed in the preceding chapter provides a theoretical value for the mobility that depends only on the polarizability of the neutral and the reduced mass of the ion neutral pair (Eq. 24). This estimate of the mobility is calculated assuming that the r^{-4} ion induced dipole potential determines the diffusion cross section of the ion-neutral pair. Substituting from Eq. (24) into Eq. (21) and rearranging gives Eq. (25) for the polarization limit for the collision frequency. The data in Table I is compared with the polarization limit in Figs. 7 and 8. In each figure $M_r^{\frac{1}{2}}/m$ is plotted against ξ/n.

$$K = \frac{0.5105}{n(4\pi\alpha M_r)^{\frac{1}{2}}} \tag{24}$$

$$\xi/n = 2.210\,\pi\,q\,\frac{M_r^{\frac{1}{2}}}{m}\,\alpha^{\frac{1}{2}} \tag{25}$$

Figure 7

The variation of the collision frequency ξ/n with $M_r^{\frac{1}{2}}/m$ for ions in methane, where M_r and m are the reduced mass of the ion neutral pair and mass of the ion, respectively. The line represents the polarization limit calculated from Eq. (25).

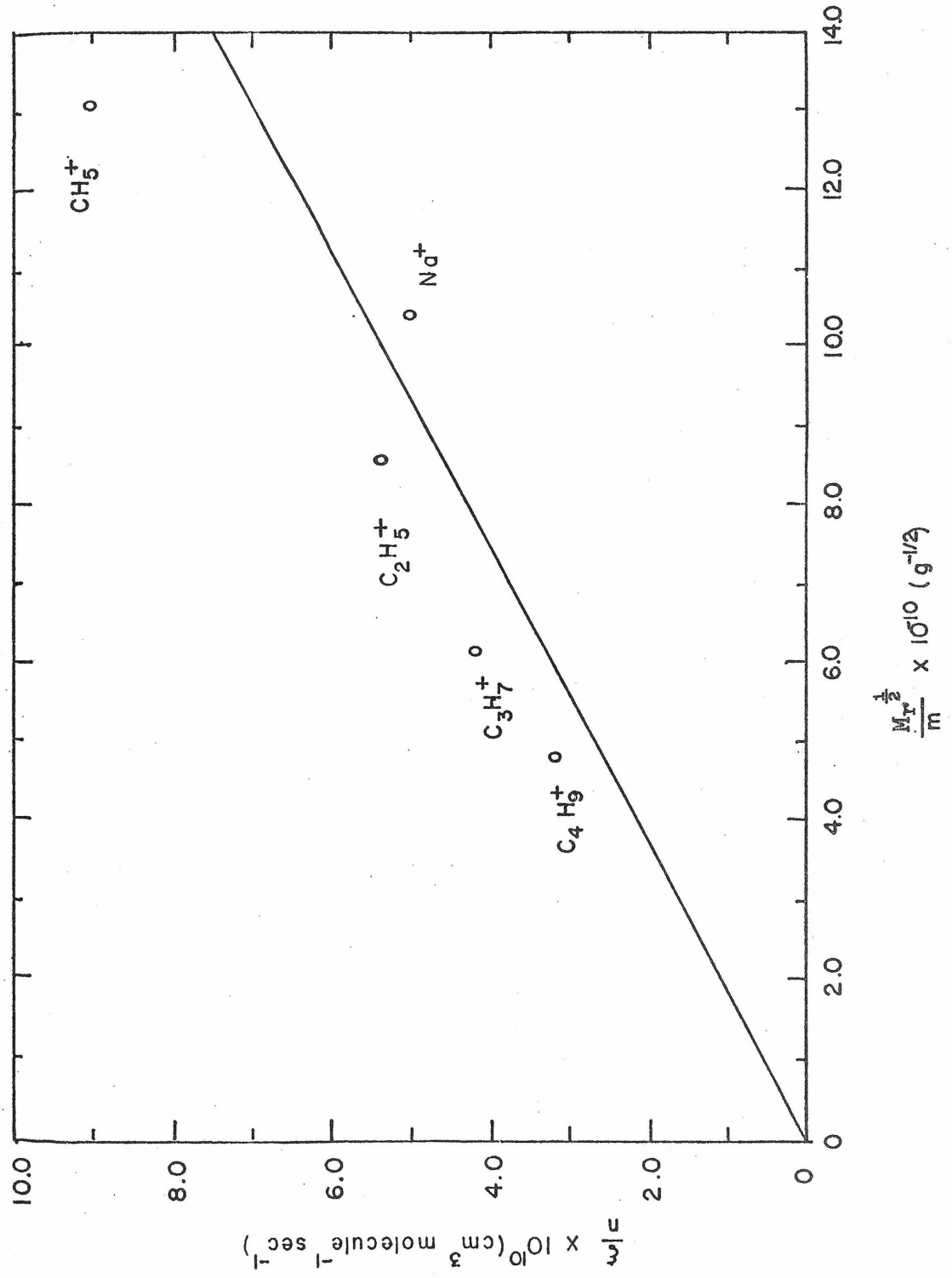
CH_5^+
Nd^+
$C_2H_5^+$
$C_3H_7^+$
$C_4H_9^+$
k_1 x 10^{10} (cm^3 molecule^{-1} sec^{-1})
$\frac{M_r^{\frac{1}{2}}}{m}$ x 10^{10} ($g^{-1/2}$)
0
2.0
4.0
6.0
8.0
10.0
12.0
14.0

Figure 8

The variation of the collision frequency ξ/n with $M_r^{\frac{1}{2}}/m$ for ions in hydrogen, where M_r and m are the reduced mass of the ion neutral pair and the ion mass, respectively. The line represents the polarization limit calculated from Eq. (25).

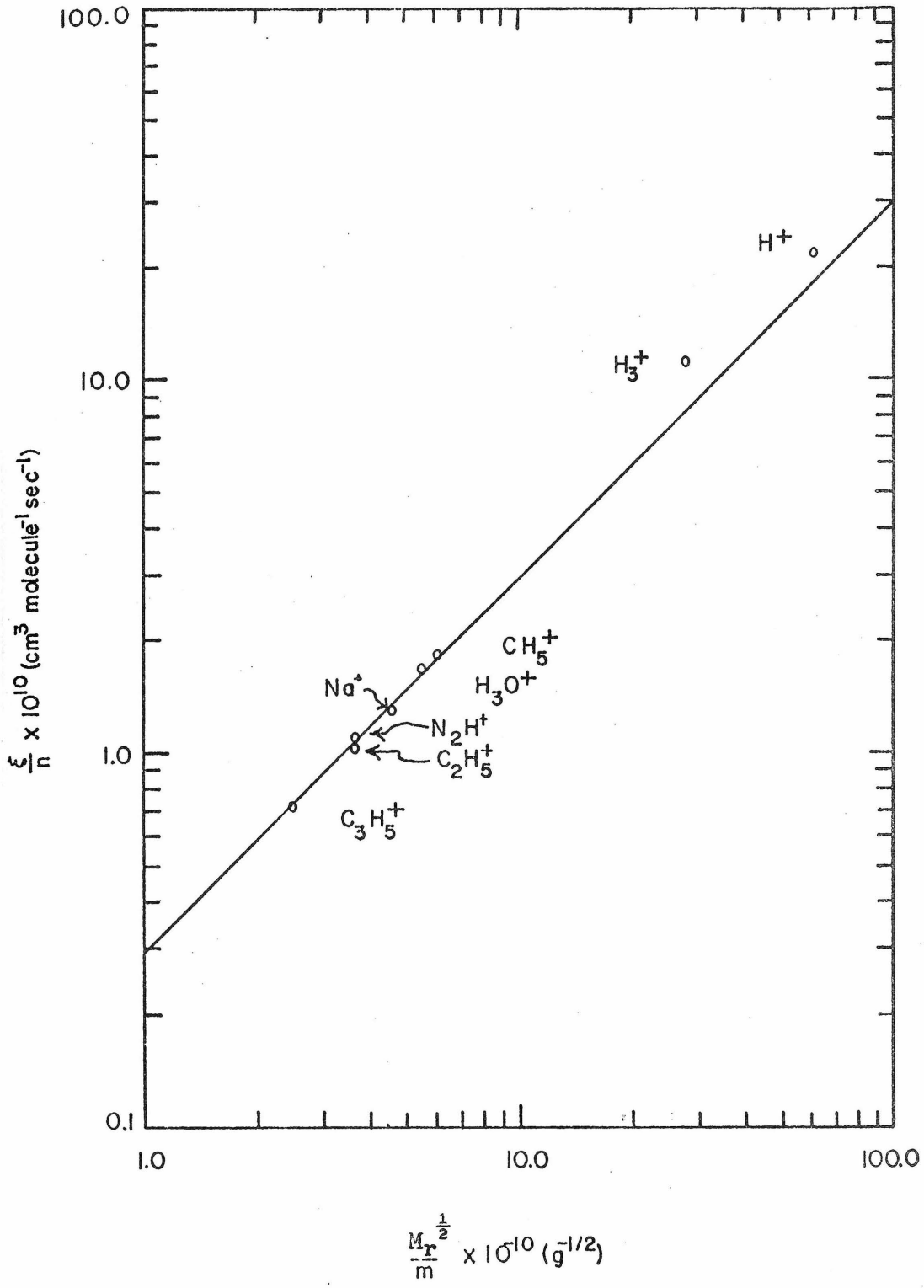
100.0
10.0
1.0
0.1
1.0
10.0
100.0
$\frac{\xi}{n} \times 10^{10}$ (cm^3 mdecule^{-1} sec^{-1})
$\frac{M_r}{m}^{\frac{1}{2}} \times 10^{10}$ ($g^{-1/2}$)
H^+
H_3^+
CH_5^+
H_3O^+
Na^+
N_2H^+
$C_2H_5^+$
$C_3H_5^+$

As expected from Eq. (25) the collision frequencies are observed to increase approximately linearly with $M_r^{\frac{1}{2}}/m$. The quantitative agreement between the model and experiment is not particularly good, however. This is not surprising since Langevin's calculations indicate that even a simple hard sphere repulsive interaction will result in a significant deviation of the mobility from the polarization limit. Thus it is surprising that the collision frequencies of the heavier ions in hydrogen agree as well as they do with the polarization limit. The agreement should probably be considered fortuitous rather than taken as evidence that only the ion induced dipole force is important in the interaction of these ions with hydrogen.

In Figs. 9 and 10 the calculations of Mason and Schamp and those of Langevin are compared with our experimental results. The calculations of Mason and Schamp[19] are based on a three term potential with attractive terms proportional to r^{-4} and r^{-6} and a repulsive term proportional to r^{-12}. The potential is given in Eq. (26) of Chapter 1, and the calculations and features of the results are described in that chapter. The calculations of Langevin[20] are based on a potential including the ion induced dipole r^{-4} interaction and a hard sphere repulsive interaction. These calculations and features of the results are also discussed in Chapter 1. The mobilities calculated from both models increase linearly with $1/M_r^{\frac{1}{2}}$ so the quantity $K_o \times M_r^{\frac{1}{2}}$ is plotted in Figs. 9 and 10 to remove the explicit mass dependence and emphasize the importance of other factors. The quantity on the abscissa increases with ion size and with temperature as discussed below. The solid lines

Figure 9

The variation of ion mobility with temperature and ion size for ion in methane. The broken line represents the polarization limit calculated from Eq. (24). The line labeled Langevin is the result of the complete Langevin calculation, including the effects of ion induced dipole and hard sphere interactions. The remaining lines were calculated from the collision integral tabulated for the 12-6-4 potential by Mason and Schamp. The coefficient of the r^{-6} term increases with γ. For an explanation of the variable on the coordinates and the significance of the data points see text.

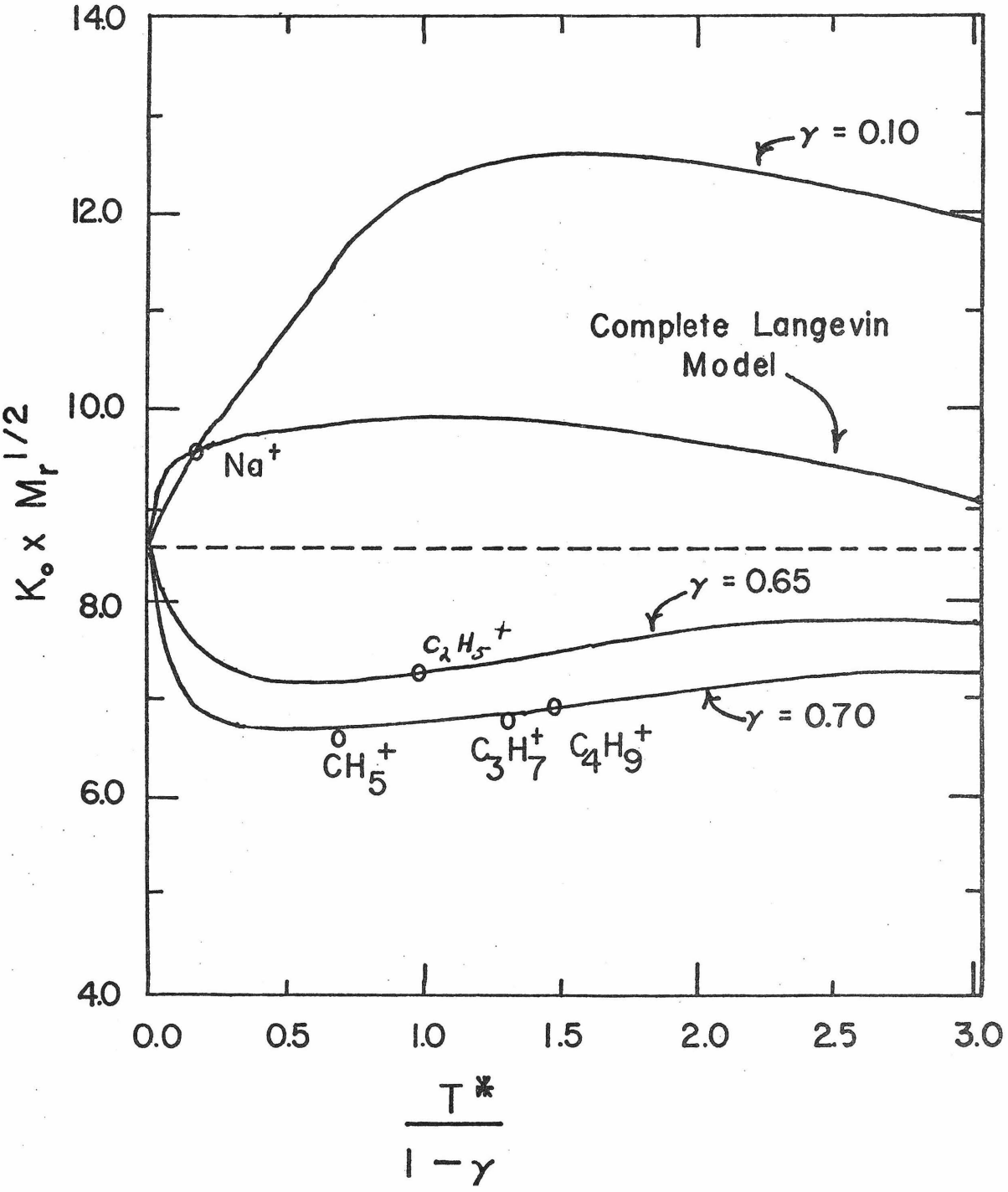
14.0
12.0
10.0
8.0
6.0
4.0
$K_o \times M_r^{1/2}$
0.0
0.5
1.0
1.5
2.0
2.5
3.0
$\frac{T^*}{1-\gamma}$
$\gamma = 0.10$
Complete Langevin Model
Na^+
$\gamma = 0.65$
$C_2H_5^+$
$\gamma = 0.70$
CH_5^+
$C_3H_7^+$
$C_4H_9^+$

Figure 10

The variation of ion mobility with temperature and ion size for ions in hydrogen. The lines and variables have the same significance as in Fig. 9.

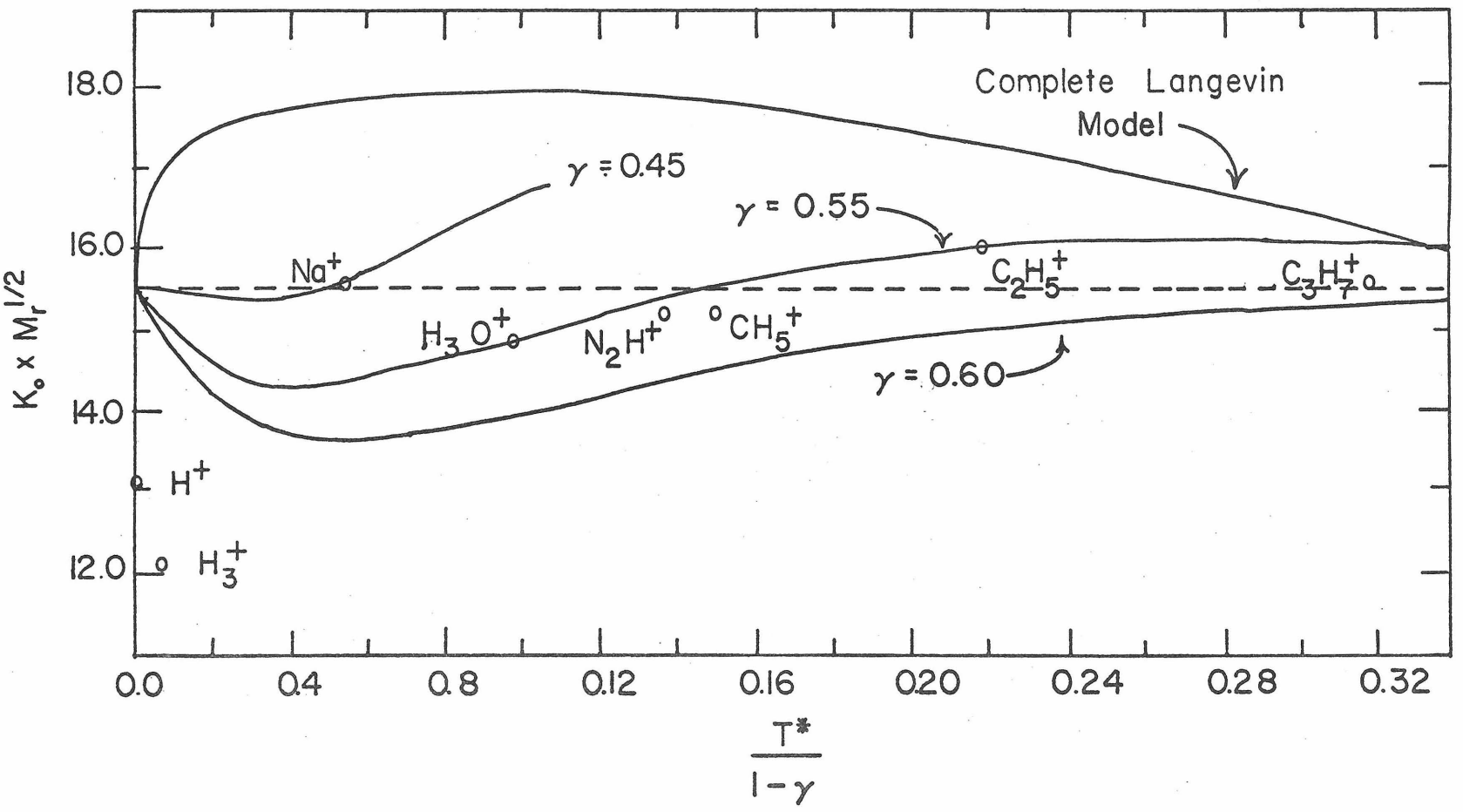
18.0
16.0
14.0
12.0
$K_o \times M_r^{1/2}$
Complete Langevin Model
$\gamma = 0.45$
$\gamma = 0.55$
$\gamma = 0.60$
Na^+
H_3O^+
N_2H^+
CH_5^+
$C_2H_5^+$
$C_3H_7^+$
H^+
H_3^+
0.0
0.4
0.8
0.12
0.16
0.20
0.24
0.28
0.32
$\frac{T^*}{1-\gamma}$

represent the mobilities calculated from the models. The broken line represents the value of the polarization limit of the mobility as calculated from Eq. (24). It is important to note in comparing Figs. 9 and 10 with Figs. 7 and 8 that the mobility is inversely proportional to the collision frequency so that the mobility decreases when the collision frequency increases and vice versa. The units of the quantity $K_0 \times M_r^{\frac{1}{2}}$ are V cm^{-2} sec $\times$ (atomic mass unit)$^{\frac{1}{2}}$.

The Langevin model accounts for the finite size of the ion and the molecule by assigning a hard sphere radius, D_{12}. In Chapter 1 we described the procedure used to obtain the mobility as a function of the parameter $1/\mu$ which is related to D_{12} by Eq. (26) (from Eq. (18) of Chapter 1). The impact parameter of classical orbiting, b_0, is given

$$1/\mu = (2\ kT/\alpha e^2)^{\frac{1}{2}} D_{12}^2 = (8/3)^{\frac{1}{2}} (D_{12}/b_0)^2 \qquad (26)$$

by Eq. (27). We note that b_0 depends only on the temperature of a gas of

$$b_0 = (4\alpha e^2/3\ kT)^{\frac{1}{2}} \qquad (27)$$

polarizability α. For a series of ions in one gas at a fixed temperature $1/\mu$ depends only on D_{12} or on ion size. The variation of K with $1/\mu$ under these circumstances reflects the variation of K with ion size. Alternatively for one ion in a gas the variation of K with $1/\mu$ reflects the variation of K with temperature.

The Mason and Schamp model adds r^{-6} and r^{-12} terms to the ion induced dipole potential to account for the finite size of the ion and the molecule and interactions other than the ion induced dipole interaction.

In Chapter 1 we discussed results of calculations in which K was determined from this potential as a function of T^* and γ. The parameter γ represents the relative importance of the r^{-6} interaction in the potential ($\gamma = 0$ implies a pure 12-4 potential and $\gamma = 1$ implies a pure 12-6 potential). The parameter T^* depends on the temperature and on r_m, the ion-molecule distance at which the potential has its minimum. Insofar as it is a measure of ion size, r_m plays the same role in the Mason and Schamp model that D_{12} plays in the Langevin model. Thus the analogy between T^* and $1/\mu$ is evident from Eq. (28) (from Eq. (27) of Chapter 1). Comparison of Eqs. (26) and (28) gives Eq. (29) relating γ

$$T^* = \left(\frac{3\ kT}{3/4\ \alpha e^2}\right)^{\frac{1}{2}} r_m^4(1-\gamma) = 4(1-\gamma)\left(\frac{r_m}{b_o}\right)^4 \tag{28}$$

$$\frac{T^*}{1-\gamma} = 3/2\left(\frac{r_m}{D_{12}}\right)^4\left(\frac{1}{\mu}\right)^2 \tag{29}$$

T^* and $1/\mu$. In order to compare the two models directly we must evaluate D_{12}/r_m. This can be done by setting $D_{12} = \sigma_{12}$ where σ_{12} is the ion-molecule distance where the 12-6-4 potential is zero. For a 12-6 potential ($\gamma = 1$) r_m/σ_{12} is $2^{1/6} = 1.122$. For a 12-4 potential ($\gamma = 0$) $r_m/\sigma_{12} = 3^{1/8} = 1.147$. For values of γ other than 0 and 1 the ratio can be approximated with sufficient accuracy for present purposes by linear extrapolation.

In order to evaluate $1/\mu$ and T^* for the ion-neutral combinations for which we have measured mobilities we estimated D_{12} from gas kinetic data. The estimates and the assumptions made in deriving the estimates are given in Table III.

Table III. Ion-Molecule Radii Used in Calculating Mobilities[a]

Ion	Neutral	D_{12} (Å)	Assumptions
H^+	H_2	0.80	estimated from data in Reference 23
H_3^+	H_2	1.85	estimated from data in Reference 24
CH_5^+	H_2	3.38	$\sigma(CH_5^+) = \sigma(CH_4)$
H_3O^+	H_2	3.06	$\sigma(H_3O^+) = \sigma(H_2O)$, $\sigma(CH_3OH) - \sigma(H_2O) = \sigma(C_2H_5OH) - \sigma(CH_3OH)$
Na^+	H_2	2.46	$\sigma(Na^+)$ = ionic radius of Na^+
N_2H^+	H_2	3.32	$\sigma(N_2H^+) = \sigma(N_2)$
$C_2H_5^+$	H_2	3.69	$\sigma(C_2H_5^+) = \sigma(C_2H_6)$
$C_3H_7^+$	H_2	4.01	$\sigma(C_3H_5^+) = \sigma(C_3H_8)$
CH_5^+	CH_4	3.80	$\sigma(CH_5^+) = \sigma(CH_4)$
$C_2H_5^+$	CH_4	4.11	$\sigma(C_2H_5^+) = \sigma(C_2H_6)$
$C_3H_7^+$	CH_4	4.43	$\sigma(C_3H_7^+) = \sigma(C_3H_8)$
$C_4H_9^+$	CH_4	4.57	$\sigma(C_4H_9^+) = \sigma(t\text{-}C_4H_{10})$
Na^+	CH_4	2.88	$\sigma(Na^+)$ = ionic radius of Na^+

[a]Calculated assuming $D_{12}(A - B) = \frac{1}{2}(\sigma(A) + \sigma(B))$ where $\sigma(A)$ is the kinetic diameter of A. The gas kinetic diameter of A is the internuclear distance at which the Lennard-Jones potential representing the interaction of two molecules of A is zero. All values of σ are taken from J. O. Hirschfeld, C. F. Curtiss, and R. B. Bird, Molecular Theory of Gases and Liquids, Appendix, John Wiley and Sons, Inc., 1954.

Since only the mobility of Na^+ in CH_4 agrees well with the complete Langevin model, the agreement could be fortuitous. On the other hand Na^+ has a low polarizability and high ionization potential, and if the hard sphere approximation fits anything it should fit Na^+.

The theoretical description which best accounts for the data is the model derived from a 12-6-4 potential with disposable parameters. With the exception of H^+ and H_3^+ in hydrogen the agreement is very good. The potential parameters which give the best agreement with experiment are summarized in Table IV. The 12-6-4 potential has, however, three disposable parameters (α, r_m, and γ) and agreement between calculated and observed mobilities is not very significant if it forces us to choose unreasonable parameters. The polarizabilities of hydrogen and methane are well-known and can be assigned with confidence. The values of r_m assigned are only estimates and could be significantly in error. The estimates are all derived in the same way, however, so that any errors should be systematic. Thus the fact that the model provides a good description of the qualitative behavior of the mobility with r_m is good evidence in support of the accuracy of the model's description of ion-molecule interactions.

The remaining parameter is γ, which represents the relative importance of the r^{-6} term. To determine whether the assigned values of γ may be considered reasonable, we consider the examples of Na^+ and CH_5^+ in methane. The r^{-6} term was introduced to account for charge induced quadrupole and London dispersion interactions, both essentially electrostatic interactions. The interactions can be estimated from ion

Table IV. Potential Parameters which Give Best Agreement with Measured Mobilities[a]

Ion	Neutral	γ	r_m (Å)	ϵ (eV)
CH_5^+	H_2	0.55	3.83	0.101
H_3O^+	H_2	0.55	3.47	0.228
N_2H^+	H_2	0.55	3.76	0.109
$C_2H_5^+$	H_2	0.55	4.18	0.067
$C_3H_7^+$	H_2	0.60	4.64	0.053
Na^+	H_2	0.45	2.99	0.232
CH_5^+	CH_4	0.70	4.29	0.121
$C_2H_5^+$	CH_4	0.65	4.64	0.077
$C_3H_7^+$	CH_4	0.70	5.00	0.066
$C_4H_9^+$	CH_4	0.70	5.16	0.059
Na^+	CH_4	0.10	3.25	0.124

[a]The reliability of these data is discussed in the text.

and neutral ionization potentials and polarizabilities and neutral oscillator strengths.[21] The necessary data are available for Na^+ and CH_4.[21] We obtain for C, the ratio of the coefficients of the r^{-6} and r^{-4} terms, a value of 1.25 Å^2. This is in good agreement with 1.56 Å^2 value of C implied by the values of γ and r_m in Table IV. An upper limit for C for CH_5^+ in methane was calculated assuming that the

polarizability of CH_5^+ is no greater than that of CH_4 and the ionization potential of CH_5^+ to be no greater than twice that of CH_4. The calculated value is 6.5 $Å^2$ which is much smaller than the value of 55.5 $Å^2$ implied by the assigned values of the parameters in Table IV. Since the calculated value of C increases with the ion polarizability and is only weakly dependent on the ion ionization potential, the value 6.5 $Å^2$ probably represents an upper limit to the electrostatic r^{-6} interaction. The disagreement between the two values is not unreasonable if there are important short range forces between CH_5^+ and CH_4 other than the ion induced quadrupole and London dispersion forces. It seems very likely that, since CH_5^+ is a good gas phase acid, there is some weak chemical bonding between CH_5^+ and CH_4 analogous to the hydrogen bonding in which acidic neutral species participate. Such bonding could be important between methane and all the hydrocarbon ions studied. They all seem to experience short range forces in their interactions with methane stronger than would be expected on the basis of electrostatic considerations.

A similar analysis can be made of the interactions of hydrogen with the heavier polyatomic ions examined. For CH_5^+, for example, the calculated value of C is 3.95 and that implied by the data is 25.9. Unlike the case of Na^+ in CH_4, however, the calculated and observed values of C do not agree well for Na^+ in H_2. The calculated value is 1.33 $Å^2$ and the value implied by the data is 6.6 $Å^2$. The disagreement is not as large as in the case of the polyatomic CH_5^+, but it must be considered significant. There is a short range attractive force between a hydrogen

molecule other than those already considered which may partly account for the large values of C. The polarizability tensor of hydrogen is anisotropic so that an ion probably aligns the H_2 molecule to maximize the ion induced dipole interaction as the two approach. The net result of this effect is an additional short range attractive force. Thus the kind of chemical bonding hypothesized to be important in the interactions of polyatomic ions in methane may also be important in hydrogen, but its effect is not clearly differentiated from the effect of the anisotropy of the hydrogen polarizability tensor.

As discussed in Chapter 1 the product of the diffusion cross section, $q_d(v_0)$, and the relative velocity, v_0, is independent of v_0 for a pure r^{-4} interaction potential. The introduction of r^{-6} and r^{-12} terms into the potential might be expected to result in some velocity dependence in $q_d(v_0)v_0$. Since the collision frequencies depend on this quantity it is therefore expected that in general a collision frequency determined in part by r^{-6} and r^{-12} interactions will depend on the ion energy and therefore on E/P. The measured collision frequencies, however, are observed to be independent of E/P. Mason and Schamp point out that the E/P dependence of the mobility is related to its temperature dependence. If the mobility is approximately independent of temperature it will be approximately independent of E/P. It is evident from Figs. 9 and 10 that a value of γ larger than about 0.5 implies that the mobility changes rather slowly with T^*. Thus the assigned potential parameters of most of the ions studied in hydrogen and methane are consistent with mobilities that are relatively independent of E/P. A possible exception is Na^+ in methane. Figure 9 indicates that this mobility should increase

quite rapidly with temperature. Evaluating the leading term in the expansion of the mobility in terms of powers of E/P given by Mason and Schamp, however, suggests that the mobility of Na^+ in methane should not vary more than 2 or 3 per cent over the range of E/P values used in the present study.

Thus we conclude that with the exception of H^+ and H_3^+ in H_2 the mobilities that have been measured are correctly predicted by the model based on a 12-6-4 potential without making any unreasonable assumptions. Although all of the parameters in Table IV make sense physically and although they give the correct values of the mobilities, they cannot be considered to be unambiguously determined. There are other values of the parameters which give the correct mobilities. In general such alternative sets of parameters include values of r_m that seem unreasonably small or large, but they cannot be eliminated on the basis of the present measurements. Measurements of the temperature dependence of these mobilities would be helpful in substantiating the assigned values of the parameters.

Patterson recently examined the mobilities of ions in helium.[7] He concluded that the mobilities were accounted for quite well by a 12-4 potential or even by a simple hard sphere model which ignores the ion induced dipole force. This is not too surprising in view of the fact that the polarizability of helium is smaller than that of hydrogen by a factor of four ($\alpha(H_2) = 0.79$ Å^3, α (He) $= 0.21$ Å^3). Patterson also measures the mobility of SF_5^- and SF_6^- in CH_4.[7] He concludes that his measurements are most consistent with a 12-6-4 potential with $\gamma = 0.62$ in good agreement with our conclusions.

Mason and Vanderslice[22] have calculated the mobilities of H^+ and H_3^+ in H_2. They use various techniques for estimating the ion-molecule interaction potentials and from these potentials calculate the mobilities by the method of Mason and Schamp. They calculate 18.3 and 22.0 V cm^{-2} sec for the room temperature mobilities at standard density of H^+ and H_3^+, respectively. The agreement between the calculated value for H^+ and the measured value ($\sim$ 16 V cm^{-2} sec) is reasonably good, but the potential used in the calculation is in poor agreement with recent ab initio calculations on the potential surface of H_3^+. They take 2.7 eV and 1.5 Å as the average over all orientations of the binding energy and position of the potential minimum, respectively. The position of the minimum is defined in terms of the distance from the center of the molecule to the approaching proton. Recent ab initio calculations[23] are in essential agreement that there is a potential minimum in the H_3^+ potential surface for an equilateral triangle configuration where the triangle is 0.88 Å on a side. The depth of the minimum relative to H_2 and a proton at large distance is 4.5 eV. The most stable colinear configuration occurs when the approaching proton is 1.2 Å from the center of the molecule. The depth of this minimum is 2.4 eV. If all orientations are considered equally likely, the average distance from the center of the H_2 molecule to the position of minimum potential for an approaching proton is 0.9 Å. The average depth of the minimum is 3.8 eV. These numbers are, of course, significantly different from the numbers used by Mason and Vanderslice in calculating the mobility. Thus the agreement between the calculated number and

the measured number must be considered fortuitous. The ab initio surface is not well represented by any simple inverse power potential for which collision integrals have been tabulated so that an explanation of the mobility H^+ in H_2 requires calculation of collision trajectories on the ab initio potential surface. The measured mobility may be a useful test of the accuracy of such trajectory calculations.

Mason and Vanderslice calculate a value of 22.0 V cm^{-2} sec for the room temperature mobility at standard density (2.69×10^{19} molecule cm^{-3}). This is a factor of 2 higher than the measured mobility and discrepancy may again be the result of an incorrect choice of potential parameters. Little information is available on the H_3^+-H_2 potential surface. No very comprehensive ab initio calculations have been done on surface, but approximate calculations of the geometry and binding energy of H_5^+ have been done.[24]

A process which could play a role in determining the mobility of H_3^+ in H_2 is proton transfer. The measured rate of proton-deuteron transfer from the isotopic variants of $(H, D)_3^+$ to $(H, D)_2$ is 3.0×10^{-10} cm^3 molecule sec^{-1} [25] which indicates that proton transfer occurs on a significant fraction of momentum transfer events. Proton transfer also occurs between CH^+ and CH_4, but the rate is much slower, 3.3×10^{-11} cm^3 $molecule^{-1}$ sec^{-1}.[26] The fact that the reaction is observed at all in methane suggests that the chemical bonding hypothesized above to play a role in the CH_5^+ - CH_4 system is real.

Conclusions

The good agreement between the present results and drift tube measurements show that ion cyclotron resonance is a useful technique for obtaining accurate ion-molecule collision frequencies and the equivalent ion mobilities.

Comparison of theory with measured mobilities suggests that a 12-6-4 potential gives a good description of the interactions of hydrogen and methane with all of the ions examined except H^+ and H_3^+. The model cannot be expected to give a good description of the interactions H^+ with H_2 since the interaction potential for that system which is known from ab initio calculations cannot be accurately represented by the 12-6-4 potential.

The results suggest that there are short range attractive forces of a chemical nature between the hydrocarbon ions studies and CH_4. The results also suggest that the anisotropy of the polarizability tensor of H_2 contributes to the short range attraction between ions and that molecule.

There is a significant amount of information about the interactions of ions with neutral molecules in measured mobilities, as is evidenced by the present study. Future studies in this promise to be interesting and instructive.

References

1. S. E. Buttrill, Jr., J. Chem. Phys., 50, 4125 (1969).
2. M. T. Bowers, D. D. Elleman, and J. R. Beauchamp, J. Chem. Phys., 72, 3599 (1968).
3. J. L. Beauchamp and S. E. Buttrill, Jr., J. Chem. Phys., 48, 1783 (1968).
4. J. H. Futrell and T. O. Tiernan, "Ion Molecule Reactions," Chap. 4 in Fundamental Processes in Radiation Chemistry, Edited by P. Ausloos (John Wiley Interscience, 1968).
5. (a) D. Wobschall, R. A. Fluegge, and J. R. Graham, Jr., J. Chem. Phys., 47, 4091 (1967); (b) D. Wobschall, Rev. Sci. Instr., 36, 466 (1965); (c) D. Wobschall, J. Graham, Jr., and D. Malone, Phys. Rev., 131, 1565 (1965).
6. T. M. Miller, J. T. Moseley, D. W. Martin, and E. W. McDaniel, Phys. Rev., 173, 115 (1968).
7. P. L. Patterson, J. Chem. Phys., 56, 3943 (1972).
8. G. Sroka, C. Chang, and G. G. Meisels, J. Amer. Chem. Soc., 95, 1052 (1972).
9. J. M. S. Henis and W. Frasure, Rev. Sci. Instr., 39, 772 (1968).
10. E. W. Rothe, J. Vacuum Sci. Technol., 1, 66 (1964).
11. S. Dushman, Scientific Foundations of Vacuum Technique (John Wiley and Sons, Inc., New York, 1962).
12. J. P. Blewett and Ernest J. Jones, Phys. Rev., 50, 464 (1936).

13. J. L. Beauchamp, J. Chem. Phys., 46, 1231 (1967).

14. (a) M. B. Comisarow, J. Chem. Phys., 55, 205 (1971); (b) A. G. Marshall, J. Chem. Phys., 55, 1343 (1971); (c) A. G. Marshall and S. E. Buttrill, Jr., J. Chem. Phys., 52, 2752 (1970); (d) See Reference 1.

15. J. L. Beauchamp, Ph.D. Thesis, Harvard University, 1967.

16. J. L. Beauchamp and J. T. Armstrong, Rev. Sci. Instr., 40, (1969).

17. F. H. Field, Acc. Chem. Res., 1, 42 (1968).

18. (a) K. J. Schmidt, Z. Phyz., 139, 251 (1954); (b) H. Schlumbohm, Z. Phyz., 182, 317 (1965).

19. E. A. Mason and H. W. Schamp, Jr., Ann. Phys., 4, 233 (1958).

20. P. Langevin, Ann. Chim. Phys., Series 8, 5, 245 (1905). See also, E. W. McDaniel, Collision Phenomena in Ionized Gases, Appendix II, (John Wiley and Sons, Inc., New York, 1964).

21. H. Margenau, Phil. Sci., 8, 603 (1941) and references therein.

22. E. A. Mason and J. T. Vanderslice, Phys. Rev., 114, 497 (1959).

23. (a) I. G. Csizmadia, R. E. Kari, J. C. Polanyi, A. C. Roach, and M. A. Robb, J. Chem. Phys., 52, 6205 (1970); (b) H. Conroy, J. Chem. Phys., 51, 3979 (1969).

24. R. D. Poshusta, J. A. Haugen, and D. F. Zetik, J. Chem. Phys., 51, 3343 (1969).

25. T. Terao and R. A. Back, J. Phys. Chem., 73, 3884 (1969). This rate has also been measured by T. B. McMahan and P. Miasek in this laboratory and found to be $\sim 3 \times 10^{-10}$ cm^3 $molecule^{-1}$ sec^{-1}.

26. R. H. Lawrence, Jr. and R. F. Firestone, "Ion Molecule Reactions in the Gas Phase," p. 278, Advances in Chemistry Series 58, American Chemical Society, 1966. This rate has also been measured in this laboratory by T. B. McMahon and P. Miasek and found to be about 3.5×10^{-11} cm^3 $molecule^{-1}$ sec^{-1}.

APPENDIX: THE RELATIONSHIP BETWEEN CYCLOTRON RESONANCE AND ION MOBILITY EXPERIMENTS

The velocity of an ion responding to the influence of a constant electric field of strength E is given by

$$v = KE \tag{A1}$$

where K is defined as the ion mobility. In a cyclotron resonance experiment the ion is subjected to a linearly polarized radio frequency electric field given by $E_1 \sin\omega t\,\hat{i}$ which can be broken down into the two circularly polarized counter-rotating components,

$$E^+(t) = \tfrac{1}{2}E_1 \sin\omega t\,\hat{i} + \tfrac{1}{2}E_1 \cos\omega t\,\hat{j} \tag{A2}$$

$$E^-(t) = \tfrac{1}{2}E_1 \sin\omega t\,\hat{i} + \tfrac{1}{2}E_1 \cos\omega t\,\hat{j}\ . \tag{A3}$$

We can transform the ion velocity into a coordinate system rotating with the electric field by writing

$$v_x = u \sin\omega t + w \cos\omega t \tag{A4}$$

and

$$v_y = u \cos\omega t - w \sin\omega t\ . \tag{A5}$$

The steady state component of velocity, u, rotates in phase with the electric field $E^+(t)$, and at resonance is given by[7]

$$u = \frac{eE_1}{2m\xi} \tag{A6}$$

A comparison of equations (A1) and (A6) gives the relation

$$K = \frac{e}{m\xi} \tag{A7}$$

with the factor of $\frac{1}{2}$ in Eq. (A6) accounting for the fact that only one circularly polarized component of the linearly polarized field is felt by the ion at resonance. Ion mobilities can thus be calculated directly from experimentally measured cyclotron resonance linewidths.

CHAPTER 3

The Interaction of Ions with Polar Neutrals: The Collision Broadening of Cyclotron Resonance Lines of Ions in the C_3H_6O Isomers

Introduction

The measurement of mobilities of ions in polar gases has been frustrated by the formation of ion clusters at the pressures utilized in conventional drift tube experiments.[1] These pressures are typically several torr to an atmosphere. Ion cyclotron resonance experiments, however, are done at pressures less than a micron where cluster formation is an unimportant process. The measurement of the cyclotron resonance linewidths of ions in polar gases is thus a unique source of information about ion polar-neutral collision processes. As discussed in Chapter 2, the width of the cyclotron resonance line of an ion in a gas provides an accurate measure of the ion neutral collision frequency for momentum transfer. This collision frequency, ξ, is directly related to the ion neutral diffusion cross section $\sigma_d(v_0)$, by Eq. (1)

$$\xi/n = \frac{M}{m+M} \langle \sigma_d(v_0) v_0 \rangle \qquad (1)$$

where m is the ion mass, M is the neutral mass, n is the neutral number density, v_0 is the relative velocity of the ion neutral pair, and the brackets indicate an average over the ion and neutral velocity distributions.[2] Estimates of the diffusion cross section can be calculated from model ion neutral interaction potentials, and comparison of the theoretical cross section with the experimental results then provides a test of the model.

Since a number of workers have measured the rates of reactions between ions and polar neutrals,[3] it is of interest to consider the relationship between reaction rate coefficients and collision frequencies for momentum transfer. The reaction rate coefficient, k, is related to the reaction cross section $\sigma_r(v_0)$, by Eq. (2), where the significance of v_0 and the brackets are the same as they are in Eq. (1). The diffusion

$$k = \langle \sigma_r(v_0) v_0 \rangle \tag{2}$$

cross section and the reaction cross section are defined in Eqs. (3) and (4).

$$\sigma_d(v_0) = 2\pi \int_0^\infty (1 - \cos\Theta)\, b\, db \tag{3}$$

$$\sigma_r(v_0) = 2\pi \int_0^\infty P_r\, b\, db \tag{4}$$

As depicted in Fig. 1, b is the impact parameter of an interacting ion molecule pair and Θ is the scattering angle. P_r is the reaction probability. In the case of a nonreactive interaction the relationship between b and Θ is defined by an ion-molecule interaction potential V(r), where r represents all the coordinates necessary to specify the relative positions of the two interacting particles. A similar ion molecule potential related b and P_r except that in the case of a reactive interaction the potential is best represented by $V(r,\rho)$ where ρ represents internuclear distances and electron probability distributions which may change as the result of making and breaking chemical bonds or the transfer of charge. The ρ dependence of $V(r,\rho)$ represents the

Figure 1

Trajectory of collision between particle A and particle B (considered infinitely massive). The solid line is the trajectory. b is the impact parameter and Θ is the scattering angle. The two are related by V(r), the interaction potential between A and B.

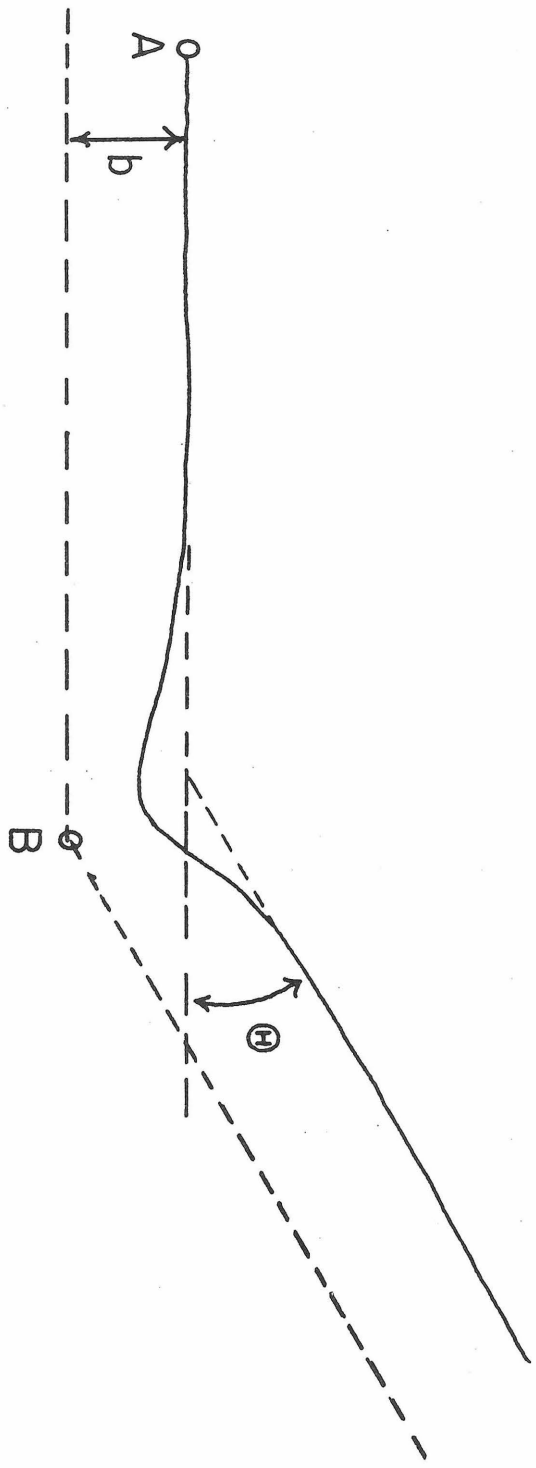
A
b
B
Θ

mechanism and reaction rates thus contains information on V(r). Generally it is not possible to measure the collision frequency of a reactive ion neutral pair since the reaction interferes with the collision frequency measurement. Thus it is not possible to separate the r and ρ dependence of $V(r,\rho)$ by direct comparison of the collision frequency and the reaction rate for a particular ion-molecule pair. The reaction rate of a reaction ion and the collision frequency of an unreactive ion with one particular neutral molecule can be measured and compared, however, and such a comparison could be helpful in characterizing the ρ dependence of $V(r,\rho)$ or the mechanism and energetics of the reaction. It is the purpose of this study to provide data so that such a comparison can be made for the interactions of ions with polar molecules.

A series of molecules was chosen for study that have the same mass and approximately the same polarizability but different dipole moments. This was done so that the effect of dipole moment could be separated from the effects of mass and polarizability. A similar approach has recently been taken in a study of the effect of dipole moment on charge exchange rates.[4] The C_3H_6O isomers fit the criteria well as indicated in Table I. The interactions of this series of molecules with one unreactive ion and two reactive ions were studied. The unreactive ion chosen was Na^+ since it could be relied upon to be unreactive with the whole series of neutrals and since it is a simple atomic species which might be expected to interact with the neutral molecules in the simplest possible way. The reactive ions chosen were CH_5^+ and $C_2H_5^+$ since they are good gas phase acids which can be expected to donate a

proton readily to all of the neutrals.[5] Both ions are formed by ion-molecule reactions which occur when methane is ionized by electron impact. Since they are good proton donors methane is frequently used as a reagent gas for chemical ionization mass spectrometry.[5] The rates of reactions of CH_5^+ and $C_2H_5^+$ with polar molecules are thus important to workers developing this promising new analytical technique.

Experimental

The ion cyclotron resonance spectrometer used for the linewidth measurements and the technique used to produce Na^+ ions are described in Chapter 2. The procedure for obtaining the spectra from which the linewidth measurements were made is identical to the procedure used to obtain the spectra from which the linewidths of ions in CH_4 and H_2 were measured. This procedure is described in Chapter 2. The C_3H_6O isomers are more subject to pyrolysis than hydrogen or methane, but the temperature of the Na^+ source was relatively low and the surface area of the filament and bead very small. The filament current was typically one amp or less, and when the filament was operated in an evacuated glass test vessel at a current of one amp the filament did not become visibly incandescent. This indicates a temperature of well below 1000 °K. No evidence of pyrolysis was observed. Pressure was measured using a capacitance manometer as described in Chapter 2. The pressure measurements were calibrated against the collision frequency of CH_5^+ in methane and the collision frequency of H_3^+ in hydrogen as described in Chapter 2. The current of ions reaching the ion collector at the end of the cell (Fig. 1 of Chapter 2) was monitored and found to be constant over the range of conditions under which the linewidth measurements were made.

As discussed in Chapter 2, the equivalence relationship between the cyclotron resonance linewidth and the ion-neutral collision frequency is invalid if the collision frequency changes significantly as the ion absorbs power from the observing field. The linewidth measurements

were therefore done in such a manner that the increase in ion energy at resonance was kept to a minimum. The marginal oscillator was set at the lowest level at which it would operate (10 mV/cm) and the pressures used were the maximum at which the signal to noise ratio was large enough above the noise level that significant linewidth measurements could be made. At 5×10^{-5} torr the lines were broadened well beyond the low pressure limit discussed in Chapter 2. The range of pressures over which the linewidth measurements were made was therefore limited to 5.0 to 50.0×10^{-5} torr. This corresponds to a range of $E_1/2P$ values from 10 V cm^{-2} sec to 100 V cm^{-2} sec.

The rates of reactions between CH_5^+ and the C_3H_6O isomers were measured using a trapped ion technique that has been described.[6] The data obtained are relative ion abundances as a function of time from which rate coefficients can be determined directly. The reactions were observed in mixtures of C_3H_6O with methane. The partial pressures of methane and C_3H_6O were determined using a Schulz-Phelps ionization gauge.[7] The ionization gauge was calibrated against a capacitance manometer for each of the gases. Two techniques were used to prepare the mixtures. One technique involved admitting methane and C_3H_6O to the spectrometer through separate sample inlets one at a time. The other involved preparing the mixtures on a vacuum manifold and admitting the mixture through a single inlet. In this latter case the Schulz-Phelps gauge was calibrated for the mixture and the known ratio of the concentrations of the two components used to determine the partial pressures. The ratio of the concentrations of the two components of

the mixtures was determined manometrically and checked by taking the mass spectrum of the mixture. Both techniques gave consistent rate measurements.

All of the C_3H_6O isomers except cyclopropanol were obtained commercially and their purity was checked by gas chromography. Trimethylene oxide was found to contain a significant impurity so it was preparatively gas chromatographed before use. The cyclopropanol was supplied by David Luippold of the California Institute of Technology.

Results

The width of the cyclotron resonance of Na^+ ions in each of the C_2H_6O isomers was plotted as a function of pressure. Least squares analysis indicated the plots to be linear to within the accuracy of the linewidth and pressure measurements. As in Chapter 2, the linearity of the plots was taken as an indication that the collision frequencies are effectively independent of ion energy over the range of ion energies sampled as the ion absorbs power from the observing field. It was therefore assumed that the linewidths are equal to the collision frequency as indicated in Eq. (4) of Chapter 2. Values of ξ/n were calculated from the slopes of the plots and are reported in Table II.

From the values of ξ/n listed in Table II and using Eq. (7) of Chapter 2, it can be determined that the ion energy at resonance for the values of E_1/P given above is never more than a factor of 4 larger than 3 kT/2 for any of the C_3H_6O isomers. The ion energy at resonance is less in cases where the ion neutral collision frequency is larger. Thus the ion energy at resonance of Na^+ ions in acetone is never more than twice 3 kT/2.

The collision frequencies of Na^+ in three of the isomers were repeated to check the reproducibility of the measurements. Fresh samples of the isomers were used. A new Na^+ filament was prepared. A different marginal oscillator was used. The gauge was recalibrated using a fresh sample of methane. The values obtained for the collision frequencies in propylene oxide, trimethylene oxide and cyclopropanol

Table II

C_3H_6O	$\xi/n \times 10^9$ [a] $cm^3\ molecule^{-1}\ sec^{-1}$		$\sigma(v)$ ($Å^2$) [b]	
	obs.	calculated	obs.	calculated
acetone	4.33±.18	4.44	897±37	920
propanol	3.93±.10	4.23	814±21	876
propylene oxide	3.36±.11	3.41	696±23	706
trimethylene oxide	2.90±.10	3.31	601±21	686
cyclopropanol	2.78±.03	3.02	576±6	626
allyl alcohol	2.90±.15	2.92	601±31	605
methyl vinyl ether	2.11±.05	2.37	437±10	491

[a] Experimental values are obtained from direct measurement of linewidths as a function of pressure. Error estimates represent standard deviation obtained in analyzing the data by the method of least squares. The calculated values are from Eq. (16) below. Polarizabilities and dipole moments used in the calculations were taken from the literature.

[b] The experimental cross sections are derived from the experimental collision frequencies using Eq. (1) below. The calculated cross sections were obtained using Eq. (15) below. Polarizabilities and dipole moments used in the calculations are the same as those used in calculating the collision frequencies. It was assumed that $1/2\ M_r v_0^2 = 3/2\ kT$.

were 3.35, 2.89, and 2.75×10^{-9} cm^3 $molecule^{-1}$ sec^{-1} in excellent agreement with the values in Table II.

The results of the trapped ion experiment in acetone are illustrated in Fig. 2. The reaction mixture is predominantly methane. The methane contains about 20% acetone. The mixture is subjected to a 10 msec ionizing pulse of 70 eV electrons. Ions formed are allowed to react for a specified time and then mass analyzed in a time short compared to the reaction time. The primary ions in methane, CH_4^+ and CH_3^+, quickly react to form CH_5^+ and $C_2H_5^+$, respectively. These two products react by proton transfer with acetone forming protonated acetone. Electron impact produces the parent ion and the fragment ion CH_3CO^+ from acetone. Both of these species react slowly to produce protonated acetone. The rate of Reaction 5 where C_3H_6O in acetone is

$$CH_5^+ + C_3H_6O \rightarrow C_3H_6OH^+ + CH_4 \qquad (5)$$

determined from the decay of CH_5^+ observed in Fig. 2. The rates of Reaction (5) and (6) where C_3H_6O is each of the other isomers in turn were similarly determined. The results are given in Table III.

$$C_2H_5^+ + C_3H_6O \rightarrow C_3H_6OH^+ + C_2H_4 \qquad (6)$$

Figure 2

The dependence of ion concentration on reaction time in a mixture of acetone and methane. Electron energy is 70 eV. The quantity on the ordinate is equal to the relative ion concentration.

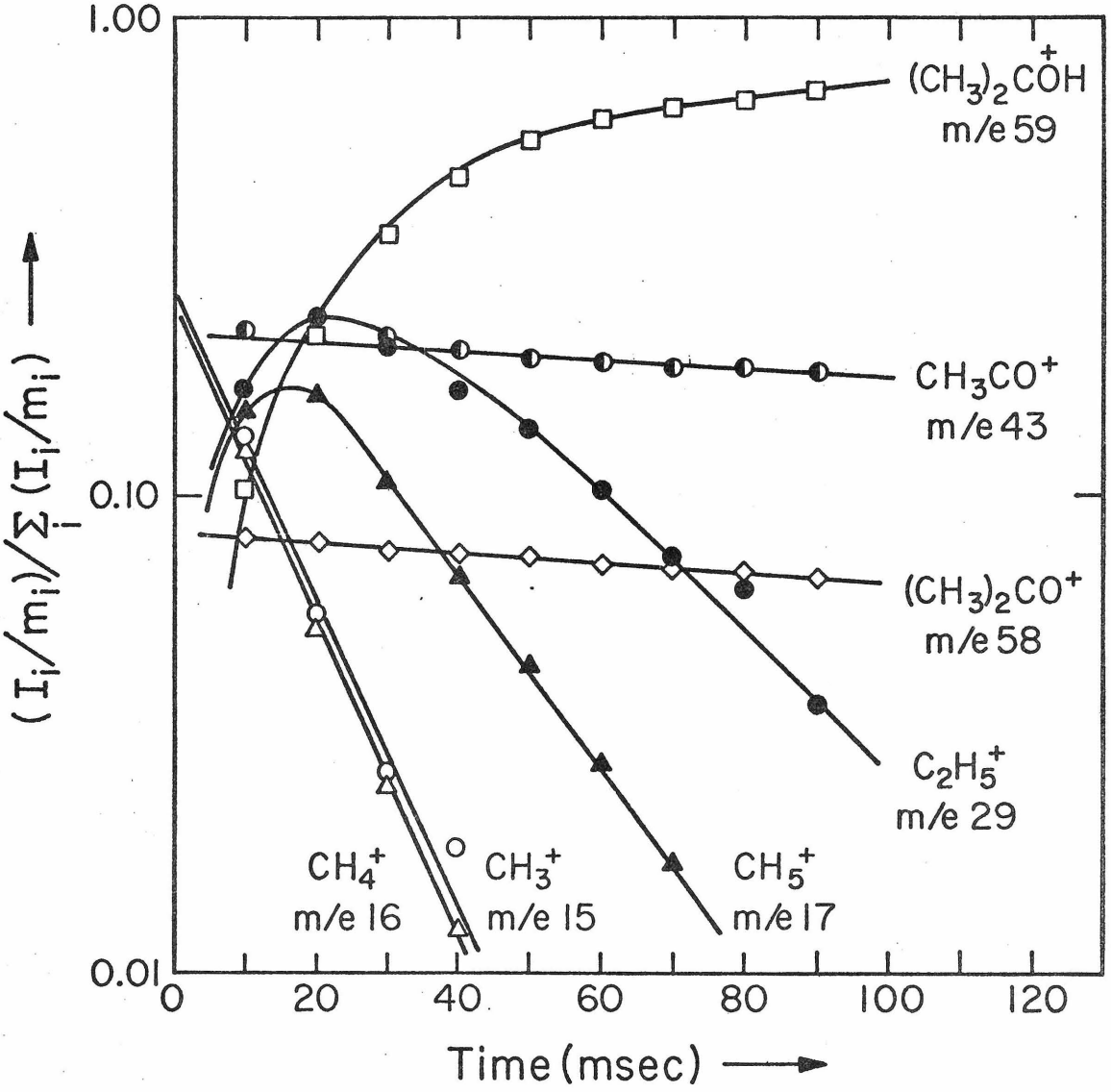
1.00
0.10
0.01
0
20
40
60
80
100
120
Time (msec)
$(I_i/m_i)/\Sigma_i (I_i/m_i)$
$(CH_3)_2\overset{+}{C}OH$
m/e 59
CH_3CO^+
m/e 43
$(CH_3)_2CO^+$
m/e 58
$C_2H_5^+$
m/e 29
CH_4^+
m/e 16
CH_3^+
m/e 15
CH_5^+
m/e 17

Table III. Rates of the Reactions of CH_5^+ With the C_3H_6O Isomers

Isomer	Rate $\times 10^9$ [a] (cm^3 $molecule^{-1}$ sec^{-1})
Acetone	3.2 ± 0.3
Acetaldehyde	2.7 ± 0.2
Propylene oxide	2.4 ± 0.2
Trimethylene oxide	2.2 ± 0.1
Allyl alcohol	1.5 ± 0.1
Methyl vinyl ether	2.1 ± 0.2

[a] Uncertainties indicate standard deviations of several measurements.

Table IV. Rates of Reactions of CH_5^+ With the C_3H_6O Isomers

Isomer	Rate $\times 10^9$ [a] (cm^3 $molecule^{-1}$ sec^{-1})
Acetone	2.15 ± 0.10
Acetaldehyde	1.6 ± 0.1
Propylene oxide	1.85 ± 0.15
Trimethylene oxide	1.1 ± 0.1
Allyl alcohol	1.1 ± 0.1
Methyl vinyl ether	0.95 ± 0.10

[a] Uncertainties indicate standard deviations of several measurements.

Discussion

The simplest theoretical model from which a collision frequency can be calculated ignores the dipole moment of the neutral and considers only the ion-induced dipole interaction. This model would be approximately valid if the polar molecule were rotating rapidly so that the dipole averaged to zero as the ion approached. In this case the potential of interaction is

$$V(r) = -\frac{\alpha e^2}{2r^4} \tag{7}$$

where α is the angle averaged polarizability of the neutral. The scattering angle Θ calculated from the ion induced dipole potential increases as the impact parameter b decreases. At a critical impact parameter b_0^p the calculated trajectory closed on itself and the collision partners move in an unstable circular orbit. At smaller impact parameter the trajectories are inward spiralling. The critical impact parameter b_0^p is given by Eq. (8)[8]

$$b_0^p = \left(\frac{4\alpha e^2}{M_r v_0^2}\right)^{\frac{1}{4}} \tag{8}$$

where M_r is the reduced mass of the ion neutral pair. If we assume that Θ is independent of b for b less than b_0^p then from Eq. (3) the diffusion cross section is given by Eq. (9). Substituting from Eq. (9)

$$\sigma_d(v_0) = \pi(b_0^p)^2 = \frac{2\pi e}{v_0}\left(\frac{\alpha}{M_r}\right)^{\frac{1}{2}} \tag{9}$$

into Eq. (1) gives Eq. (10) for the collision frequency. If we assume that the reaction probability P_r is unity for inward spiralling collisions

$$\xi/n = 2\pi e \left(\frac{M_r}{m}\right)^{\frac{1}{2}} \alpha^{\frac{1}{2}} \tag{10}$$

and zero otherwise, then Eq. (4) for the reaction cross section becomes Eq. (11). Substituting from Eq. (11) into Eq. (2) gives Eq. (12) for the

$$\sigma_r(v_0) = \pi b_0^2 = \frac{2\pi e}{v_0} \left(\frac{\alpha}{M_r}\right)^{\frac{1}{2}} \tag{11}$$

reaction rate coefficient.

$$k = 2\pi e \left(\frac{\alpha}{M_r}\right)^{\frac{1}{2}} \tag{12}$$

The effect of the dipole moment can be included in V(r) by adding a term to account for the charge dipole interaction. This gives

$$V(r) = -\frac{\alpha e^2}{2r^4} - \frac{\mu \cos\gamma}{r^2} \tag{13}$$

where μ is the neutral dipole moment and γ is the angle between the direction of the dipole moment vector and the radius vector between the ion and the molecule.

Setting this potential at its minimum ($\gamma = 0$) and calculating a critical impact parameter for orbiting collisions, b_0^p, gives Eq. (14).[9]

$$b_0^d = \left[\left(\frac{4\alpha e^2}{M_r v_0^2}\right)^{\frac{1}{2}} + \frac{2\mu e}{M_r v_0^2}\right]^{\frac{1}{2}} \tag{14}$$

The cross section for orbiting collisions $\sigma_0(v_0)$ is then given by Eq. (15).

$$\sigma_0(v_0) = \pi(b_0^d)^2 = \pi(b_0^p)^2 + \frac{2\pi\mu e}{M_r v_0^2} \tag{15}$$

If we set $\sigma_0(v_0)$ equal to $\sigma_d(v_0)$ in Eq. (1) we obtain Eq. (16).

$$\xi/n = 2\pi e \frac{M_r}{m}^{\frac{1}{2}} \left(\alpha^{\frac{1}{2}} + \frac{\mu e}{(M_r v_0^2)^{\frac{1}{2}}}\right) \tag{16}$$

Setting $\sigma_0(v_0)$ equal to $\sigma_r(v_0)$ in Eq. (2) gives Eq. (17). Note that

$$k = \frac{2\pi e}{M_r^{\frac{1}{2}}} \left(\alpha^{\frac{1}{2}} + \frac{\mu e}{(M_r v_0^2)^{\frac{1}{2}}}\right) \tag{17}$$

Eqs. (16) and (17) go to Eqs. (11) and (12) if μ is equal to zero.

The potential in Eq. (13) with γ set at zero is referred to as the locked dipole potential since setting γ at zero implies that the dipole is locked in the direction of the approaching ion keeping the attraction between the two particles at a maximum. Thus the cross section $\sigma_0(v_0)$ may be considered an upper limit for the cross section for close approach collisions. In reality the ion dipole interaction has a repulsive phase which is not accounted for in the locked dipole model. Although repulsive collisions would not be expected to lead to reaction they could

involve a large change in Θ and therefore contribute to the collision frequency. Thus $\sigma_0(v_0)$ is best considered upper limit for $\sigma_r(v_0)$ and an approximation for $\sigma_d(v_0)$. In most real situations $\sigma_d(v_0)$ would be expected to be larger than $\sigma_r(v_0)$. It could be misleading to compare experimental results to Eqs. (16) and (17) without noting these restrictions.

Such a comparison is, however, both interesting and instructive. In Fig. 3 the measured collision frequencies are plotted as a function of dipole moment. The collision frequencies of Na^+ in the C_3H_6O isomers increases linearly with the increasing dipole moment of the C_3H_6O isomer. The intercept at zero dipole moment of a line through the points agrees reasonably well with the polarization limit for the collision frequency of Na^+ interacting with a neutral having the mass and polarizability of the C_3H_6O isomers. This is the behavior predicted by the locked dipole model. In fact as indicated in the figure the quantitative agreement between the locked dipole limit for the collision frequency and the observed collision frequencies is very good for most of the isomers.

In Figs. 4 and 5 the rates of the proton transfer reactions of CH_5^+ and $C_2H_5^+$ with the C_3H_6O isomers are compared with the locked dipole and polarization limits for the rates. In both cases the rates increase with dipole moment reaching a value above the polarization limit but considerably below the locked dipole limit. This is the general trend observed in other systems where rate coefficients have been measured for reactions between ions and polar neutrals.[3]

Figure 3

The dependence of the collision frequencies of the C_3H_6O isomers with Na^+ on dipole moment. The line marked "locked dipole" was calculated from Eq. (16). The line marked "least squares" is the result of a least squares analysis of the data.

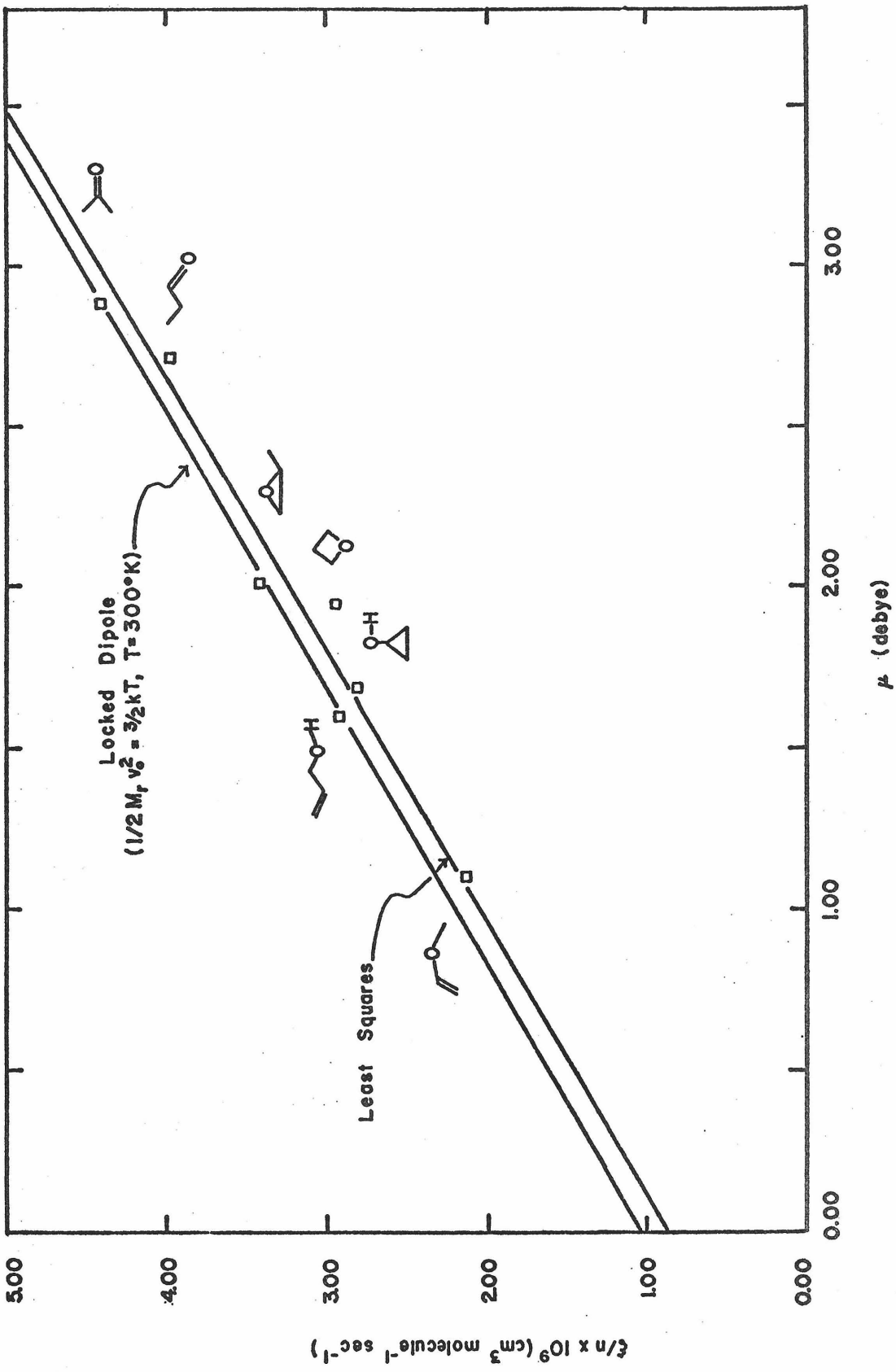
Locked Dipole
(1/2 M_r v_0^2 = 3/2 kT, T=300°K)
Least Squares
ε/n x 10^9 (cm^3 molecule^-1 sec^-1)
μ (debye)
5.00
4.00
3.00
2.00
1.00
0.00
0.00
1.00
2.00
3.00

Figure 4

The dependence of rates of reaction between CH_5^+ and the C_3H_6O isomers on dipole moment. The line marked "locked dipole" was calculated from Eq. (17). The line marked "polarization" was calculated from Eq. (12).

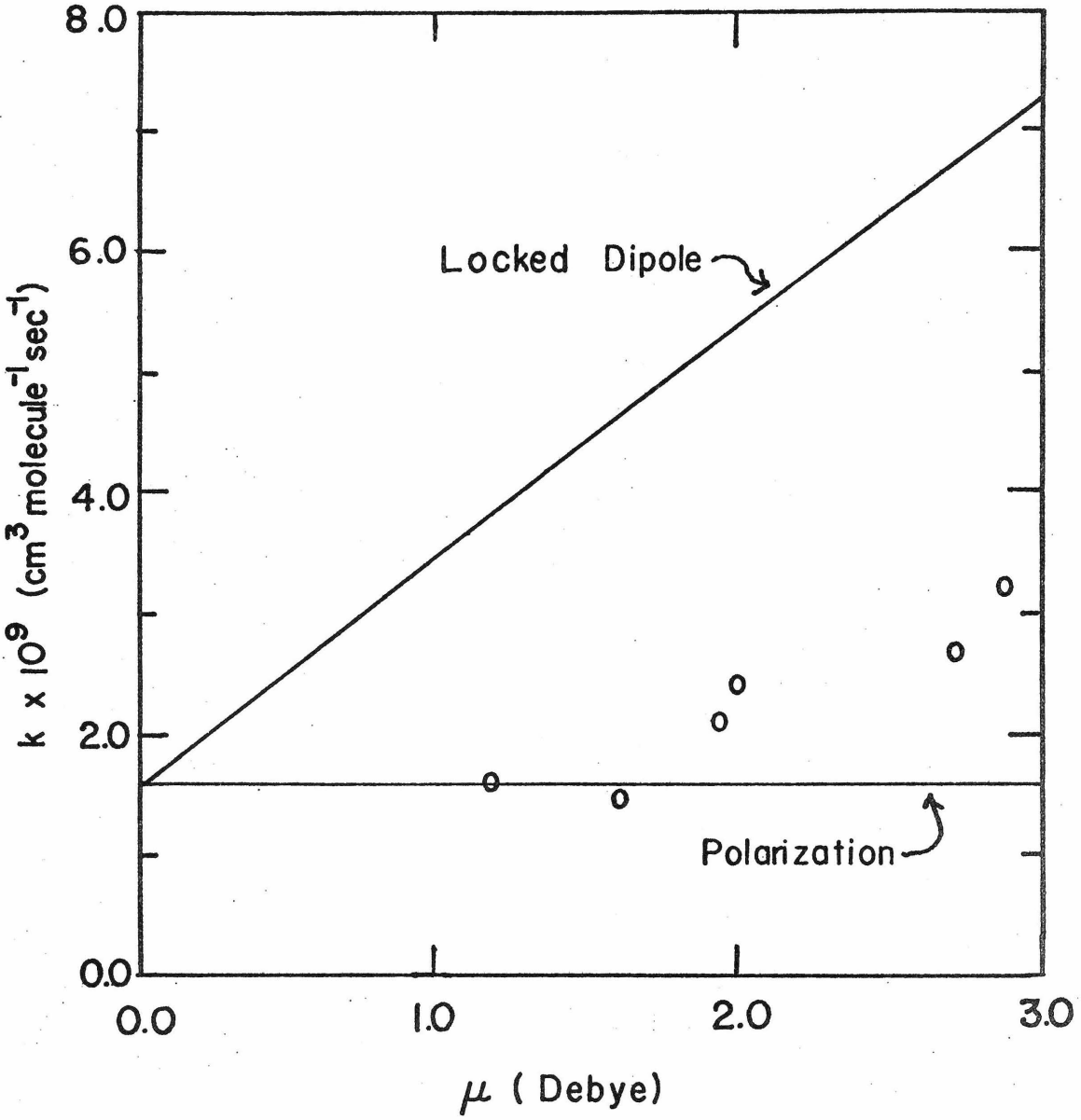
8.0
6.0
4.0
2.0
0.0
k x 10^9 (cm^3 molecule^-1 sec^-1)
Locked Dipole
Polarization
0.0
1.0
2.0
3.0
μ (Debye)

Figure 5

The dependence of the rates of reaction between $C_2H_5^+$ and the C_3H_6O isomers on dipole moment. The line marked "locked dipole" was calculated from Eq. (17). The line marked "polarization" was calculated from Eq. (12).

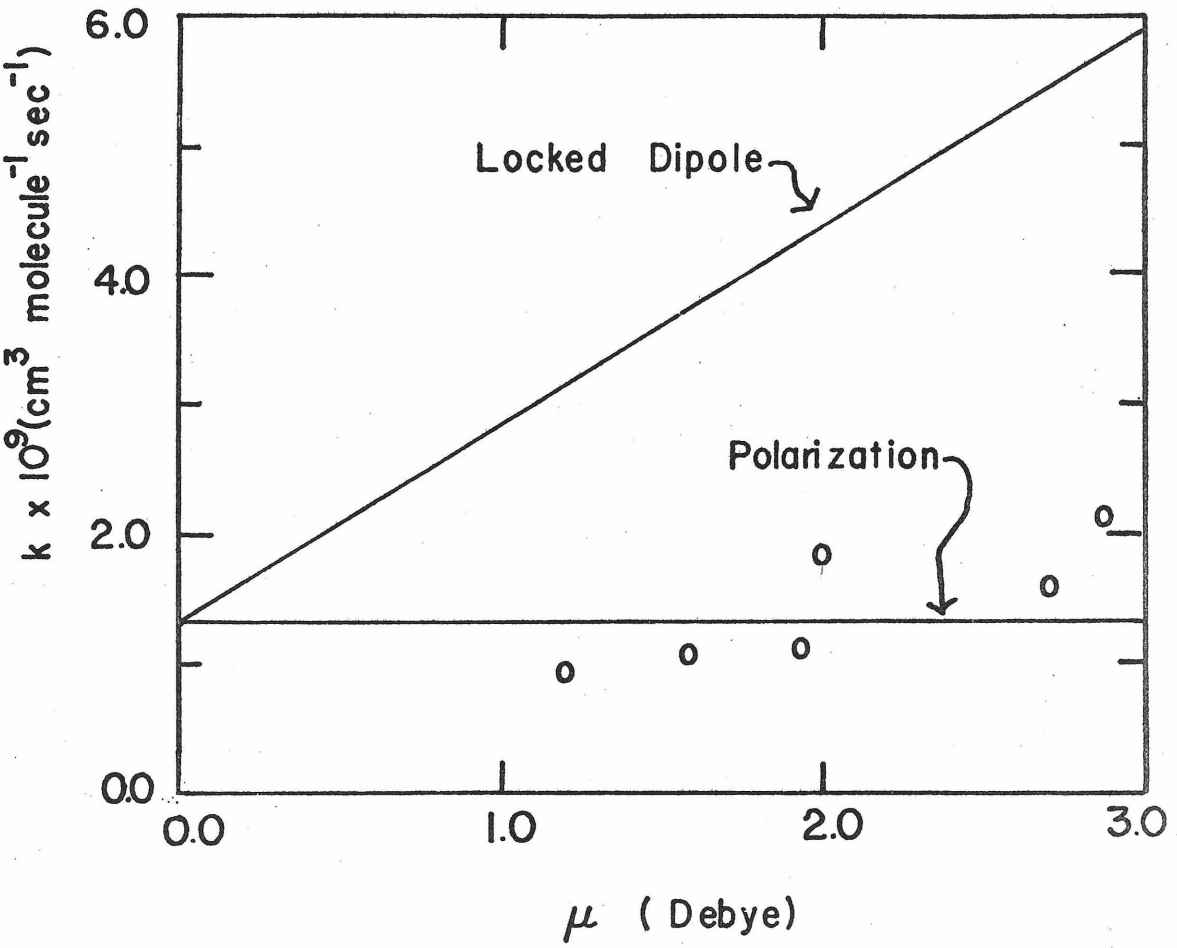
6.0
4.0
2.0
0.0
0.0
1.0
2.0
3.0
k x 10^9(cm^3 molecule^-1 sec^-1)
μ (Debye)
Locked Dipole
Polarization

If it is assumed that the general behavior of the reaction rates reflects the behavior of the cross section for close approach collisions, then these results suggest a straightforward description of the dynamics of ions with polar neutrals. If the ion and neutral approach each other at an impact parameter less than or equal to b_0^p the probability that close approach occurs and a long-lived complex is formed is close to one. If the impact parameter is between b_0^p and b_0^d then the probability that a close approach occurs drops to something less than one half. If b is between b_0^c and b_0^d, then even if a close approach does not occur there is significant interaction between the dipole moment of the neutral and the ion so that the relative velocity of the colliding pair changes in magnitude or direction or both. The result is momentum transfer so that such collisions are counted in the collision frequency but not in the reaction rate. If b is larger than b_0^d then the probability that a close approach complex forming collision occurs is zero, and the probability that momentum transfer occurs is small.

As stated above this description is merely suggested and not unambiguously implied by the present results. The description is, however, consistent with the results of the comprehensive trajectory calculations reported over the past several years.[10] The calculations were accomplished by numerical integration of the equations of motion. Trajectories are calculated for various initial conditions and a capture ratio is determined. The capture ratio is the probability that the ion and molecule approach within some specified distance (usually 2 Å is chosen). The capture ratio is found to be a decreasing function of

impact parameter. It remains relatively large up to b_0^p and drops off between b_0^p and b_0^d. The rate at which the capture ratio drops off above b_0^p increases with increasing rotational energy of the polar molecule and with decreasing dipole moment.

The close relationship observed between the dipole moment and the collision frequency suggests that dipole moments may be measured using this technique. Substituting the measured collision frequency of cyclopropanol gives 1.6 D for the previously measured dipole moment of cyclopropanol which is in the range of the dipole moments of other aliphatic alcohols. This application requires further investigation.

A number of other experiments are suggested by the present results. Studies designed to examine the effects of the mass and structure of the ion, the anisotropy of the polarizability tensor and the presence of two polar functional groups free to rotate with respect to one another on the measured collision frequencies should all prove instructive.

References

1. R. J. Munson and A. M. Tyndall, Proc. Roy. Soc. (London), A172, 28 (1939).
2. J. L. Beauchamp, J. Chem. Phys., 46, 1231 (1967).
3. (a) T. J. Moran and W. H. Hamill, J. Chem. Phys., 39, 1413 (1963); (b) S. K. Gupta, E. G. Jones, A. G. Harrison, and J. J. Myher, Can. J. Chem., 45, 3107 (1967); (c) Lucette Hellner and L. Wayne Sieck, J. Res. N. B. S., 75A, 487 (1971).
4. M. T. Bowers and J. B. Laudenslager, J. Chem. Phys., 56, 4711 (1972).
5. F. H. Field, Accts. Chem. Res., 1, 42 (1968).
6. (a) R. T. McIver, Jr., Rev. Sci. Instr., 41, 555 (1970); (b) T.B. McMahon and J. L. Beauchamp, Rev. Sci. Instr., 43, 509 (1972).
7. F. Rosenburg, Handbook of Electron Tube Techniques, (Addison Wesley, Reading, Mass., 1965).
8. E. W. McDaniel, Collision Phenomena in Ionized Gases, (John Wiley and Sons, Inc., New York, 1964) p. 70.
9. J. V. Dugan, Jr. and J. L. Magee, J. Chem. Phys., 47, 103 (1967).
10. J. V. Dugan, Jr., and J. L. Magee, Chemical Dynamics, (John Wiley and Sons, Inc., New York, 1971) pp. 207-235.

SECTION II

Studies of the Gas Phase Ion Chemistry of Fluoroethanes

CHAPTER 1

Fluorocarbonium Ion Stabilities: The Positive Ion Chemistry of Fluoroethanes in the Gas Phase

Introduction

The effect of a heteroatom substituent on the stability of methyl cations has been extensively studied.[1-6] Relatively little is known, however, about the stabilities of heteroatom substituted ethyl cations. The purpose of the present study is to provide information about the stabilities of a series of fluoroethyl cations.

The thermodynamic data on fluoroethyl cations available in the literature is summarized in Table I. The reason the data are few and somewhat inconsistent is that they are not readily accessible to measurement using conventional methods. Measurements of appearance potentials of fluoroethyl fragments of fluoroalkanes and measurements of ionization potentials of fluoroethyl radicals gives the energies required for vertical processes.[1b] The energy required for an adiabatic process may be quite different from that required for a vertical process. There is still uncertainty about thermochemical properties of the extensively studied fluoromethyl cations because of difficulty in characterizing differences between vertical and adiabatic processes.[1] A considerably larger body of thermochemical data than that tabulated in Table I is necessary, however, to an understanding of the bonding in fluoroethyl cations and the ion chemistry of fluoroalkyl cations and the ion chemistry of fluoroalkanes. The thermochemical information obtained in the present study is deduced from chemical processes other than electron or photon impact induced

Table I. Thermochemical Properties Related to Fluoroethyl Cation Stabilities [a]

R	AP (R^+) from RF [b]	AP (R^+) from RH [b]	$\Delta H^\circ_{f298}(RF)$	$\Delta H^\circ_{f298}(RH)$	$\Delta H^\circ_{f298}(R)$	IP (R) [b]	$\Delta H^\circ_{f298}(R^+)$ [c]	$D(R^+-F^-)$ [c]	$D(R^+-H^-)$ [c]
C_2H_5			-60.05 [j]	-20.24 [k]	25.9±1.3 [l]	8.38 [m]	219.1±1.3	218.6±1.3	297.8±1.3
CH_3CHF	14.80 [n]						204.4±1 [d]	261.95 [d]	297.8±1 [d]
	14.90 [p]		-118±1 [s]	-60.05 [j]			206.7±1 [e]	264.25 [e]	300.1±1 [e]
CH_3CF_2	15.14 [n]						152.1 [f]	269.79 [f]	303.5±1 [f]
	14.9±0.2 [r]						146.5±4.6 [g]	264.26±4.6 [g]	297.9±4.6 [g]
		12.33 [p]	-178.2 [s]	-118±1 [s]			114.1±1 [h]	231.8±1 [h]	265.50 [h]
CH_2FCHF			-158.9 [s]	-109 [u]					
CHF_2CHF			-209 [t]	-158.9 [s]					
CF_3CF_2			-318.2 [v]	-265.8 [w]			8.09 [v]	265.82	307.28

Table I (Cont'd)

[a] All values are in kcal/mole except ionization potentials and appearance potentials which are in eV.

[b] AP is an abbreviation for the mass spectrometric electron impact appearance potential. IP is an abbreviation for ionization potential.

[c] Values in these columns are calculated from data in preceding columns using $\Delta H^{\circ}_{f298}(H) = 52.10$, $\Delta H^{\circ}_{f298}(H^-) = 33.39$, $\Delta H^{\circ}_{f298}(F) = 18.72$, $\Delta H^{\circ}_{f298}(F^-) = -61.3 \pm 0.5$. The data on hydrogen are taken from Reference k. The data on fluorine are based on data given in W. A. Chupka and J. Berkowitz, J. Chem. Phys., 54, 5126 (1971).

[d] Calculated from AP (R^+) from RF = 14.80.

[e] Calculated from AP (R^+) from RF = 14.90.

[f] Calculated from AP (R^+) from RF = 15.14.

[g] Calculated from AP (R^+) from RF = 14.9.

[h] Calculated from AP (R^+) from RF = 12.33.

[j] Calculated from group equivalents given in Reference k.

[k] J. L. Franklin, J. G. Dillard, H. M. Rosenstock, J. T. Herron, K. Draxl, and F. H. Field, "Ionization Potentials, Appearance Potentials and Heats of Formation of Gaseous Positive Ions," Nat. Stand. Ref. Data Ser., Nat. Bur. Stand., 26 (June 1969).

[ℓ] D. B. Hartley and S. W. Benson, J. Chem. Phys., 39, 132 (1963).

[m] F. P. Lossing and G. P. Semelnk, Can. J. Chem., 48, 955 (1970).

[n] J. M. Simmie and E. Techuikow-Roux, Int. J. Mass. Spec. and Ion Physics, 7, 41 (1971).

[p] C. Lifshitz and F. A. Long, J. Phys. Chem., 69, 3731 (1965).

Table I (Cont'd)

[r] W. C. Stule and F. G. A. Stone, J. Amer. Chem. Soc., 84, 3450 (1962).

[s] J. R. Lacher and H. A. Skinner, J. Chem. Soc. A, 1034 (1968).

[t] G. E. Millward, R. Hartig and E. Tschuikow-Roux, J. Phys. Chem., 75, 3195 (1971).

[u] Estimate.

[v] R. E. Marcotte and T. O. Tiernan, J. Chem. Phys., 54, 3385 (1971).

[w] Calculated using $D(C_2F_5-H) = 103.0 \pm 1.0$ (J. E. Bassett and E. Whittle, J. Chem. Soc. Faraday I, 68, 492 (1972)) and $\Delta H^{\circ}_{f_{298}}(C_2F_5) = 214.9$ (Reference v).

ionization processes. It is most probable that the ion-molecule reactions observed are adiabatic processes so that they reflect the thermochemistry of ground state ions. Difficulties with regard to the vertical or adiabatic nature of ionization processes are thus largely obviated.

There are several possible criteria for the stability of a fluoroalkyl cation, R^+. These include the ionization potential of R, the hydride affinity of R^+, $D(R^+-H^-)$; the fluoride affinity of R^+, $D(R^+-F^-)$; and the heat of formation of R^+ relative to the heats of formation of its constituent elements in their standard states, $\Delta H^\circ_{f298}(R^+)$. These quantities are all related through the heats of formation of R, RH and RF so that measurement of any of them implies values for the others. The consequences of adopting any one of these parameters as a criterion for the stability of methyl cations has been discussed.[2] The results of the present study combined with the thermochemical data available in the literature will provide the basis for a discussion of criteria for the stability of fluoroethyl cations.

The parameter characterized by the present study is the fluoride affinity of the ions studied. A convenient means of ordering the fluoride affinities of two fluoroalkyl cations, R_1^+, and R_2^+, is to determine the direction is which equilibrium lies for Reaction 1

$$R_1^+ + R_2F \rightleftharpoons R_2^+ + R_1F . \qquad (1)$$

Ion cyclotron resonance techniques have recently been used to establish the order of fluoride affinities of the fluoromethyl cations.[3] In the present study ion cyclotron resonance techniques are used to extend the ordering of fluoride affinities to include the fluoroethyl cations.

The order of fluoride affinities together with data in Table I provides a basis for comparing the effects of hydrogen atom, fluorine atom and methyl group substituents on the stability of a methyl cation. The order also reflects the relative importance of α and β fluorine substituents in determining ethyl cation stability.

The interaction between an α fluorine atom substituent and the α carbon atom of a fluoroalkyl cation has been described in various ways. Dative π bonding between the unshared pair of electrons on the fluorine and the empty p-orbital on the carbon is the proposed mechanism by which fluoromethyl cations are stabilized.[4-6] Ab initio calculations suggest that in addition to the stabilizing π-bonding effect a destabilizing inductive effect is important in determining the overall behavior of the substituent.[4] The present study provides data useful in understanding the relative importance of the two effects.

Recently one of the fluoroethyl cations ($CH_3CF_2^+$) was observed directly in solution.[7] This and other solution studies will be given particular attention in the discussion of results of the present study.

Experimental

All gases except 1, 1 difluoroethane were obtained from Peninsular Chemresearch. The 1, 1 difluoroethane was obtained from Matheson Gas Products. They were purified by freeze-pump-thaw cycles at 78°K. Mass spectra indicated satisfactory purity in all cases. Pressures were measured using a Schulz-Phelps ionization gauge[8] calibrated against a Baratron capacitance manometer for each of the gases used. The ion trapping techniques used to obtained the relative ion abundances as a function of reaction time are described in the literature.[9,3] The standard ion cyclotron resonance apparatus and the single and double-resonance techniques are also described in the literature.[10]

Results

The 70 eV fragmentation patterns of the fluoroethanes examined are given in Table II. The primary fragmentation processes involve cleavage of the carbon-fluorine or the carbon-carbon bond. These processes are generally important in the electron impact induced fragmentation of alkyl halides.[11] Cleavage of a carbon-hydrogen bond also plays a major role in the fragmentation of some of the fluoroethanes. As a result of these processes the major fragment ions are fluoromethyl and fluoroethyl cations. Figure 1 illustrates the behavior of the fragmentation pattern with electron energy in a typical case, CH_3CHF_2. The only ion that is not a fluoromethyl or fluoroethyl cation is $C_2H_2F^+$, which is formed by a complex high-energy process and consequently disappears at low electron energy. Carbon-carbon bond cleavage gives only CF_2H^+ because the ionization potential of CF_2H is lower than that of CH_3.[2] The increasing importance of carbon-hydrogen bond cleavage relative to carbon-carbon bond cleavage with decreasing electron energy suggests that carbon-hydrogen bond cleavage is a lower energy process. This is consistent with appearance potential studies on CH_3CHF_2 (see Table I). The trifluoro- and tetrafluoroethanes form a small amount of parent ion which increases in relative abundance as the electron energy is decreased. They also lose a hydrogen atom but to a much smaller extent than ethyl fluoride and difluoroethane. The chemistry of the various fragments with their parent neutrals is discussed below.

Table II. Mass Spectra of Fluoromethanes [a]

m/e	Probable structural formula	CH_3CH_2F [b]	CH_3CHF_2	CH_3CF_3	CH_2FCHF_2	CHF_2CHF_2
15	CH_3^+			.027		
27	$C_2H_3^+$	.097				
28	$C_2H_4^+$	.038				
29	$C_2H_5^+$	.011				
31	CF^+			.017	.029	.034
32	CHF^+	.011				.024
33	CH_2F^+	.145	.018	.037	.116	.154
44	C_2HF^+		.023	.012	.020	.011
45	$C_2H_2F^+$	.038	.080	.058	.154	
46	$C_2H_3F^+$	.054	.028			
47	CH_3CHF^+	.536	.159			
48	$CH_3CH_2F^+$	.059				
51	CHF_2^+		.421		.422	.378

Table II. (Cont'd)

m/e	Probable structural formula	CH_3CH_2F [b]	CH_3CHF_2	CH_3CF_3	CH_2FCHF_2	CHF_2CHF_2
63	$C_2HF_2^+$				.019	.028
64	$C_2H_2F_2^+$		.024	.041	.042	
65	$C_2H_3F_2^+$		.229	.247	.145	
69	CF_3^+			.542		
82	$C_2HF_3^+$					.026
83	$CH_2FCF_2^+$				.014	.278
84	$CH_2FCHF_2^+$			.012	.035	.010
101	$CHF_2CF_2^+$					.035
102	$CHF_2CHF_2^+$					.022

[a] At 70 eV ionizing electron energy. The numbers given correspond to fraction of total ionization for each fragment. Fractions less than .01 are not reported.

[b] From F. W. McLafferty, Anal. Chem., 34 (1), 2 (1962).

Figure 1

Relative ion abundances as a function of electron energy in CH_3CHF_2. The quantity (I_i/m_i) is the single resonance signal intensity of the i^{th} ion divided by its mass and is proportional to its relative abundance (Reference 21). The data were taken at a pressure of approximately 1×10^{-6} Torr.

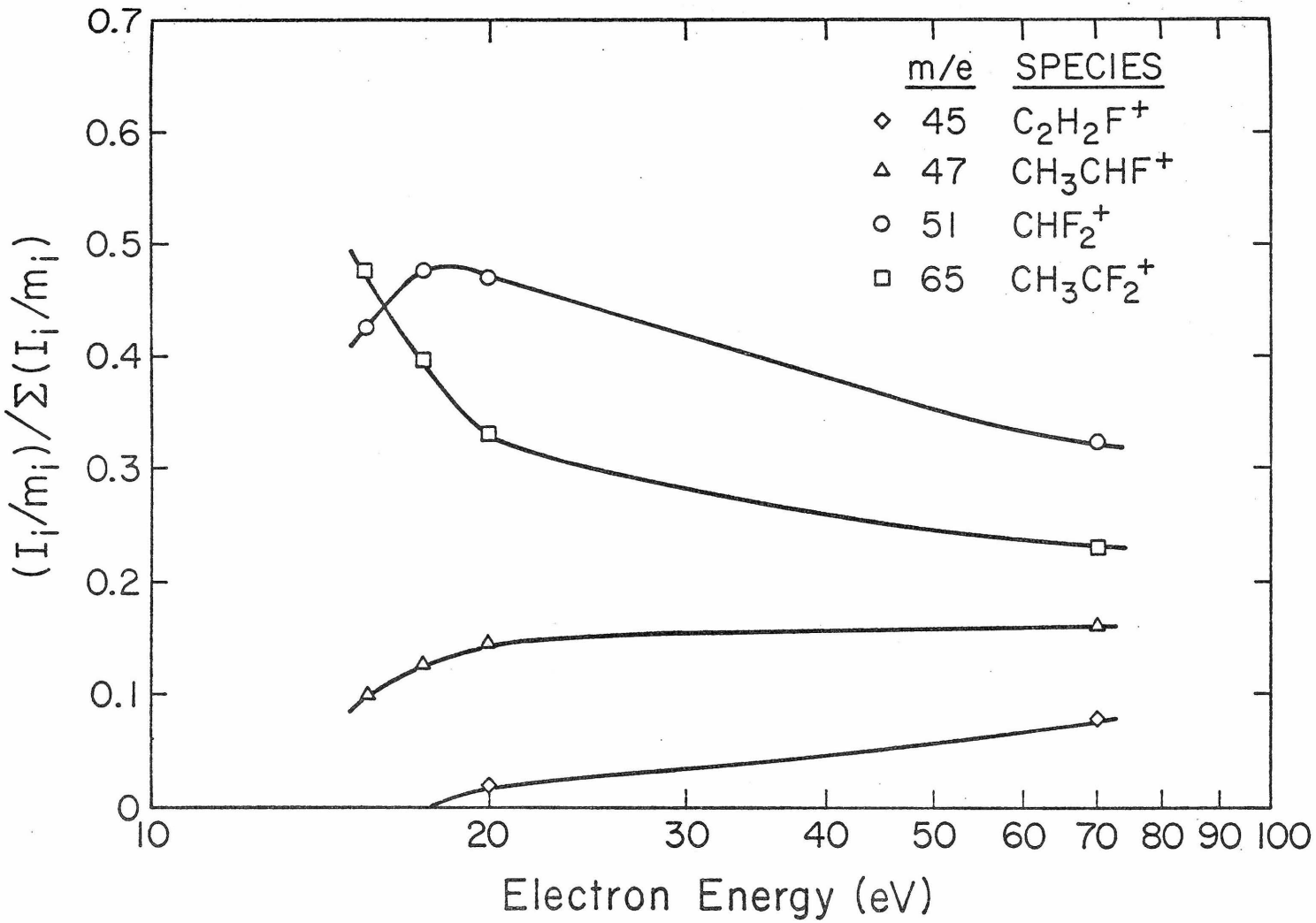
m/e SPECIES
45 $C_2H_2F^+$
47 CH_3CHF^+
51 CHF_2^+
65 $CH_3CF_2^+$
$(I_i/m_i)/\Sigma(I_i/m_i)$
0.7
0.6
0.5
0.4
0.3
0.2
0.1
0
10
20
30
40
50
60
70
80
90
100
Electron Energy (eV)

Ethyl Fluoride

The chemistry of the fragment ions of ethyl fluoride with the parent neutral have been studied previously.[12] At 13.5 eV, the electron energy used in this previous study, the only ions produced are $C_2H_5F^+$ and CH_3CHF^+. The reaction between CH_3CHF^+ and C_2H_5F has three channels as indicated in Reactions (1) to (3).

$$CH_3CHF^+ + C_2H_5F \longrightarrow \left[CH_3-\overset{\overset{F}{|}}{C}-H \quad \overset{|}{F^+}-CH_2CH_3 \right] \begin{cases} \xrightarrow{63\%} C_2H_5^+ + C_2H_4F_2 & (1) \\ \xrightarrow{<1\%} C_2H_4F_2H^+ + C_2H_4 & (2) \\ \xrightarrow{37\%} C_4H_7^+ + 2\,HF & (3) \end{cases}$$

As indicated, channel 1 accounts for 63% of the overall reaction, channel 3 for 37% and channel 2 for less than 1%. The parent ion and $C_2H_5^+$ react with the neutral in a series of rather complex reactions that will not be discussed here.

The structure of the CH_3CHF^+ ion and the mechanism of Reaction (1) have been verified by a study of the ion chemistry of CD_3CH_2F.[13] At 13.5 eV the only ions observed were $CD_3CH_2F^+$ and CD_3CHF^+. The only isotopic product of Reaction (1) was $CD_3CH_2^+$. The overall rate of Reactions (1), (2) and (3) was found to be $6.8 \pm .7 \times 10^{-10}$ cm^3 molecule^{-1} sec^{-1}. The rate of Reaction (1) is included in Table III with the rates measured in the present study.

Table III. Reactions in Pure Gases

	Reaction	Rate $\times 10^{10}$ (cm^3 $mole^{-1}$ sec^{-1})	dk/dE[b]	Thermochemical Inference[a]
2	$CH_3CHF^+ + CH_3CH_2F \rightarrow C_2H_5^+ + CH_3CHF_2$	4.3 ± 0.8	< 0	$CH_3CHF^+ > C_2H_5^+$
5	$CH_2F^+ + CH_3CHF_2 \rightarrow CH_3CHF^+ + CH_2F_2$	11 ± 2	< 0	$CH_2F^+ > CH_3CHF^+$
6	$CH_3CF_2^+ + CH_3CHF_2 \rightarrow CH_3CHF^+ + CH_3CF_3$	2.7 ± 0.5	< 0	$CH_3CF_2^+ > CH_3CHF^+$
7	$CF_3^+ + CH_2FCF_3 \rightarrow CH_3CF_2^+ + CHF_3$	6 ± 1	< 0	$CF_3^+ > CH_3CF_2^+$
8	$CH_2F^+ + CH_2FCHF_2 \rightarrow CH_2FCHF^+ + CH_2F_2$	10 ± 2	< 0	$CH_2F^+ > CH_2FCHF^+$
9	$CHF_2^+ + CH_2FCHF_2 \rightarrow CH_2FCHF^+ + CHF_3$	10 ± 2	< 0	$CHF_2^+ > CH_2FCHF^+$
12	$CHF_2^+ + CHF_2CHF_2 \rightarrow CHF_2CHF^+ + CHF_3$	< 0.2	< 0	$CHF_2^+ > CHF_2CHF^+$
13	$CH_2F^+ + CHF_2CHF_2 \rightarrow CHF_2CHF^+ + CH_2F_2$	1.8 ± 0.4	< 0	$CH_2F^+ > CHF_2CHF^+$

[a] In this column $R_1^+ > R_2^+$ meant $D(R_1^+ - F^-) > D(R_2^+ - F^-)$.

[b] dk/dE is the rate of change of the reaction with in energy as determined by double resonance.

1, 1 Difluoroethane

The chemistry of the remaining fluoroethanes is dominated by fluoride transfer processes. Two such processes, Reactions (4) and (5), are observed in 1, 1 difluoroethane. The relative abundance of the major ionic species at 17.5 eV electron energy as a function of pressure at fixed reaction time and as a function of reaction time at fixed pressure are illustrated in Figures 2 and 3.

$$CHF_2^+ + CH_3CHF_2 \longrightarrow CH_3CHF^+ + CHF_3 \qquad (4)$$

$$CH_3CF_2^+ + CH_3CHF_2 \longrightarrow CH_3CHF^+ + CH_3CF_3 \qquad (5)$$

From the data in Figure 3 the rates of Reactions (4) and (5) can be calculated. They are $k_4 = 11 \pm 2 \times 10^{-10}$ cm^3 molecule^{-1} sec^{-1} and $k_5 = 2.7 \pm .5 \times 10^{-10}$ cm^3 molecule^{-1} sec^{-1}. Reactions (4) and (5) were also observed by double resonance and in both cases dk/dE, the derivative of the reaction rate with respect to ion energy, is negative.

1, 1, 1 Trifluoroethane

Only one process is observed in 1, 1, 1 trifluoroethane, Reaction (6). The rate of Reaction (6) determined from data similar

$$CF_3^+ + CH_3CF_3 \longrightarrow CH_3CF_2^+ + CHF_3 \qquad (6)$$

to that illustrated in Figure 3 is $6.2 \pm .6 \times 10^{-10}$ cm^3 molecule^{-1} sec^{-1}. Double resonance indicates that dk/dE is negative. The parent ion does not react with the parent neutral to an observable extent.

Figure 2

Relative ion abundances as a function of pressure in CH_3CHF_2. The electron energy is 17.5 eV.

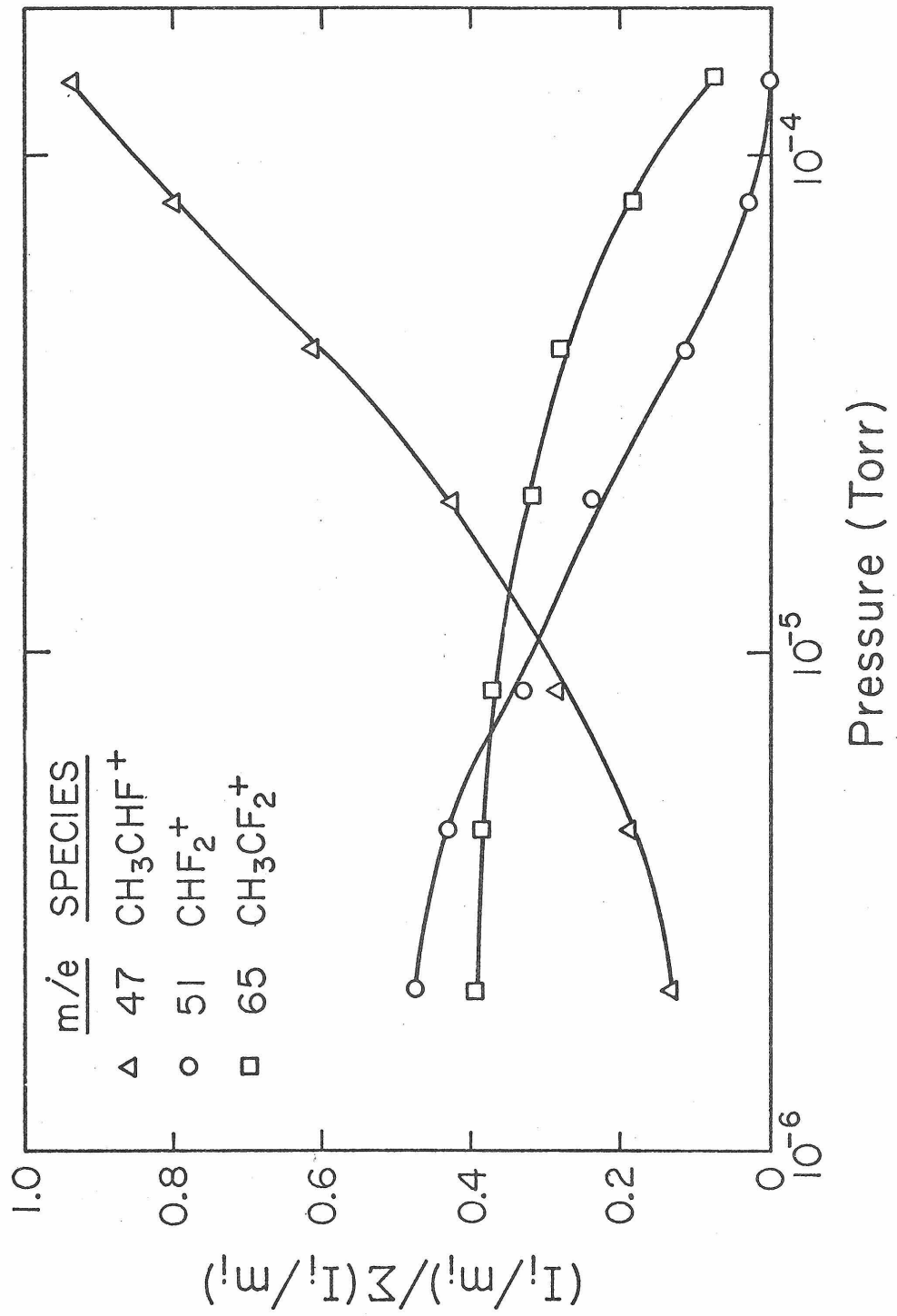
m/e SPECIES
47 CH_3CHF^+
51 CHF_2^+
65 $CH_3CF_2^+$
$(I_i/m_i)/\Sigma(I_i/m_i)$
1.0
0.8
0.6
0.4
0.2
0
10^{-6}
10^{-5}
10^{-4}
Pressure (Torr)

Figure 3

Relative ion abundances as a function of reaction time in CH_3CHF_2. The pressure is 7.0×10^{-7} Torr. The electron energy is 17.5 eV.

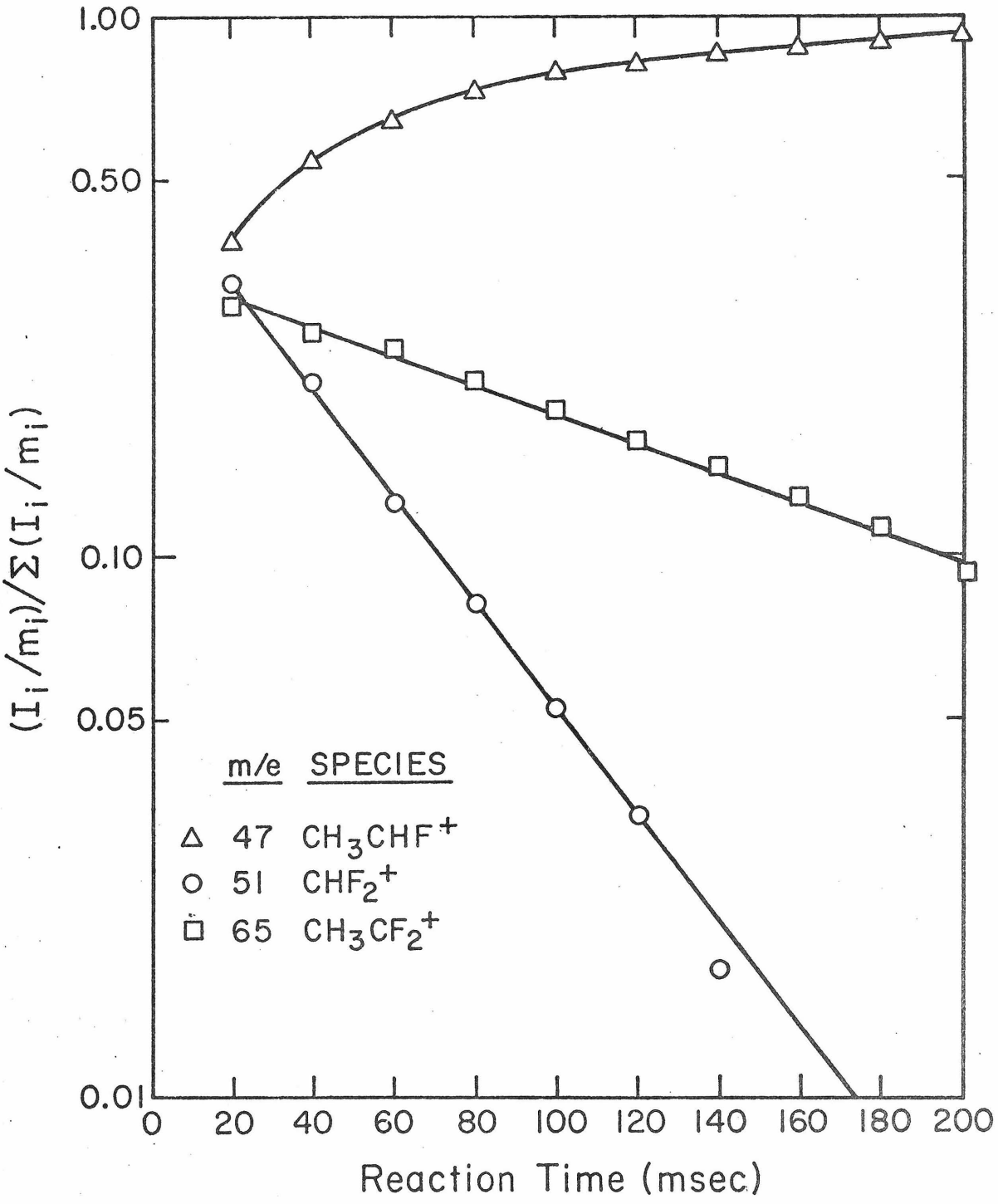
1.00
0.50
0.10
0.05
0.01
$(I_i/m_i)/\Sigma(I_i/m_i)$
m/e SPECIES
△ 47 CH_3CHF^+
○ 51 CHF_2^+
□ 65 $CH_3CF_2^+$
0 20 40 60 80 100 120 140 160 180 200
Reaction Time (msec)

1, 1, 2 Trifluoroethane

The major fragments in the 70 eV mass spectrum of 1, 1, 2 trifluoroethane are CHF_2^+ and CH_2FCHF^+. Also present are the parent ion, CH_2F^+ and $C_2H_2F^+$. The product of all observed reactions is CH_2FCHF^+ which is stable to further reaction. Reactions (7) to (9) are fluoride transfer reactions and double resonance indicates that dk/dE is negative in each case. Reaction (10) is probably a

$$CH_2F^+ + CH_2FCHF_2 \longrightarrow CH_2FCHF^+ + CH_2F_2 \quad (7)$$

$$CHF_2^+ + CH_2FCF_2H \longrightarrow CH_2FCHF^+ + CHF_3 \quad (8)$$

$$C_2H_2F^+ + CH_2FCHF_2 \longrightarrow CH_2FCHF^+ + C_2H_2F_2 \quad (9)$$

$$CH_2FCHF_2^+ + CH_2FCHF_2 \longrightarrow CH_2FCHF^+ + CH_2FCHF_2 + F \quad (10)$$

collision induced decomposition since double resonance indicates that dk/dE is positive for this reaction. Since $CHF_2CH_2^+$ is destabilized by two β-fluorine substituents, the product of Reactions (7) to (10) is considered to be CH_2FCHF^+. The mass 65 fragment ion formed by electron impact on CH_2FCHF_2 is considered to be predominantly CH_2FCHF^+ for the same reason. The destabilizing effect of β-fluorine substitution is verified by results reported below. The rates obtained are $k_7 = k_8 = k_9 = 10 \pm 2 \times 10^{-10}$ cm^3 molecule^{-1} sec^{-1}, and $k_{10} = 2.3 \pm .5 \times 10^{-10}$ cm^3 molecule^{-1} sec^{-1}. The measurements of relative ion abundance as a function of time were done at 70 eV since this was found to introduce no interfering chemistry and significantly increased the signal intensity.

1, 1, 2, 2 Tetrafluoroethane

The major fragment ion is CHF_2^+ which reacts only slowly with CHF_2CHF_2 to form CHF_2CHF^+ (Reaction (11)). The CHF_2CHF^+ ion is a significant fragment, and it is unreactive towards the parent. The CH_2F^+ ion, which must be the product of a rearrangement rather than a bond cleavage, appears in the spectrum only at electron energies above 17.5 eV and reacts according to Reaction (12). The rate

$$CHF_2^+ + CHF_2CHF_2 \longrightarrow CHF_2CHF^+ + CHF_3 \qquad (11)$$

$$CH_2F^+ + CHF_2CHF_2 \longrightarrow CHF_2CHF^+ + CH_2F_2 \qquad (12)$$

measured for reaction (12) is $1.8 \pm .4 \times 10^{-10}$ cm^3 $molecule^{-1}$ sec^{-1}, and double resonance indicates that dk/dE is negative. Although dk/dE for 11 was found to be negative and the CHF_2^+ ion decayed slowly with pressure, the ion decayed so slowly with time that only an upper limit could be established for the rate. That upper limit is 2×10^{-11} cm^3 $molecule^{-1}$ sec^{-1}.

Mixture I: $CH_3CHF_2 + CH_3CF_3$

In this mixture at long times the only ions present are CH_3CHF^+ (m/e = 47) and $CH_3CF_2^+$ (m/e = 65). In an 18.3:1 mixture of CH_3CF_3 and CH_3CHF_2 the relative abundances of the mass 65 ion and the mass 47 ion approach constant values as illustrated in Figure 3. The data illustrated in Figure 3 suggest that the equilibrium constant for Reaction (13) is 18 ± 3. If after 500 msec the

Figure 4

Relative ion abundance as a function of pressure in an 18.3 : 1 mixture of CH_3CF_3 and CH_3CHF_2. The total pressure is 1.36×10^{-6} Torr and the electron energy is 70 eV.

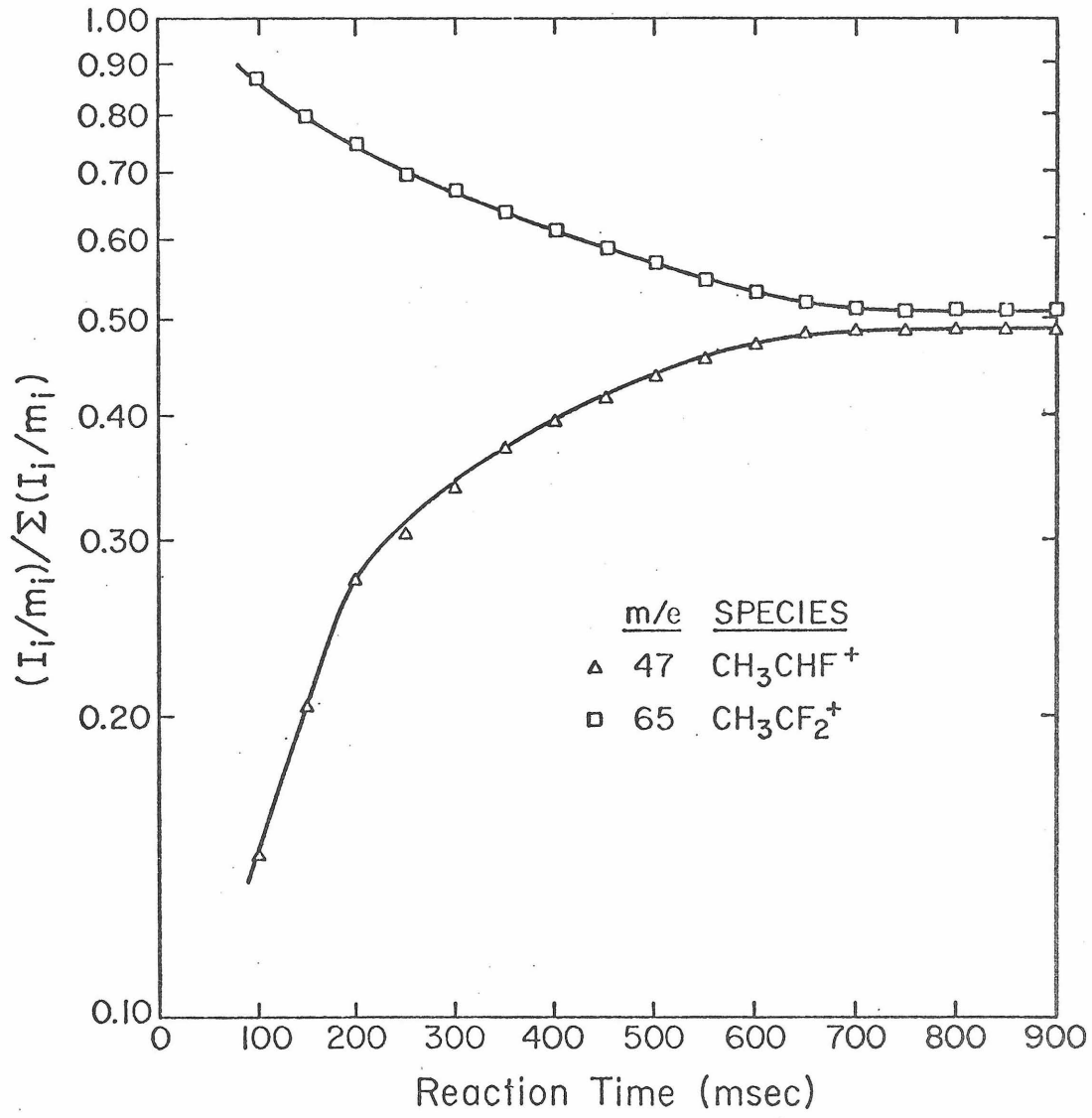
1.00
0.90
0.80
0.70
0.60
0.50
0.40
0.30
0.20
0.10
$(I_i/m_i)/\Sigma(I_i/m_i)$
0
100
200
300
400
500
600
700
800
900
Reaction Time (msec)
m/e SPECIES
47 CH_3CHF^+
65 $CH_3CF_2^+$

Figure 5

The quantity (I/I_0) represents the ratio of the single resonance signal intensity of the mass 47 ion at a time after ejection of the mass 65 into the mass 47 signal intensity just before injection. The ions are formed by 70 eV electron impact in an 18.3 : 1 mixture of CH_3CF_3 and CH_3CHF_2 at a total pressure of 1.36×10^{-6} Torr. The ions are allowed to react for 500 msec before the mass 65 is injected. As discussed in the text, the decrease in the relative signal intensity is the result of Reaction (14) in the reverse direction.

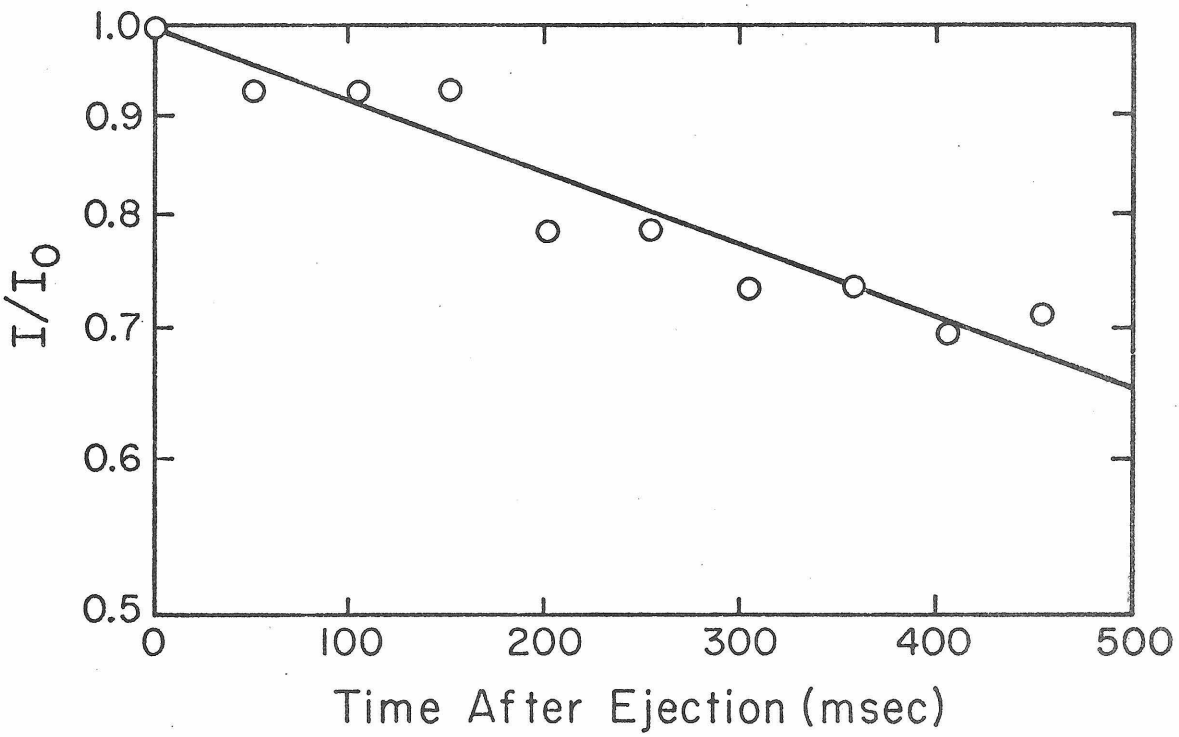
1.0
0.9
0.8
0.7
0.6
0.5
I/I0
0
100
200
300
400
500
Time After Ejection (msec)

mass 65 ion is ejected from the cell,[14] the abundance of the mass 47

$$\underset{65}{CH_3CF_2^+} + CH_3CHF_2 \longrightarrow \underset{47}{CH_3CHF^+} + CH_3CF_3 \qquad (13)$$

ion is observed to decrease exponentially as shown in Figure 4. This is direct evidence that the reverse reaction of (13) (m/e 47 → m/e 65) is important under the conditions of the present experiment and the observed approach to equilibrium is real. The rate constant for the reverse reaction determined from the data illustrated in Figure 5 is $1.8 \pm .3 \times 10^{-11}$ cm^3 molecule^{-1} sec^{-1}. The rate constant for the forward reaction (Reaction (5) above) is $2.7 \pm .5 \times 10^{-10}$. The ratio of the forward and reverse rate constants is thus 15 ± 3 in good agreement with the directly measure equilibrium constant. The average of the two equilibrium constants is 16.5 ± 3.0 which implies that for Reaction (13), $\Delta G = -1.7 \pm .1$ kcal/mole.

Mixture II: $CH_2F_2 + CHF_2CHF_2$

The chemistry of CH_2F_2 by itself has been described.[15] The major ions in the mixture are CHF_2^+, CH_2F^+ and CHF_2CHF^+. The CHF_2^+ reacts with CH_2F_2 according to 14.[3, 15]

$$CHF_2^+ + CH_2F_2 \longrightarrow CH_2F^+ + CHF_3 \qquad (14)$$

$$CH_2F^+ + CHF_2CHF_2 \longrightarrow CHF_2CHF^+ + CH_2F_2 \qquad (15)$$

The CH_2F^+ ion, which is unreactive with CH_2F_2 alone, decays in the mixture by means of Reaction (15). The rate for Reaction (15) $3.0 \pm 0.6 \times 10^{-10}$ cm^3 molecule^{-1} sec^{-1}. The decay of CH_2F^+ is

exponential even in a 10:1 mixture of CH_2F_2 and CHF_2CHF_2 at long times. The ratio of the abundances of the mass 83 and 33 ions reaches 4.2 and is still increasing in the 10:1 mixture at 400 msec. The equilibrium constant for Reaction (15) is thus greater than 42, corresponding to $\Delta G \leq -2.2$ kcal/mole for Reaction (15).

Mixture III: $CHF_2CH_2F + CHF_2CHF_2$

In this mixture the major ions at short times are CHF_2^+ and CHF_2CHF^+. As determined above CHF_2^+ reacts only slowly with CHF_2CHF_2. The decay of CHF_2^+ in this mixture is therefore attributed to Reaction (8). The rate observed is $9 \pm 2 \times 10^{-10}$ cm^3 molecule^{-1} sec^{-1} in good agreement with the rate determined in CHF_2CH_2F alone. The CHF_2CHF^+ ion decays as a result of Reaction (16). The rate constant for (16) is $3.3 \pm 6 \times 10^{-10}$ cm^3 molecule^{-1} sec^{-1}. At 350 msec

$$CHF_2CHF^+ + CH_2FCHF_2 \longrightarrow CH_2FCHF^+ + CHF_2CHF_2 \quad (16)$$

the ratio of the abundance of CH_2FCHF^+ to the abundance of CHF_2CHF^+ reached 16 in a one to one mixture. The equilibrium constant for Reaction (16) is thus greater than 16, corresponding to $\Delta G \leq -1.7$ kcal/mole.

Mixture IV: $CH_3CHF_2 + CHF_2CH_2F$

In this mixture the mass 65 ion ($C_2H_3F_2^+$) is observed to decay rapidly as CH_3CHF^+ is formed. Since the 65 ion does not decay at all in CH_2FCHF_2 alone, and slowly in CH_3CHF_2 alone, it is assumed

that Reaction (17) is the cause of the observed decay. This assumption

$$CH_2FCHF^+ + CHF_2CH_3 \longrightarrow CH_3CHF^+ + CHF_2CH_2F \qquad (17)$$

is substantiated by the observation of rapid decay of the 65 ion in a 10:1 mixture of CHF_2CH_2F and CHF_2CH_3. The rate constant for Reaction (17) is $7.8 \pm 1.6 \times 10^{-10}$ cm^3 molecule^{-1} sec^{-1}. At 400 msec in the 10:1 mixture the ratio of the abundances of the mass 47 and 65 ions reaches 4.5 and is still increasing. The equilibrium constant for Reaction (17) is thus greater than 45, corresponding to $\Delta G \leq -2.3$ kcal/mole.

Discussion and Conclusions

Since the ions in the cell are at thermal kinetic energies only thermoneutral or exothermic processes are observed. A process that is endothermic for ground state reactants may be observed if the ionic reactant is generated with sufficient vibrational energy to render the process exothermic. If several vibrational states of an ion are populated and each state reacts at a different rate, the ion will decay non-exponentially with increasing reaction time. In a mixture where both reactant and product neutral are present, a process rendered exothermic by vibrational excitation of the reactant ion would have to compete with the reverse process which is exothermic from ground state species. The result would again be non-exponential decay of the reactant ion. The only case where non-exponential decay is observed is Reaction (14). In that case, however, the final ratio of reactant and product ions gives an equilibrium constant in good agreement with the ratio of forward and reverse reaction rate constants. The observed non-exponential decay is thus best explained as the result of approach to equilibrium. Since no evidence to the contrary was obtained it is assumed that only processes exothermic for ground state ions were observed.

The following order of the fluoride affinities of fluoromethyl cations was obtained in the study described in References 3 and 15.

$$CF_3^+ > CH_3^+ > CH_2F^+ > CHF_2^+$$

A recent study of the chemistry of perfluoroalkanes establishes that $D(C_2H_5^+-F^-) > D(CF_3^+-F^-)$.[16] Combining these results with the results of the present study gives the following sequence of fluoride affinities

$$C_2F_5^+ > CF_3^+ > CH_3^+ > CH_2F^+ > CHF_2^+ > CHF_2CHF^+ >$$

$$CH_2FCHF^+ > CH_3CF_2^+ > CH_3CHF^+ > C_2H_5^+ .$$

The thermochemical inferences from the observed reactions that lead to this order of fluoride affinities are summarized in Tables III and IV.

Several of the conclusions derived from the reactions observed in mixtures of gases require comment. The limits on K_{eq} are calculated from the ratio of reactant and product ions observed at long reaction times. The limits are valid if all reactant and product species have Boltzmann kinetic energy distributions and the same temperature. The ions are not accelerated by any fields during the reaction time so this condition is satisfied. The assumption that $K_{eq} = k_f/k_r$ is used to estimate limits for k_r except in the case of Reaction (14) where k_r was measured directly.

The values of ΔS°_{f298} for each reaction were estimated using the methods of Benson.[17] The major contribution to the entropy changes were assumed to be the result of changes in symmetry numbers. Other contributions were assumed to be less than 0.3 e.u. One of the inequalities in the order of fluoride affinities could not be unequivocally verified in an appropriate mixture of gases. It was

Table IV. Reactions in Mixtures [a]

	Reaction	dK/dE	K_{eq}	$K_f \times 10^{10}$ ($cm^3\ mole^{-1}\ sec^{-1}$)	$K_r \times 10^{10}$ ($cm^3\ mole^{-1}\ sec^{-1}$)	$T\Delta S$ [b] (kcal/mole)	Relative fluoride affinity (kcal/mole)
14	$CH_3CF_2^+ + CH_3CHF_2 \rightleftharpoons CH_3CHF^+ + CH_3CF_3$	<0	16.5	2.7	0.18	+.25	$D(CH_3CF_2^+-F^-) - D(CH_3CHF^+-F^-) = 1.4$
16	$CH_2F^+ + CHF_2CHF_2 \rightleftharpoons CHF_2CHF^+ + CH_2F_2$	<0	>42	3.0	<0.07	-.42	$D(CH_2F^+-F^-) - D(CHF_2CHF^+-F^-) > 2.6$
17	$CHF_2CHF^+ + CH_2FCHF_2 \rightleftharpoons CH_2FCHF^+ + CHF_2CHF_2$	<0	>16	3.3	<0.21	+.42	$D(CHF_2CHF^+-F^-) - D(CH_2FCHF^+-F^-) > 1.3$
18	$CH_2FCHF^+ + CHF_2CH_3 \rightleftharpoons CH_3CHF^+ + CHF_2CH_2F$	<0	>45	7.8	<0.17	.00	$D(CH_2FCHF^+-F^-) - D(CH_3CHF^+-F^-) > 2.3$

[a] Data measured as explained in the text, except as noted. Estimates of experimental error given in text.

[b] Estimated as explained in the text.

deduced from results in other mixtures. The inequality $CH_2FCHF^+ > CH_3CF_2^+$ depends on the observation that Reaction (18) is more exothermic than Reaction (14). If the estimate of ΔS°_{f298} for Reactions (14) and (18) are in error the sense of the inequality could be reversed. The combined error, however, would have to exceed 3 e. u. for the inequality to be reversed. An error of this magnitude is improbable.

There are significant discrepancies between the thermochemical data in Table I and the ordering of fluoride affinities given above. These discrepancies can be removed if it is assumed that the appearance potentials of the $CH_3CF_2^+$ and CH_3CHF^+ ions from the fragmentation of CH_3CF_3 and CH_3CHF_2 do not represent the adiabatic threshold for the fragmentation processes. This assumption is supported by the fact that ΔH°_{f298} $(CH_3CF_2^+)$ derived from the appearance potential of $CH_3CF_2^+$ from CH_3CHF_2 is 35 kcal/mole less than the enthalpy of formation derived from the appearance potential of $CH_3CF_2^+$ from CH_3CF_3. The preferred value for the fluoride affinity of $CH_3CF_2^+$ is thus 231. 8 kcal/mole.

The values of the fluoride affinities and hydride affinities which are implied by the present results are summarized in Table V. The values were calculated using the data in Table I and the limits and inequalities in Table IV. Also included are the fluoride affinities and hydride affinities of the fluoromethyl cations from Reference 3.

Table V. Preferred Values of Thermochemical Parameters Related to Fluoromethyl [a] and Fluoroethyl [b] Cation Stabilities

R	$\Delta H^{\circ}_{f298}(R^+)$	$D(R^+-F^-)$	$D(R^+-H^-)$
CH_3	260.9	255.5	312.2
CH_2F	200.3	247.1	289.6
CHF_2	142.4	247.4	283.9
CF_3	99.3	260.0	299.0
CH_3CH_2	219.1	218.6	272.7
CH_3CHF	172.9 [c]	230.4 [c]	266.3 [c]
CH_3CF_2	114.1	231.8	265.5
CH_2FCHF	139.9 ± 5.7 [d]	238.3 ± 5.7 [d]	282.3 ± 5.7 [d]
CHF_2CHF	91.1 ± 5.7 [d]	239.6 ± 5.7 [d]	283.4 ± 5.7 [d]
CF_3CF_2	8.1	265.8	307.3

[a] Data for methyl cations taken from Table II of Reference 3. The fluoride affinities of the methyl cations were corrected for the difference in the value of $\Delta H^{\circ}_{f298}(F^-)$ given in footnote a of Table I and that used in Reference 3.

[b] Data from Table I selected as explained in the text with exceptions as noted.

[c] Data derived from equilibrium studies summarized in Table IV.

[d] See Results for a discussion of the limits on these numbers.

Using data from Table V we can construct a complete ordering of hydride affinities to be compared with the ordering of fluoride affinities. The order is as follows:

$$CH_3^+ > CF_3CF_2^+ > CF_3^+ > CH_2F^+ > CHF_2^+ \sim CHF_2CHF^+ > CH_2FCHF^+ > C_2H_5^+ > CH_3CHF^+ > CH_3CF_2^+$$

There are several significant differences between the sequence of hydride affinities and the sequence of fluoride affinities. An explanation of these differences is suggested by Reaction Scheme (19). The relationship between the bond strength, D(R–X), the ionization

$$\begin{array}{ccccc} & RX & \xrightarrow{D(R^+-X^-)} & R^+ + X^- & \\ D(R-X) & \downarrow & & \downarrow & -EA(X) \\ & R + X & \xrightarrow{IP(R)} & R^+ + X & \end{array} \qquad (19)$$

potential of R, IP(R); the electron affinity of X, EA(X), and the X^- affinity of R^+, $D(R^+–X^-)$, implied by (19) is given in Equation (20)

$$D(R^+–X^-) = D(R–X) + IP(R) - EA(X). \qquad (20)$$

The important consequence of Equation (20) is that the X^- affinity of R^+ depends on the R–X bond strength. The R–F bond strengths in fluoromethanes change markedly with increasing fluorine substitution while the R–H bond strengths change only slightly (Table VI). This suggests that the R–F and R–H bond strengths in fluoroethanes behave similarly accounting for the differences in the sequences of fluoride and hydride affinities.

Table VI. Bond Strengths in Fluoromethanes

R	D(R–H)	D(R–F)
CH_3	104.0 [a]	107.8 [a, b]
CH_2F	100.2 [b]	119.0 [b]
CHF_2	101.0 [b]	125.8 [b]
CF_3	105.8 [b, c]	128.1 [c]

[a] Reference K of Table I.

[b] J. A. Kerr and D. M. Timlin, Int. J. Chem. Kinet., III, 427 (1971).

[c] J. Heicklen, Advan. Photochem., 7, 57 (1969).

Replacement of a hydrogen atom by a methyl group decreases both the fluoride and hydride affinities of the methyl cation by about 39 kcal/mole. Replacement of a hydrogen atom by a fluorine atom decreases the fluoride affinity about 5 kcal/mole and the hydride affinity about 23 kcal/mole.

The relative hydride affinities of $C_2H_5^+$, CH_3CHF^+ and $CH_3CF_2^+$ parallel the hydride affinities of CH_3^+, CH_2F^+ and CHF_2^+ in that they decrease with increasing fluorine substitution. Analogous behavior is not observed for the relative fluoride affinities. Since, as explained above, the fluoride affinities could be quite strongly affected by neutral bond strengths, the hydride affinities probably reflect the electronic properties of the ion more directly. Thus we conclude that one or two β fluorine substituents stabilize the charge in fluoroethyl cations. The additional effect of the second fluorine is much less than the effect of the first fluorine. Recent molecular orbital calculations indicate that in the case of fluoromethyl cations the stabilizing effect of carbon-fluorine dative π bonding does not increase as much with increasing fluorine substitution as the destabilizing inductive effect which is the result of the electronegativity of fluorine. The present results thus suggest that the bonding in fluoroethyl cations responds to increasing fluorine substitution in a similar way.

Not surprisingly, fluoroethyl cations are destabilized by β fluorine substituents. Both fluoride and hydride affinities increase with substitution. The destabilization can be considered the result of

electrostatic interaction between the charge on the α carbon and group dipole of the fluoromethyl substituent. In fact, calculated charge dipole interaction energies are in rather good agreement with observed changes in hydride affinity with β fluorine substitution. The calculations are summarized in Table VI. The observed destabilization of a fluoroethyl cation R^+ as listed in Table VII is the hydride affinity of R^+ less the hydride affinity of R_1^+ where R_1^+ has the same number of α fluorines as the R^+ but no β fluorines. The calculated destabilization energies are calculated charge-dipole interaction energies. The dipole moments of the CH_2F, CHF_2 and CF_3 groups were taken to be equal in magnitude to the dipole moments of C_2H_5F, CH_3CHF_2 and CH_3CF_3.[18] The direction of the dipole was taken as the direction of the vector sum of the β carbon-fluorine bonds. The effective position of the dipole was taken as the middle of that vector sum. The vector sum was calculated using neutral bond lengths and angles.[18] The charge was assumed to be shared by the α carbon and its hydrogen and fluorine substituents. The center of charge was calculated from assigned bond lengths and angles and charge densities about the α carbon. The bond angles used were 120°. The bond lengths used were those used by Baird and Datta in their molecular orbital calculations on fluoromethyl cations (C–F bonds, 1.26 Å, and C–H bonds, 1.08 Å).[4] The charge densities on the carbon hydrogens and fluorines for each fluoroethyl cation were assumed to be proportional to charge densities calculated by Baird and Datta for fluoromethyl cations with the same number of fluorine substituents on

Table VII. Calculated and Observed Destabilization Energies of β-Substituted Fluoroethanes

R^+	Destabilization Energy[a] calculated[b]	observed[b]
CH_2FCHF^+	17.3	16.0 ± 5.7
CHF_2CHF^+	24.4	17.1 ± 5.7
$CF_3CF_2^+$	40.5	41.8

[a] Values in kcal/mole.

[b] Determined as explained in the text.

the trivalent carbon. For example, the charge densities on carbon, hydrogen and fluorine in CH_2F^+ calculated by Baird and Datta are +.346, +.254 and +.146, respectively. The charge density on the α fluorine in CH_2FCHF^+, and CHF_2CHF^+ thus was set at (.146)/(.346 + .254 + .146). It was also assumed that the polarizability of a methyl group does not change with fluorine substitution.

The agreement between observed and calculated values in Table VII suggests that similar calculations might be useful in estimating unmeasured thermochemical properties of other fluorine substituted organic ions.

Comparison with Solution Results

Recently the $CH_3CF_2^+$ ion was observed by nmr in a mixture of CH_3CF_3, SbF_5 and SO_2ClF at -78°C.[7] Attempts to form CH_3CHF^+ from CH_3CHF_2 under similar conditions were unsuccessful. These results were interpreted as indicating that $CH_3CF_2^+$ was stabilized relative to CH_3CHF^+ by back donation of electrons (dative π-bonding) from the second fluorine atom in $CH_3CF_2^+$. The results of the present gas phase study suggest that the energy gained from backbonding from a second fluorine atom is just about balanced by the additional inductive withdrawal of electronic charge by that fluorine. The result of this balance is that while the hydride affinity of $CH_3CF_2^+$ is slightly lower than that of CH_3CHF^+, the fluoride affinity of $CH_3CF_2^+$ is higher than that of CH_3CHF^+. The fluoride affinity of the two ions should be a measure of their relative stability in the solvent systems used in

the solution studies described above, since these solvent systems ionize by fluoride abstraction. Evidently the relative magnitude of the fluoride affinities is reversed in the presence of solvent.

Although $CH_3CF_2^+$ is the only fluoroethyl cation to be observed directly in solution, evidence was obtained that CH_3CHF_2 exchanges fluorine atoms with the solvent system SbF_5-SO_2ClF. The CH_3CHF^+ ion is probably an intermediate in the exchange. It has also been found that an intimate ion pair between ethyl cation and SbF_6^- is formed when ethyl fluoride is introduced into SbF_5-SO_2 solutions at -78°C.[20] Thus there is some evidence that fluoroethyl cations are capable of playing an interesting role in solution chemistry. As more data become available a more extensive comparison between the characteristics of solvated and gas phase fluoroethyl cations may become possible.

References

1. (a) F. P. Lossing, Bull. Soc. Chim. Belges, 81, 125-134 (1972); (b) I. P. Fisher, J. B. Homer and F. P. Lossing, J. Amer. Chem. Soc., 87, 957 (1965).
2. A. G. Harrison, C. D. Finney and J. A. Sherk, Org. Mass Spec., 1313 (1971).
3. T. B. McMahon, R. J. Blint, D. P. Ridge and J. L. Beauchamp, J. Amer. Chem. Soc., submitted for publication.
4. N. C. Baird and R. K. Datta, Can. J. Chem., 49, 3708 (1971).
5. R. W. Taft, R. H. Martin and R. W. Lampe, J. Amer. Chem. Soc., 87, 2490 (1965).
6. R. H. Martin, F. W. Lampe and R. W. Taft, J. Amer. Chem. Soc., 88, 1353 (1966).
7. G. A. Olah and Y. K. Mo, J. Org. Chem., 37, 1028 (1972).
8. This gauge is similar in construction to that described in F. Rosenburg, Handbook of Electron Tube Techniques, (Addison Wesley, Reading, Mass., 1965).
9. T. B. McMahon and J. L. Beauchamp, Rev. Sci. Instr., 43, 509 (1972).
10. J. L. Beauchamp, Ann. Rev. Phys. Chem., 22, 527 (1971).
11. F. W. McLafferty, Anal. Chem., 34, 3 (1962).
12. J. L. Beauchamp, D. Holtz, S. D. Woodgate, and S. L. Patt, J. Amer. Chem. Soc., 94, 2798 (1972).
13. J. Park, D. P. Ridge and J. L. Beauchamp, to be published.

14. See Reference 3 for a more complete description of this technique.

15. R. J. Blint, Ph.D. Thesis, California Institute of Technology, 1972.

16. See Reference v of Table I.

17. S. W. Benson, Thermochemical Kinetics, (John Wiley and Sons, Inc., New York, 1968).

18. 1.94 D, 2.27 D, and 2.31 D, respectively from Ralph D. Nelson, Jr. and Arthur A. Maryott, "Selected Values of Electric Dipole Moments for Molecules in the Gas Phase," NSRDS-NBS 10 (1967).

19. Values taken from Handbook of Chemistry and Physics, Edition 51, Robert C. Weast, Ed. (The Chemical Rubber Company, Cleveland, Ohio, 1970).

20. G. A. Olah, J. R. DeMember, R. H. Schlossberg and Y. Halpern, J. Amer. Chem. Soc., 94, 156 (1972).

21. S. E. Buttrill, Jr., J. Chem. Phys., 50, 4125 (1969).

CHAPTER 2

Based Induced Elimination Reactions in the Gas Phase Negative Ion Chemistry of Fluoroethanes: A Chemical Consequence of Strong Hydrogen Bonding

Introduction

The strong hydrogen bond, formed by the binding of two n-donor bases to a labile proton, participates in a variety of gas phase ion-molecule reactions. The processes in which strong hydrogen bonding has been observed to play an important role include nucleophilic substitution reactions,[1-3] acid induced elimination reactions,[3-5] and a novel class of associative fragmentation reactions.[6] These reactions involve at one or more stages the binding of the base A to the conjugate acid of the base B, forming AHB^+ (Reaction (1)).

$$A + BH^+ \longrightarrow AHB^+ \qquad (1)$$

Strong hydrogen bonding of the type illustrated in Reaction (1) is, for example, effective in promoting gas phase acid induced elimination reactions such as the dehydration of alcohols illustrated in Reaction (2).[3-5]

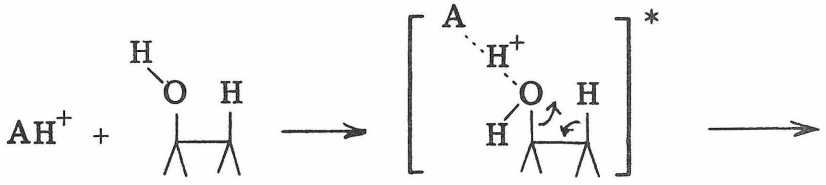

(2)

As indicated in Table I the strength of the bond between A and BH^+ (the negative enthalpy change for Reaction (1)) can be as large as 35 kcal/mole. The bond strengths in Table I were measured

Table I. Hydrogen Bond Strengths in Some Proton Bound Dimers

Process	$-\Delta H$, kcal/mol	Ref.
$H_3O^+ + H_2O \rightarrow (H_2O)_2H^+$	32, 36	a, b
$CH_3OH_2^+ + CH_3OH \rightarrow (CH_3OH)_2H^+$	31	c
$NH_4^+ + NH_3 \rightarrow (NH_3)_2H^+$	27	d

[a] M. DePaz, J. J. Levanthal, and L. Friedman, J. Chem. Phys., 51, 3748 (1969).

[b] P. Kebarle, S. K. Searles, Z. Zolla, J. Scarborough, and M. Ashadi, J. Amer. Chem. Soc., 89, 6393 (1967).

[c] P. Kebarle, R. N. Haynes, and J. G. Collins, ibid., 89, 5753 (1967).

[d] S. K. Searles and P. Kebarle, J. Phys. Chem., 72, 742 (1968).

by Kebarle and co-workers using a mass spectrometer with a high pressure source designed for observing equilibrium concentrations of ions in gases. Equilibrium constants for reactions such as Reaction (1) are measured as a function of temperature, and the free energy, entropy and enthalpy changes for the reaction are determined from a van't Hoff plot.[7] Kebarle and his co-workers have made similar measurements on systems of the type

$$X^- + YH \longrightarrow XHY^- . \qquad (3)$$

The results of these measurements, summarized in Table II, indicate that the bond between the base X^- and the acid YH can be nearly as strong as that between the base A and the acid BH^+. This suggests that by analogy with Reaction (2) the type of strong hydrogen bonding illustrated in Reaction (3) may be expected to participate in the base induced elimination reaction generalized by Reaction (4). The enthalpy

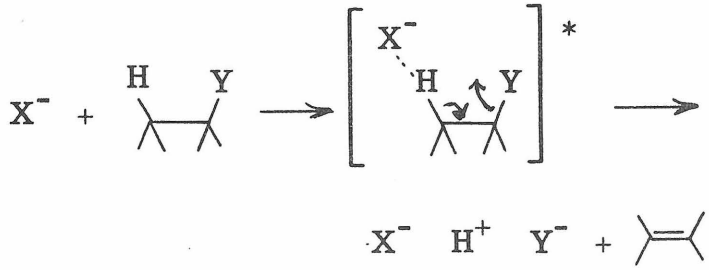

(4)

changes for the removal of HY (hydrogen halides and water) from a number of compounds of the type RY (haloethanes and ethanol) are listed in Table III. Comparison of these enthalpy changes with the bond strengths in Table II suggest that sufficient energy is available

Table II. Bond Strengths in Anionic Dimers[a]

X^-	HY	$D(X^- - HY)$	$D(XH - Y^-)$[e]
F^-	HOH	23[b]	44
F^-	CH_3OH	24[d]	40
F^-	HF	30[c]	30
Cl^-	HOH	13.1[b]	70.1
Cl^-	CH_3OH	14.1[b]	66
Cl^-	HCl	24[c]	24
Cl^-	HF	14[c]	50

[a] Bond strengths in kcal/mole.

[b] Experimentally measured bond strengths from Reference 7.

[c] Estimated bond strengths from Reference 7. Estimates based on trends observed in measured bond strengths.

[d] Calculated assuming $D(CH_3OH - F^-) - D(HOH - F^-) = D(CH_3OH - Cl^-) - D(CH_3OH - Cl^-)$.

[e] These values calculated from $D(X^- - H^+)$, $D(Y^- - H^+)$ and $D(X^- - HY)$. Values of $D(X^- - H^+)$ and $D(Y^- - H^+)$ were taken from Reference 7 except $D(CH_3O^- - H^+)$ which was taken as 385 kcal/mole (D. Holtz, J. L. Beauchamp and J. R. Eyler, J. Amer. Chem. Soc., 92, 7045 (1970)).

Table III. Enthalpy Changes for Removal of HX from RX[a]

RX	HX	ΔH[b]	$\Delta H - D(CH_3O^- - HX)$[c]	$\Delta H - D(F^- - HX)$[c]
CH_3CH_2Cl	HCl	16.7	-49	-33
CH_3CHCl_2	HCl	17.1	-49	-33
CH_3CCl_3	HCl	12.8	-53	-37
CH_3CH_2OH	HOH	10.9	–	-12
CH_3CH_2F	HF	7.8	-32	-22
CH_3CHF_2	HF	25.2	-15	-5
CH_3CF_3	HF	33.4	-7	+3
CH_2FCHF_2	HF	14.1[d]	-26	-16
CHF_2CHF_2	HF	25.7	-14	-4

[a] All data in kcal/mole.

[b] Calculated using the heats of formation of the haloethanes (except CHF_2CHF_2), CH_2CF_2 and CF_2CHF from J. R. Skinner and H. A. Lacher, J. Chem. Soc. A, 1968, 1034. The heat of formation of CHF_2CHF_2 used is from G. E. Millward, R. Hartig and E. Tschuikow-Roux, J. Phys. Chem., 75, 3195 (1971). All other heats of formation ised in the calculations are from J. L. Franklin, J. G. Dillard, H. M. Rosenstock, J. T. Herron, K. Draxl and F. H. Field, "Ionization Potentials, and Heats of Formation of Gaseous Positive Ions," NSRDS-NBS 26, U. S. Government Printing Office, Washington, D. C., 1969.

[c] Calculated using bond strengths from Table II.

[d] Calculated assuming the product is CH_2CF_2. The reaction actually observed is believed to involve formation of CHFCHF (see Results below), but a reliable heat of formation for CHFCHF is not available.

from the formation of a bond between an anionic base and the leaving group HY to render Reaction (4) exothermic for an appropriate choice of reactants. This is verified for specific cases by the numbers in columns 4 and 5 of Table III. Reaction (4) where RY is ethyl fluoride and X^- is F^-, for example, is predicted to be 22 kcal/mole exothermic. If X^- is CH_3O^- and RY is ethyl fluoride then Reaction (4) is 33 kcal/mole exothermic. Exothermicity may be considered a necessary (but not sufficient) condition for a reaction between thermal energy reactions to proceed.[8] The data in Table III thus suggest that 1, 2 elimination of hydrogen halide may be important in the reactions of basic anions with alkyl halides. Efforts to characterize the elimination process of Reaction (4) thus led to the investigation of the reactions of CH_3O^-, a relatively strong base in the gas phase,[9] with a series of alkyl halide substrates. The results of this investigation are reported below.

Some trends observed in the bond strength measurements of Kebarle are useful in interpreting the results of the present experiments. The bond strength $D(RH-X^-)$ was observed to increase with the acidity of RH and decrease with the acidity of XH.[7] The acidity of RH is defined as $-D(R^- - H^+)$. These trends imply that if RH has several protons an anion X^- will be most strongly bound to the most acidic proton. An obvious example is that F^- is expected to form a stronger bond to the hydroxylic hydrogen in methanol than to the methyl hydrogens. A second implication of these trends is that if Reaction (5) is exothermic then R_1H is more acidic than R_2H.

$$R_1HX^- + R_2H \longrightarrow R_2HX^- + R_1H \qquad (5)$$

Experimental

All experiments were performed using a standard ion cyclotron resonance spectrometer modified as noted.

The reactant ion CH_3O^- can be generated from CH_3ONO by low energy electron attachment.[9,10] The process is probably analogous to that by which ethoxide anion is formed from ethyl nitrite.[11] Methyl nitrite-d_3 was used in the present experiments so that CH_3O^- (mass 31) could be distinguished from HNO^- (mass 31). In CD_3ONO at 1.75 eV electron energy the major ions are CD_3O^- (mass 34) and DNO^- (mass 32). These two species appear in a ratio of 10 to 1. In addition, small peaks at masses 46 (NO_2^-), 62 ($CD_2NO_2^-$) and 64 ($CD_3NO_2^-$) are present in the spectrum. As the electron energy is raised, the intensity of the mass 34 signal first decreases and then around 20 eV increases again. This increase at higher electron energy is probably the result of attachment of scattered electrons but could be in part the result of a pair process. The methoxide anion is observed to react slowly with methyl nitrite to form NO_2^-.[12] No other reactions were observed in methyl nitrite alone.

In a typical experiment CD_3ONO is admitted to the analyzer of the ion cyclotron resonance spectrometer to a pressure of 10^{-6} torr. The alkyl halide is admitted through a second sample inlet so that its pressure could be varied independently. Reactions were identified both by double-resonance experiments and by the variation of relative

single-resonance intensities with partial pressure of the alkyl halide.[13] No negative ions were observed in any of the alkyl halides alone. The range of alkyl halide partial pressures was 1 to 20×10^{-5} torr. Reactions with CD_3ONO neutrals are assumed unimportant under these conditions.

In the normal single-resonance experiment the power absorbed by the ions from the detecting RF field is modulated in some way to produce an AC signal which can be detected more efficiently than a DC signal. For positive ions this can be accomplished by modulating the electron energy since at low electron energies no ionization occurs and power absorption drops to zero. Since, as noted above, negative ions are formed at both high and low electron energies another modulation scheme is necessary. The scheme chosen was trapping voltage modulation. Applying a positive potential to the trapping plates quickly removes all negative ions from the cell and the drops the power absorption to zero.

Since negative ionization processes cannot be stopped simply by changing the energy of the electron beam, it was not possible to measure negative ion reaction rates using ion trapping techniques that have been used in this laboratory to measure positive ion reaction rates.[14] Rates were therefore determined from single-resonance intensity versus pressure data by the method of Marshall and Butrill.[15]

The CD_3ONO was prepared by the method described by D'Amore[12] using CD_3OH of 99 atom % purity supplied by Stohler Isotope Chemical Company. The single-resonance spectrum of the CD_3ONO indicated acceptable purity. The CH_3ONO used in several of the experiments was prepared by the same method. Its purity was checked by nmr. All the fluoroethanes were supplied by Peninsular Chemresearch except 1, 1 difluoroethane which was supplied by Matheson. Ethyl chloride was also supplied by Matheson. They were used as supplied except for freeze-pump-thaw cycles to remove non-condensable gases. Samples of cis and trans 2-chlorocyclopentanol were generously provided by Jhong Kim of the University of California at Riverside. The CD_3CH_2F was supplied by John Park of the California Institute of Technology. The 1, 1, 1 trichloroethane, the ethyl bromide and the β-chloroethanol were supplied by Matheson, Coleman and Bell. The β-bromoethane was supplied by Eastman Kodak.

Results

As ethyl fluoride is added to methyl nitrate-d_3 the CD_3O^- disappears and the ions of masses 19 (F^-), 39 (FHF^-), 47 ($^-CH_2CHF$), 54 (CD_3OHF^-) and 67 ($CH_2FCH_3F^-$) appear. Double-resonance indicates that CD_2O^- reacts to form F^-, $^-CH_2CH_2F$ and CD_3OHF^-; that $^-CH_2CH_2F$ reacts to form $CH_2FCH_3F^-$ and that F^- reacts to form FHF^-. In CD_3CH_2F the products are F^-, FDF^-, $^-CD_2CH_2F$, CD_3ODF^-, and $CH_2FCD_3F^-$. These are the only isotopic products observed. The variation of ion abundances with CD_3CH_2F pressure is illustrated in Figure 1. Double resonance in CD_3CH_2F indicates that CD_3O^- reacts to form F^-, $^-CD_2CH_2F$ and CD_3ODF^-; that F^- reacts to form FDF^- and that $^-CD_2CH_2F$ reacts to form $CH_2FCD_3F^-$. These data are consistent with the proposed Reactions (6)-(10) and suggest that the β-protons are more acidic than the α-protons.

$$CH_3O^- + CH_3CH_2F \xrightarrow{29\%} \underset{54}{CD_3OHF^-} + CH_2CH_2 \qquad (6)$$

$$CH_3O^- + CH_3CH_2F \xrightarrow{34\%} \underset{47}{^-CH_2CH_2F} + CD_3OH \qquad (7)$$

$$CH_3O^- + CH_3CH_2F \xrightarrow{37\%} \underset{19}{F^-} + CD_3OCH_2CH_3 \text{ or } CD_3OH + CH_2CH_2 \qquad (8)$$

$$\underset{47}{^-CH_2CH_2F} + CH_3CH_2F \longrightarrow \underset{67}{CH_2FCH_3F^-} + CH_2CH_2 \qquad (9)$$

$$\underset{19}{F^-} + CH_3CH_2F \longrightarrow \underset{39}{FHF^-} + CH_2CH_2 \qquad (10)$$

Figure 1

Relative negative in abundances as a function of the partial pressure of CD_3CFH_2 in a mixture of CD_3CFH_2 and CD_3ONO. The pressure of CD_3ONO is kept constant as the CD_3CFH_2 pressure is varied. The quantity I_i/m_i used in this and subsequent figures is the ratio of the single resonance signal intensity and the mass of "ith" ion and is proportional to the concentration of the "ith" ion (Reference 25).

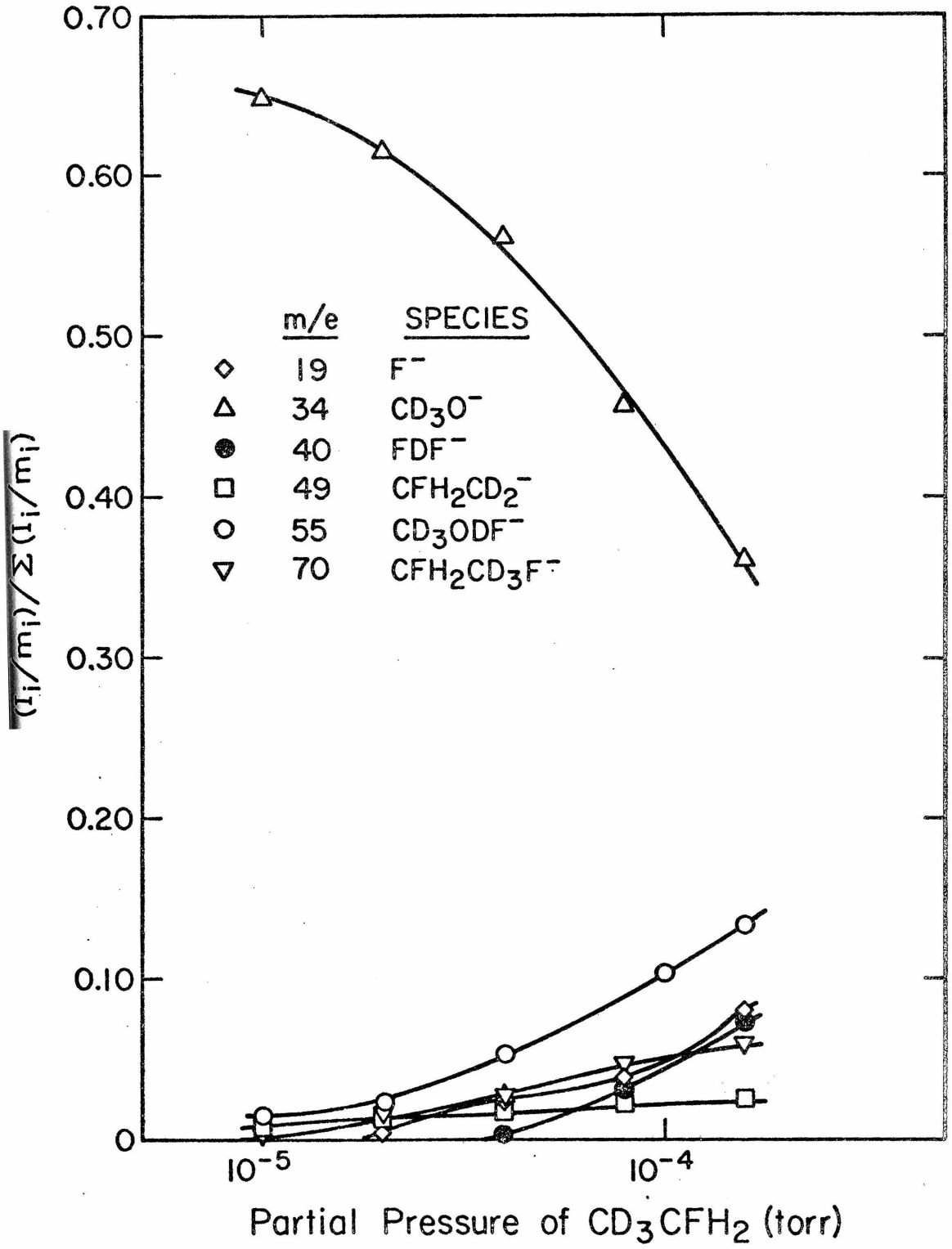
0.70
0.60
0.50
0.40
0.30
0.20
0.10
0
$(I_i/m_i)/\Sigma(I_i/m_i)$
m/e SPECIES
19 F^-
34 CD_3O^-
40 FDF^-
49 $CFH_2CD_2^-$
55 CD_3ODF^-
70 $CFH_2CD_3F^-$
10^{-5}
10^{-4}
Partial Pressure of CD_3CFH_2 (torr)

When a mixture of CD_3CH_2F and CH_3CH_2F is added to CD_3ONO ions of mass 67 ($CH_2FCH_3F^-$) and 70 ($CH_2FCD_3F^-$) appear, but no ions of mass 68 ($CH_2FCH_2DF^-$) and 69 ($CH_2FCD_2HF^-$) are observed. Double resonance indicates that $^-CH_2CH_2F$ and $^-CD_2CH_2F$ each react to form both 67 and 70. These data show that as indicated in Reaction (11)

$$\underset{49}{^-CD_2CH_2F} + CH_3CH_2F \longrightarrow \underset{67}{CH_2FCH_3F^-} + CD_2CH_2 \qquad (11)$$

Reaction (9) proceeds by the transfer of F^- from the ion to the neutral rather than by the transfer of DF from the neutral to the ion. Double resonance in this mixture indicates that Reaction (12) proceeds with $dk/dE < 0$ in both directions indicating that the mass 67 and 70 ions

$$^-FCH_3CH_2F + CH_3CH_2F \longrightarrow {}^-FCD_3CH_2F + CH_3CH_2F \qquad (12)$$

have a labile fluorine. The labile fluorine is assumed to be attached to one of the acidic β protons. This is consistent with the finding of Kebarle et al.[7] that the strength of the X^-–HR bond increases with the acidity of HR. Product neutrals are not directly identified. The neutral products written for Reactions (6)-(10) are the most thermodynamically stable products consistent with the ionic products observed. The added gas, CH_3CH_2F, is assumed to be the reactant neutral in each case since the product ions only appear when CH_3CH_2F is present. In addition, the product ions increase in relative concentration when the partial pressure of CH_3CH_2F is increased.

Under the conditions of the experiment, product neutrals are present only in concentrations smaller than the CH_3CH_2F concentrations by at least a factor of 10^5. Products of their reactions are therefore not observed. The bimolecular rate constants were invariant within the accuracy of the method over a tenfold increase in pressure. The rates are summarized in Table IV. The uncertainties are standard deviations of determinations based on data taken at pressures ranging from 20×10^{-5} torr to 18.5×10^{-5} torr. Thus the reactant and product ions and the reactant neutrals for Reactions (6)-(10) are definitely identified. The processed are bimolecular, and the reactions as written are consistent with isotopic labeling results.

1, 1 Difluoroethane

The product ions observed when CH_3CHF_2 is added to CD_3ONO have masses of 54 (CD_3OHF^-), 65 ($^-CH_2CHF_2$) and 85 ($CHF_2CH_3F^-$). The variation of ion abundance with CH_3CHF_2 pressure is illustrated in Figure 2. Double resonance indicates that CD_3OHF^- and $^-CH_2CHF_2$ come from CD_3O^- and that $CHF_2CH_3F^-$ comes from $^-CH_2CHF_2$ and CD_3OHF^-. These data are consistent with Reactions (13) to (16). At 70 eV a small amount of F^- was observed. Double resonance gave no indication that it was the product of any reaction. It disappeared when the electron energy was dropped to 1.75 eV. It was therefore assumed to be the product of electron impact induced ion pair formation from CH_3CHF_2. The mass 65 ion is written $^-CH_2CHF_2$ implying loss of a β proton by analogy with ethyl fluoride where loss of a β

Table IV. Negative Ion Reactions in Fluoroethanes

Reactant gas		Reactant ion		Product ion		Product neutral	Rate × 10^{19} (cm^3 $mole^{-1}$ sec^{-1})	
CH_3CH_2F	+	CD_3O^-	→	CD_3OHF^-	+	CH_2CH_2	0.38 ± 0.12	(6)
			→	$^-CH_2CH_2F$	+	CD_3OH	0.44 ± 0.09	(7)
			→	F^-	+	$CH_3CH_2OCD_3$	0.47 ± 0.06	(8)
	+	F^-	→	FHF^-	+	CH_2CH_2	1.32 ± 0.06	(9)
CH_3CH_2F	+	$^-CH_2CH_2F$	→	$CH_2FCH_3F^-$	+	CH_2CH_2	1.87 ± 0.24	(10)
CH_3CF_3	+	CD_3O^-	→	CD_3OHF^-	+	CH_2CF_2	14.4 ± 2.0	(17)
			→	$^-CH_2CF_3$	+	CD_3OH	1.1 ± 0.4	(18)
	+	$^-CH_2CF_3$	→	$CF_3CH_3F^-$	+	CH_2CF_2	7.9 ± 0.9	(19)
CH_3CHF_2	+	CD_3O^-	→	CD_3OHF^-	+	CH_2CHF	9.0 ± 2.4	(13)
			→	$^-CH_2CHF_2$	+	CD_3OH	3.6 ± 1.5	(14)
	+	$^-CH_2CHF_2$	→	$CHF_2CH_3F^-$	+	CH_2CHF	1.5 ± 0.4	(15)

Table IV. (Cont'd)

CHF_2CH_2F	+	CD_3O^-	→	CD_3OHF^-	+	CHFCHF	8.4 ± 1.0 (21)
			→	CHF_2CHF^-	+	CD_3OH	5.6 ± 0.4 (22)
			→	F^-	+	$CD_3OC_2H_3F_2$	2.8 ± 0.3 (23)
	+	CHF_2CHF^-	→	$CHF_2CF_2HF^-$	+	CHFCHF	1.5 ± 0.2 (24)
	+	F^-	→	FHF^-	+	CHFCHF	2.8 ± 1.5 (25)
CHF_2CHF_3	+	CD_3O^-	→	CD_3OHF^-	+	CF_2CHF	2.5 ± 0.4 (26)
			→	$CHF_2CF_2^-$	+	CD_3OH	2.9 ± 0.1 (27)
	+	$^-CF_2CHF_2$	→	$CHF_2CF_2HF^-$	+	CF_2CHF	10.7 ± 1.0 (29)

Figure 2

Relative negative ion abundances as a function of the partial pressure of CH_3CF_2H in a mixture of CH_3CF_2H and CD_3ONO.

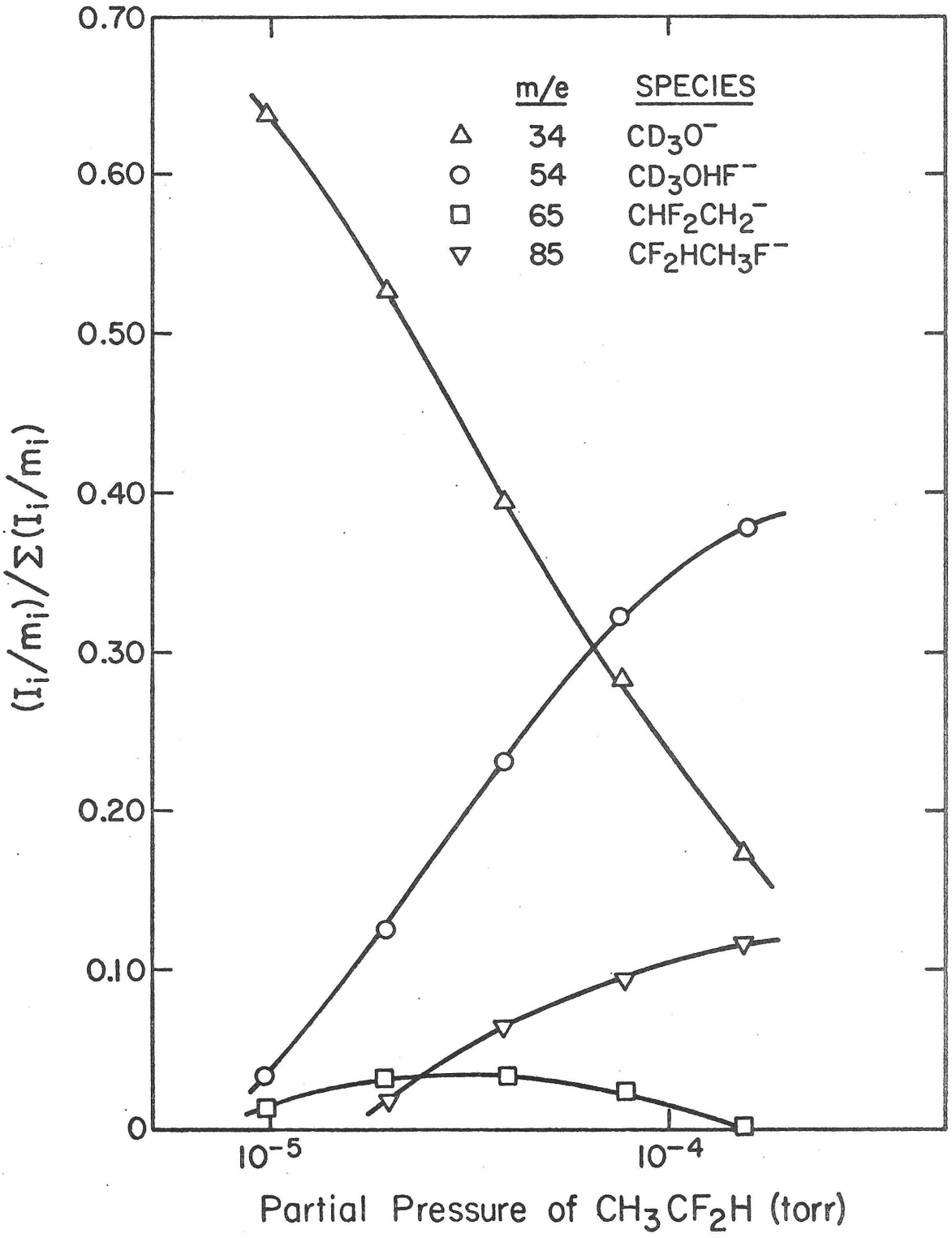
0.70
0.60
0.50
0.40
0.30
0.20
0.10
0
m/e
SPECIES
34
CD_3O^-
54
CD_3OHF^-
65
$CHF_2CH_2^-$
85
$CF_2HCH_3F^-$
$(I_i/m_i)/\Sigma(I_i/m_i)$
10^{-5}
10^{-4}
Partial Pressure of CH_3CF_2H (torr)

proton is confirmed by isotopic labeling. In addition, the β protons are found to be the most acidic in solution.[16] The mass 85 ion is written $CHF_2CH_3F^-$ also by analogy with ethyl fluoride and because the β protons are believed to be more acidic than the α protons and are therefore better sites for binding an anion. The method of Marshall and Buttrill for determining rates can not be used in cases where two reactant ions form the same product ion. Reactions (15) and (16) give the same product ion, but it was estimated that Reaction (16) is much slower than Reaction (15) so Reaction (16) was ignored in calculating the rates from the data. The rate data for

$$\underset{34}{CD_3O^-} + CH_3CHF_2 \xrightarrow{71\%} \underset{54}{CD_3OHF^-} + CH_2CHF \qquad (13)$$

$$\xrightarrow{29\%} \underset{65}{{}^-CH_2CHF_2} + CD_3OH \qquad (14)$$

$$\underset{65}{{}^-CH_2CHF_2} + CH_3CHF_2 \longrightarrow \underset{85}{CHF_2CH_3F^-} + CH_2CHF \qquad (15)$$

$$\underset{54}{CD_3OHF^-} + CH_3CHF_2 \longrightarrow \underset{85}{CHF_2CH_3F^-} + CD_3OH \qquad (16)$$

these reactions were determined at three different pressures from 0.9×10^{-5} to 3.6×10^{-5}. The large standard deviations reflect the inaccuracy of the Baratron at pressures less than about 2×10^{-5} torr. Reactions (13) to (15) are thus bimolecular processes for which the reactants and the product ion are unambiguously identified.

1, 1, 1 Trifluoroethane

The predominant product that appears when CF_3CH_3 is added to CD_3ONO is the mass 54 (CD_3OHF^-) ion. At higher pressures an ion of mass 103 ($CF_3CH_3F^-$) appears. Double resonance indicates that CD_3O^- is the precursor of CD_3OHF^- and that $^-CH_2CF_3$ and CD_3OHF^- are precursors of $CF_3CH_3F^-$. These data are consistent with Reactions (17) to (20). The variation of ion concentrations with

$$CD_3O^- + CH_3CF_3 \xrightarrow{93\%} \underset{83}{CD_3OHF^-} + CH_2CF_2 \qquad (17)$$

$$CD_3O^- + CH_3CF_3 \xrightarrow{7\%} \underset{83}{{}^-CH_2CF_3} + CD_3OH \qquad (18)$$

$$\underset{83}{{}^-CH_2CF_3} + CH_3CF_3 \longrightarrow \underset{103}{CF_3CH_3F^-} + CH_2CF_2 \qquad (19)$$

$$\underset{54}{CD_3OHF^-} + CH_3CF_3 \longrightarrow \underset{103}{CF_3CH_3F^-} + CD_3OH \qquad (20)$$

CH_3CF_3 partial pressure is illustrated in Figure 3. Reaction (29) is sufficiently fast that no $^-CH_2CF_3$ was observed in the series of spectra from which the illustrated data are taken. The ion was observed and the rates of (17) to (19) determined from spectra taken with a relatively high partial pressure of CD_3ONO, about 5×10^{-6} torr. The rates were determined at three CH_3CF_3 pressures ranging from 1.0 to 4.0×10^{-5} torr. As in the case of Reaction (16), the rate of Reaction (20) was estimated to be relatively slow and was considered to be zero in determining the rates. As is the case with the other fluoroethanes

Figure 3

Relative negative ion abundances as a function of the partial pressure of CH_3CF_3 in a mixture of CH_3CF_3 and CD_3ONO.

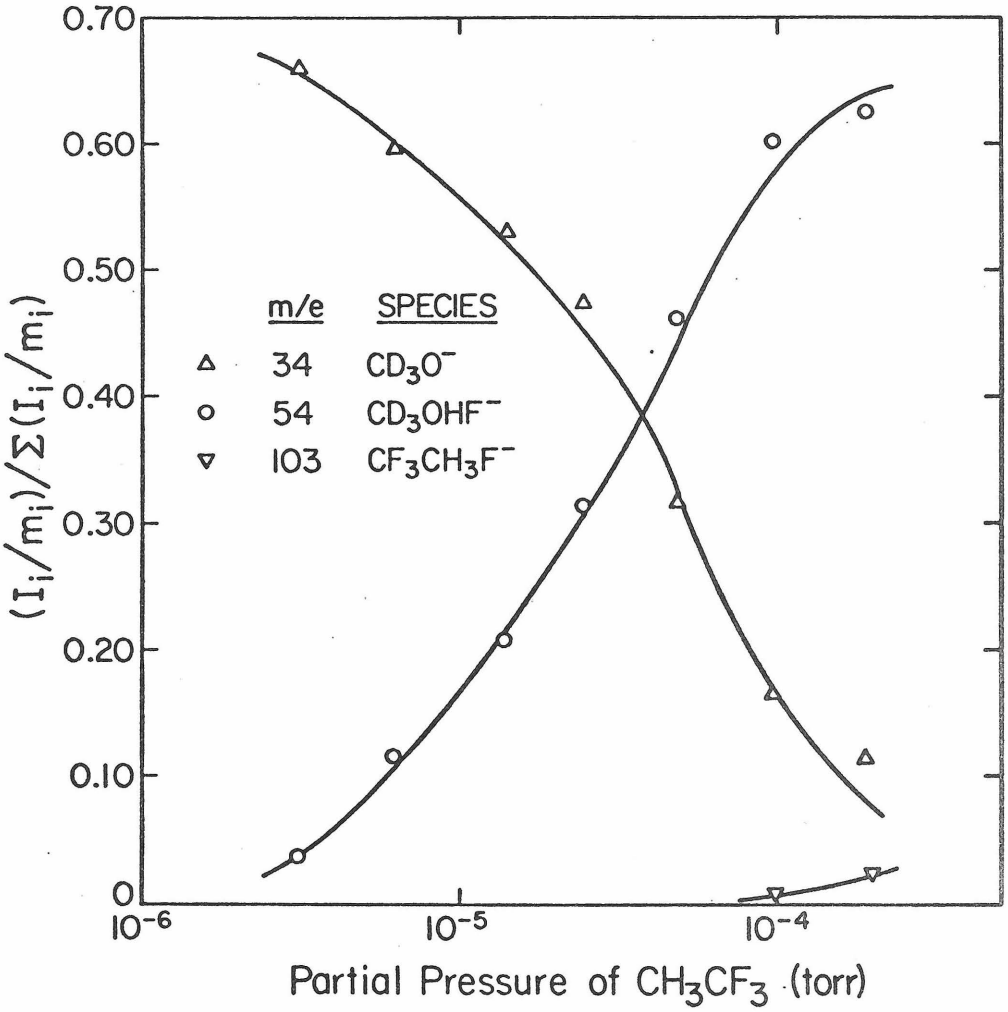
0.70
0.60
0.50
0.40
0.30
0.20
0.10
0
$(I_i/m_i)/\Sigma(I_i/m_i)$
m/e SPECIES
34 CD_3O^-
54 CD_3OHF^-
103 $CF_3CH_3F^-$
10^{-6}
10^{-5}
10^{-4}
Partial Pressure of CH_3CF_3 (torr)

all the data are consistent with bimolecular kinetics, and the ionic and neutral reactants and the ionic products are unequivocally identified for the reactions of CH_3CF_3.

1, 1, 2 Trifluoroethane

The reactions observed in CH_2FCHF_2 are analogous to those observed in ethyl fluoride. Ions of masses 54 (CD_3OHF^-), 83 (^-CHFCHF), 19 (F^-), 103 ($CHF_2CFH_2F^-$) and 39 (FHF^-) appear as the partial pressure of CH_3CHF_2 is increased. The variation of ion abundances with CHF_2CH_2F pressure is illustrated in Figure 4. Double resonance indicates that CD_3O^- is the precursor of CD_3OHF^-, $^-CHFCHF_2$ and F^-; that $^-CHFCHF_2$ is the precursor of $CHF_2CFH_2F^-$ and that F^- is the precursor of FHF^-. These data are consistent with Reactions (21) to (25). The β fluorine introduces an ambiguity in the identifies of the products of these reactions. Reactions (21) to (25)

$$\underset{34}{CD_3O^-} + CH_2FCHF_2 \xrightarrow{50\%} \underset{54}{CD_3OHF^-} + CHFCHF \qquad (21)$$

$$\underset{34}{CD_3O^-} + CH_2FCHF_2 \xrightarrow{33\%} \underset{83}{^-CHFCHF_2} + CD_3OH \qquad (22)$$

$$\underset{34}{CD_3O^-} + CH_2FCHF_2 \xrightarrow{17\%} \underset{19}{F^-} + CD_3OCHFCH_2F \text{ or } CD_3OH + CHFCHF \qquad (23)$$

$$\underset{83}{^-CHFCHF_2} + CH_2FCHF_2 \longrightarrow \underset{103}{^-FCH_2FCHF_2} + CHFCHF \qquad (24)$$

$$\underset{19}{F^-} + CH_2FCHF_2 \longrightarrow \underset{39}{FHF^-} + CHFCHF \qquad (25)$$

Figure 4

Relative negative ion abundances as a function of the partial pressure of CFH_2CF_2H in a mixture of CFH_2CF_2H and CD_3ONO.

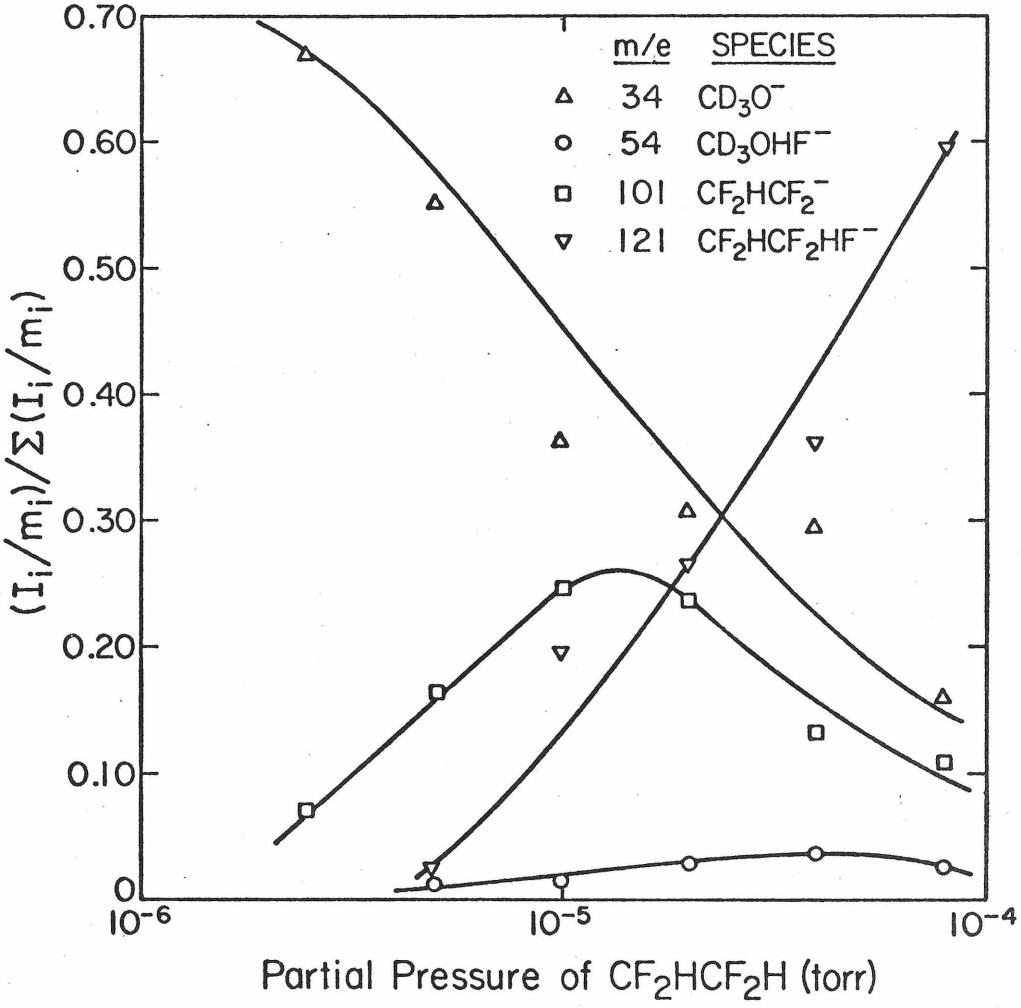
0.70
0.60
0.50
0.40
0.30
0.20
0.10
0
$(I_i/m_i)/\Sigma(I_i/m_i)$
m/e SPECIES
34 CD_3O^-
54 CD_3OHF^-
101 $CF_2HCF_2^-$
121 $CF_2HCF_2HF^-$
10^{-6}
10^{-5}
10^{-4}
Partial Pressure of CF_2HCF_2H (torr)

are written assuming that the β protons in CH_2FCHF_2 are more acidic than the α protons. The reactivities of the ethyl fluoride and 1, 1 difluoroethane suggest this to be the case. The data do not establish unambiguously, however, that only β protons are transferred to the CD_3O^- ion in Reaction (22). It could be that α protons are also transferred. Similarly Reactions (21) and (25) could involve transfer of an α hydrogen and a β fluorine from the neutral to the ion. In that case the neutral product of these reactions would be CH_2CF_2. The rate given in Table I for Reactions (21)-(25) were obtained at three partial pressures of CH_2FCHF_2 varying from 1.0 to 4.0×10^{-5} torr. The data are again consistent with bimolecular kinetics.

1, 1, 2, 2 Tetrafluoroethane

The product ions that appear when CHF_2CHF_2 is added to CD_3ONO have masses 54 (CD_3OHF^-), 101 ($^-CF_2CHF_2$), and 121 ($CHF_2CF_2HF^-$). The variation of ion abundances with CHF_2CHF_2 pressure is illustrated in Figure 5. Double resonance indicates that CD_3O^- reacts to form CD_3OHF^- and $^-CF_2CHF_2$ both of which react to form $CHF_2CF_2HF^-$. These data are consistent with Reactions (26) to (29).

$$\underset{34}{CD_3O^-} + CHF_2CHF_2 \begin{cases} \longrightarrow \underset{54}{CD_3OHF^-} + CF_2CHF & (26) \\ \longrightarrow \underset{101}{{}^-CF_2CHF_2} + CD_3OH & (27) \end{cases}$$

$$\underset{54}{CD_3OHF^-} + CHF_2CHF_2 \longrightarrow \underset{121}{CHF_2CF_2HF^-} + CD_3OH \qquad (28)$$

Figure 5

Relative negative ion abundances as a function of the partial pressure of CF_2HCF_2H in a mixture of CF_2HCF_2H and CD_3ONO.

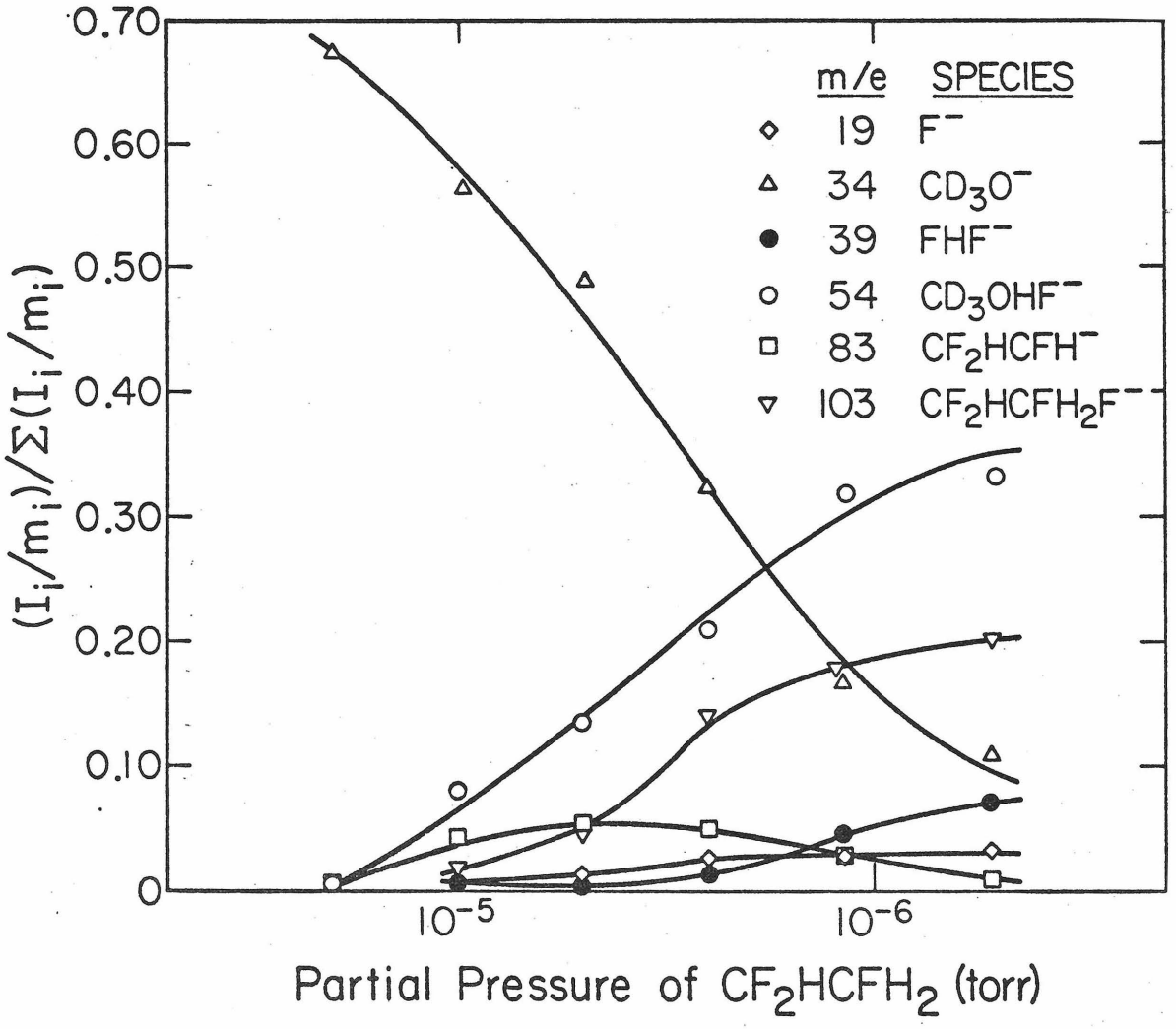
0.70
0.60
0.50
0.40
0.30
0.20
0.10
0
$(I_i/m_i)/\Sigma(I_i/m_i)$
m/e SPECIES
19 F^-
34 CD_3O^-
39 FHF^-
54 CD_3OHF^-
83 CF_2HCFH^-
103 $CF_2HCFH_2F^-$
10^{-5}
10^{-6}
Partial Pressure of CF_2HCFH_2 (torr)

$$\underset{101}{CF_2CHF_2} + CHF_2CHF_2 \longrightarrow \underset{121}{CHF_2CF_2HF^-} + CF_2CHF \qquad (29)$$

The rates given in Table I for Reactions (26), (27) and (29) are calculated assuming the rate of Reaction (28) to be negligible. The rates are calculated from data taken at three pressures ranging from 0.5 to 2.0×10^{-5} torr. The data are consistent with bimolecular kinetics.

Other Alkyl Halides

The only products observed in CH_3CH_2Cl and CH_3CH_2Br are the Cl^- and Br^- ions, respectively. Double resonance indicates that CH_3O^- reacts with neutrals to form the halide ions. In a mixture of CH_3ONO and CH_3CCl_3 ions of mass 67 and 69 appear in addition to the Cl^- ion. The concentrations of the mass 67 and 69 ions are in a ratio of 3:1 and double resonance indicates that 34 is their precursor. These data suggest that Reaction (30) occurs in CH_3CCl_3. CD_3OHCl^- was never greater than 1% of the total ionization. For this reason an accurate rate constant could not be determined for Reaction (30).

$$CD_3O^- + CH_3CCl_3 \longrightarrow CD_3OHCl^- + CH_2CCl_2 \qquad (30)$$

β-Chloroethanol

Ions of masses 35, 37, 67 and 69 appear as CH_2OHCH_2Cl is added to CH_3ONO. Double resonance indicates that all four ions are formed by reaction of CH_3O^- with CH_2OHCH_2Cl. The relative

abundance of the mass 35 and mass 37 ions are in a ratio of 3:1 as are the relative abundances of the 65 and 67 ions. These data are consistent with Reactions (31) and (32). As the product of a simple

$$CH_3O^- + CH_2OHCH_2Cl \begin{cases} \xrightarrow{83.5\%} Cl^- + CH_3OCH_2CH_2OH \quad (31) \\ \qquad\quad 35, 37 \\ \xrightarrow{16.5\%} CH_3OCHCl^- + \text{ethylene oxide} \quad (32) \\ \qquad\quad 67, 69 \end{cases}$$
(34)

nucleophilic displacement the β methoxy methanol is the most likely of the several possible neutral products of Reaction (31). Ethylene oxide is similarly the most mechanistically accessible of the several possible neutral products of Reaction (32). No rates were determined. Products were observed in a one to one mixture of methyl nitrite and CH_2OHCH_2Cl at 10^{-5} torr and above.

The negative ion reactions of CH_2OHCH_2Cl in the presence of SO_2F_2 were examined also. In SO_2F_2 alone at 3.5 eV, the major negative ions are at masses 19 (F^-), 38 (F_2^-), 83 (SO_2F^-) and 102 ($SO_2F_2^-$). These ions are 66.9%, 11.8%, 20.5% and 0.7% of the ionization, respectively, at 10^{-5} torr. Double resonance indicates that 19 reacts to form 38. As CH_2OHCH_2Cl is added ions of mass 35, 37, 55 and 57 appear. Double resonance indicates that 19 is the precursor of the four product ions. The concentrations of the 35 and 37 ions are in a ratio of 3 to 1 as are the concentrations of the 55 and 57 ions. These data are consistent with Reactions (33) and (34).

The neutral products written are again those that are mechanistically most readily accessible.

$$F^- + CH_2OHCH_2Cl \xrightarrow{73.8\%} Cl^- + CH_2OHCH_2F \quad (33)$$

$$F^- + CH_2OHCH_2Cl \xrightarrow{26.2\%} FHCl^- + \text{(cyclic ether)} \quad (34)$$

cis and trans 2-Chlorocyclopentanol

Neither the cis or the trans compound reacted with methoxide anions. Mixtures of the chloro alcohol with CD_3ONO in a ratio of ten to one were examined at pressures as high as 7×10^{-4} torr and the only product ion observed was an ion of mass 84 which appeared in small concentrations at the highest pressures. This ion is probably cyclopentoxy anion formed from an impurity of cyclopentanol in the chlorocyclopentanols.

β-Bromoethanol

In a 5 to 1 mixture of CH_2BrCH_2OH and CH_3ONO at 6×10^{-5} torr, very small concentrations of negative ions of masses 111 and 113 are observed in addition to ions of mass 31, 79 and 81. The 79 and 81 ions are present in CH_2BrCH_2OH by itself and are Br^- ions formed by electron attachment. Double resonance on the mixture indicates that Br^- is also formed by reaction between CH_3O^- and the alcohol. Double resonance also indicates the mass 111 and mass 113 ions to be products of reaction between CH_3O^- and the alcohol.

The concentrations of the 79 and 81 ions are in a ratio of one to one as are the concentrations of the mass 111 and 113 ions. These data are consistent with Reactions (35) and (36).

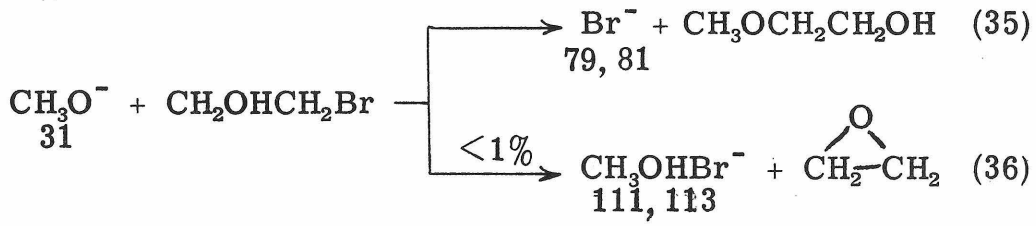

Discussion

The evidence is very good that Reactions (6) and (17) are the type of base induce 1, 2 elimination generalized by Reaction (4). The evidence may be summarized as follows:

1. The ionic reactant is CD_3O^- as determined by isotopic labeling in CH_3ONO and CD_3ONO.
2. The neutral reactants for the reactions as written are the only neutrals present in sufficient concentration to account for the appearance of product ions in observable concentrations.
3. The reactions are one step bimolecular processes. This is evident from the fact that the kinetics are consistently bimolecular over a range of pressures.
4. The double resonance results clearly and unambiguously identify CD_3O^- as the precursor of CD_3OHF^-.
5. Since CH_3CF_3 has only β protons and CD_3CH_2F has only β deuterons, the reactions involve loss of a β hydron consistent with the proposed mechanism.

On the basis of similar evidence and by analogy with Reactions (6) and (17) it is probable that Reactions (13), (17), (21), (25) and (26) are also 1, 2 base induced eliminations. Reaction (30) is probably also the same type of reaction. Thus enough examples of the elimination have been observed that some generalizations about the

reaction can be made. First of all, it appears that the probability for elimination of HX increases in the order HF > HCl > HBr. This could be the result of the fact that a fluorine substituent is less susceptible to nucleophilic attack than a chlorine or bromine substituted carbon.[17] Nucleophilic substitution is less likely to compete with the elimination in fluorides. Another important effect could be the acidity of the protons in fluoroethanes,[16] which facilitates the formation of a strong bond between the attacking anion and the fluoroethane substrate. The strength of this bond is the excitation energy of the intermediate complex depicted in Reaction (4). Factors which increase the bond strength increase the excitation energy available to effect the elimination and may thus be expected to increase the probability of elimination. The probability of proton transfer from substrate to base is also expected to increase with the acidity of the substrate, and other factors may control which of the two processes is predominant.

A second trend is that the relative importance of the elimination increases markedly with increasing α fluorine substitution. The elimination accounts for 29% of the reaction between CD_3O^- and CH_3CH_2F. That fraction increases to 71% in the case of CH_3CHF_2 and 93% in the case of CH_3CF_3. A probable explanation of this trend is that the elimination requires that the hydrogen and fluorine of the leaving group HF be in a <u>cis</u> configuration as depicted in Reaction (4). Increased α fluorine substitution statistically favors such a configuration. In addition, the direction of the dipole moment relative to the rest of the molecule changes significantly in this series of fluoro-

ethanes. This may effect the direction of approach of the attacking anion. If a molecule of CH_3CH_2F, for example, rotates to maximize the attraction between the approaching anion and the carbon-fluorine bond dipole moment,[18] then the anion will tend to bind to a proton trans to the fluorine. Since the elimination requires the proton to which the anion is bound and the leaving fluorine to be cis to one another, the elimination will be less probable to the extent that ion dipole alignment occurs. Similarly, ion dipole alignment might be expected to reduce the probability of elimination somewhat in CH_3CHF_2 but not to the extent that it does in ethyl fluoride. In CH_3CF_3 on the other hand, ion dipole alignment would not be expected to reduce the probability of elimination at all.

The trends observed for the elimination are consistent with the results in solution.[19] The process depicted in Reaction (4) can be classified formally as a syn-E2H reaction in which the component of the leaving group are in a cis configuration. Such processes are known to be promoted in solution by strong bases, poor leaving groups, substituents which acidify the β hydrogen and factors which promote the syn configuration of the intermediate base-substrate complex.

The fact that the elimination is observed corroborates that the bond between methoxide anion and hydrogen fluoride is sufficiently strong to render dehydrofluorination of a number of fluoroethanes exothermic. In fact, the observation of elimination of HF from CH_3CF_3 implies that $D(CH_3O^- - HF)$ is at least 33.4 kcal/mole (see Table III). This is, of course, consistent with the estimated value of

40 kcal/mole given in Table II. An interesting extension of the present study suggested by this result is the examination of the chemistry of F^- ions with several of the fluoroethanes. A wide range of values of $D(F^- - HF)$ have been reported in the literature,[7] and observation of fluoride induced elimination of HF would imply limits on that bond strength that would be useful in evaluating the various measurements.

The observed reactions also include a number of reactions that are best characterized on the basis of the data as proton transfer reactions between a fluoroethane and CD_3O^-. These include Reactions (7), (14), (18), (22) and (27). Proton transfer decreases in relative importance with increasing fluorine substitution in the series CH_3CH_2F, CH_3CHF_2 and CH_3CF_3. This is presumably because the elimination reaction becomes increasingly important with fluorine substitution in this series. Fluorine substitution at the β carbon seems to increase the relative importance of proton transfer. It is observed in solution that β fluorine substituents increase the acidity of β hydrogens in fluoroethanes.[16] This increased acidity may account for the increased importance of proton transfer.

Observation of these proton transfer reactions implies that the reactant fluorocarbons are better acids than methanol. The fact that CD_3OHF^- is observed to transfer a fluoride to several of the fluoroethanes (Reactions (16), (20) and (28)) is thus consistent with the implication discussed in the Introduction of this Chapter that if R_1H is a better acid than R_2H then Reaction (5) is exothermic. Limits on the

acidity of methanol have been determined so that a lower limit for the acidities of the fluoroethanes can be assigned. If it is assumed that the carbon-hydrogen bond strength in all of the fluoroethanes is the same as that in ethane (98 kcal/mole[20]) then a limit on the electron of the fluoroethyl radicals affinities can also be assigned. It is concluded in this way that the proton transfer reactions imply that the electron affinity of the fluoroethyl radicals CH_2CH_2F, CH_2CHF_2, CH_2CF_3, $CHFCHF_2$ and CF_2CHF_2 are all greater than 1.2 eV. The only fluoroethyl radical for which an electron affinity has been measured is CF_2CF_3.[21] The measured value is 2.1 eV which is consistent with what might be expected from the limit obtained above.

Another interesting general type of reaction observed is fluoride transfer. Reaction (9) was shown to be a fluoride transfer reaction by isotopic labeling. Reactions (15), (19), (24) and (28) are probably also fluoride transfer reactions. The observation of these reactions suggests that it may be possible to determine a sequence of gas phase fluoride affinities of various neutral species in the same way that a sequence of proton affinities has been determined.[13] The fluoride affinity of A may be defined as $D(A-F^-)$. On the basis of Reaction (9), for example, we can say that the fluoride affinity of CH_2CH_2 is less than that of CH_3CH_2F. The possibility of determining fluoride affinities of fluoroethylenes is particularly interesting because from the fluoride affinity of ethylene, for example, the heat of formation of $CH_2FCH_2^-$ and consequently an estimate of the electron affinity of $CH_2FCH_2\cdot$ can be determined.

In the reaction of CD_3O^- with CH_3CH_2F and with CH_2FCHF_2 some F^- is formed (Reactions (8) and (23)). The present experiments do not distinguish between several possible mechanisms for the production of fluoride ion. One possibility is nucleophilic substitution, but as mentioned above, fluorine substituted carbon atoms are not very susceptible to nucleophilic attack. Two other processes that would form F^- from ethyl fluoride are shown in Reaction (37).

$$CD_3O^- + CH_3CH_2F \begin{cases} \xrightarrow{a} [{}^-CH_2CH_2F]^* + CD_2OH \xrightarrow{a} \\ \xrightarrow{b} [CD_3OHF^-]^* + CH_2CH_2 \xrightarrow{b} \end{cases} F^- + CD_3OH + CH_2CH_2 \qquad (37)$$

Analogous processes would produce F^- from CH_2FCHF_2. The overall enthalpy change is the same for both path a and path b, but it can best be calculated from data in Tables II and III by considering path b. The enthalpy change for the first step is the enthalpy change for the elimination reaction which is given as -32 kcal/mole in Table II (under the column heading $\Delta H - D(CH_3O^- - HF)$). The enthalpy change for the second step is $D(CH_3OH - F^-)$ which is given as +24 kcal/mole in Table II. The overall process is thus exothermic for both CH_3CH_2F and CH_2FCHF_2. In a similar way it can be determined that processes analogous to those depicted in Reaction (37) are endothermic for the other fluoroethanes. This supports the conjecture that either path a or path b (or both) of Reaction (37) is the mechanism by which F^- is formed in the reactions of CD_3O^- with CH_3CH_2F and CH_2FCHF_2.

It should be noted that the above thermodynamic conclusions are subject to inaccuracies in the data in Tables II and III. The overall enthalpy changes for Reaction (37) and its analogs, however, are independent of the bond strengths listed in Table II. This is because the enthalpy change depends only on the heats of formation of the products and reactants and not the heat of formation of intermediate species formed.

In each system where F^- ions are generated, they go on to eliminate HF from the parent neutral. Fluoride ions did not, in either case, abstract a proton. This may indicate that the acidities of CH_3CH_2F and CHF_2CH_2F are both between those of F^- and CH_3O^-. These limits on the acidities of CH_3CH_2F and CHF_2CH_2F imply that the electron affinities of CH_2FCH_2 and CHF_2CHF (or CH_2FCH_2) are between 1.2 and 1.9 eV. It should be noted that the lower limit on the acidities (and the upper limit on the electron affinities) is merely suggested and not rigorously established by the observed chemistry.

The overall reaction rates between CD_3O^- and each of the fluoroethanes indicate reaction proceeds on approximately every collision except in the case of ethyl fluoride.[22] There may be some entropy or enthalpy of activation for reaction between CD_3O^- and ethyl fluoride.

The elimination of HCl from β chloroethanol (Reaction (32)) is an interesting reaction to discuss in Conclusion. It suggests that elimination of HX is strongly assisted by the intramolecular hydrogen bond between the hydroxy proton and the chlorine in β chloroethanol.[23]

This effect is easily understood in terms of the mechanism depicted in Reaction (4). The reaction also suggest that a variety of substrates may be susceptible to base induced elimination. Very recently, for example, a series of reactions of the type illustrated in Reaction (37) have been observed in alkyl formates.[24]

$$R_1O^- + HC(=O)OR_2 \longrightarrow R_1OHOR_2^- + CO \qquad (37)$$

Reaction (37) also points out the interesting variety of species XHY^- that can be generated in base induced elimination reactions. As is illustrated by the chemistry described, the formation of a strong hydrogen bond involves the release of considerable energy. Since the anionic dimers are formed in the gas phase, this energy is not rapidly dissipated to the solvent but is available to facilitate a variety of chemical changes in the dimer itself. Formation of the strong hydrogen bond is thus a means of chemical activation, and the chemistry that follows the formation of the bond can provide insight into the energetics and mechanisms of a variety of chemical processes.

References

1. D. Holtz, J. L. Beauchamp, and S. D. Woodgate, J. Amer. Chem. Soc., 92, 7484 (1970).
2. J. L. Beauchamp, D. Holtz, S. D. Woodgate and S. L. Patt, J. Amer. Chem. Soc., in press.
3. J. L. Beauchamp and M. C. Caserio, J. Amer. Chem. Soc., in press.
4. J. L. Beauchamp, J. Amer. Chem. Soc., 91, 5925 (1969).
5. J. L. Beauchamp and R. C. Dunbar, J. Amer. Chem. Soc., 92, 1477 (1970).
6. D. P. Ridge and J. L. Beauchamp, J. Amer. Chem. Soc., 93, 5925 (1971).
7. R. Yamdagni and P. Kebarle, J. Amer. Chem. Soc., 93, 7139 (1971).
8. There are no large ion accelerating fields in an ion cyclotron resonance spectrometer. The primary ions in the present study are formed by low energy electron attachment processes. The chemistry observed is therefore assumed to be that of thermal energy reactants.
9. J. I. Brauman and L. K. Blair, J. Amer. Chem. Soc., 92, 5986 (1960).
10. D. Holtz, J. L. Beauchamp and J. R. Eyler, J. Amer. Chem. Soc., 92, 7045 (1970).
11. K. Jaeger and A. Henglein, Z. Naturforsch., A22, 700 (1967).
12. M. D'Amore, Ph.D. Thesis, California Institute of Technology, 1971.

13. For a recent review of ion cyclotron resonance techniques and results see J. L. Beauchamp, Ann. Rev. Phys. Chem., 22, 527 (1971).

14. T. B. McMahon and J. L. Beauchamp, Rev. Sci. Instr., 43, 509 (1972).

15. A. G. Marshall and S. E. Buttrill, Jr., J. Chem. Phys., 52, 1752 (1970). Computer program courtesy of T. B. McMahon.

16. M. Hudlicky, Chemistry of Organic Fluorine Compounds, (MacMillan, New York, 1962). See also, J. A. Pople and D. L. Beveridge, Approximate Molecular Orbital Theory, (McGraw-Hill, New York, 1970), pp. 119-121.

17. M. Hudlicky, op. cit., p. 200.

18. For a discussion of ion dipole interactions see Part 1 of this thesis.

19. For a recent review see J. F. Bunnett, Surv. Progr. Chem., 5, 53 (1969).

20. S. W. Benson, Thermochemical Kinetics, (John Wiley and Sons, Inc., New York, 1968), p. 215.

21. P. W. Harland and J. C. J. Thynne, Int. J. Mass Spectrom. Ion Phys., 253 (1972).

22. Because of long range attractive forces, ion neutral collision frequencies are 1 to 2×10^{-9} cm^3 $molecule^{-1}$ sec^{-1} or larger. See Part I of this thesis for further discussion of ion neutral collision frequencies.

23. R. G. Azrak and E. B. Wilson, J. Chem. Phys., 52, 5299 (1970).

24. Jose Riveros, private communication.

25. S. E. Buttrill, Jr., J. Chem. Phys., 50, 4125 (1969).